
AFM-basierte Assemblierung biomolekularer Bausteine auf Festkörperoberflächen

Stefan K. Kufer

Dissertation



München Juni 2008

AFM-basierte Assemblierung biomolekularer Bausteine auf Festkörperoberflächen

Stefan K. Kufer

Dissertation

vorgelegt von
Stefan K. Kufer
aus
Freising

angefertigt an der
Ludwig-Maximilians-Universität München
Fakultät für Physik

München Juni 2008

Erstgutachter: Prof. Dr. Hermann E. Gaub
Zweitgutachter: Prof. Dr. Friedrich Simmel
Tag der mündlichen Prüfung: 05. August 2008

Inhaltsverzeichnis

Zusammenfassung	iii
1 Einleitung	1
2 Grundlagen zur Einzelmolekülkraftspektroskopie an DNA-Molekülen	5
2.1 Das Kraftmikroskop	5
2.2 Dissoziation von DNA-Duplexen unter Einfluss einer äußeren Kraft	7
2.3 Das Kraftsystem	11
3 Grundlagen zur Einzelmolekülfluoreszenzspektroskopie	15
3.1 Das Rayleigh Kriterium - das beugungslimitierte Objekt und seine Position	15
3.2 Fluoreszenzspektroskopie	17
3.3 Hochauflösende Mikroskopiemethoden	18
4 Ausblick	21
A Modular multichannel surface plasmon spectrometer	25
B Covalent immobilization of recombinant fusion proteins with hAGT for single molecule force spectroscopy	31
C Single-Molecule Cut-and-Paste Surface Assembly	41
D Super-Resolution Imaging of Fluorophore Patterns Deposited by Single-Molecule Cut-and-Paste	59
E Nanoparticle self-assembly on a DNA-scaffold written by single-molecule cut-and-paste	75
F Methoden zur Oberflächenfunktionalisierung für SMCP-Experimente	89
G SMCP als entkoppeltes Transportsystem für verschiedenste molekulare Bausteine	95
H Verbesserungsmöglichkeiten bei der SMCP-Oberflächenassemblierung	99

Abkürzungsverzeichnis	101
Literaturverzeichnis	109
Danksagung	111
Curriculum Vitae	113

„You don't make a girl and a boy fall in love by pushing them together (although this is often a step in the right direction)“

Richard E. Smalley

„Wir haben eine ältere Offenbarung als jede geschriebene - die Natur.“

Friedrich W. J. von Schelling

Zusammenfassung

Im Rahmen dieser Dissertation wurde erstmals eine Methode zur mechanisch kontrollierten Assemblierung einzelner molekularer Bausteine unter physiologischen Bedingungen entwickelt, die *Single-Molecule Cut-and-Paste (SMCP)-Oberflächenassemblierung*. Der Zusammenbau der molekularen Einheiten erfolgte auf Siliziumdioxidoberflächen und wurde mit einem Rasterkraftmikroskop (AFM) durchgeführt. Die aufgebauten Strukturen wurden mit zueinander komplementären Messverfahren (Fluoreszenz- und AFM-basierter Kraftspektroskopie) nachgewiesen.

Die Eigenschaft des DNA-Moleküls, aus zwei zueinander komplementären Strängen, selbstfindend eine Doppelhelix zu formen, wurde verwendet, um ein hierarchisches Kraftsystem zu etablieren. Dabei wurde ausgenutzt, dass die mechanische Stabilität eines Doppelstranges nicht nur von Art und Anzahl der Basenpaare, sondern auch von dessen Belastungsgeometrie abhängt. Einzelsträngige DNA-Moleküle (Transfer-DNA-Moleküle) wurden mit Hilfe einer Ankersequenz in einem wohlsortierten Depot mit der Kraft F_{Depot} spezifisch angebunden. Die Transfer-DNA besaß zusätzlich zur Ankersequenz eine Henkelsequenz, die es ermöglichte, einzelne Transfer-DNA-Moleküle über die Kraft $F_{Cantilever} > F_{Depot}$ mit einem AFM-Cantilever vom Depot aufzupicken. Anschließend wurde die Transfer-DNA mit Nanometerpräzision an die Zielstelle bewegt und mittels einer Kraft $F_{Ziel} > F_{Cantilever}$ abgesetzt. Auf diese Weise war es möglich, mit einer einzigen AFM-Spitze mehrere tausend SMCP-Zyklen durchzuführen und damit ausgedehnte Strukturen Molekül für Molekül aufzubauen.

Die Herstellung der Depot- und Zielbereiche sowie die Ankopplung der molekularen Bausteine wurde mit Hilfe eines Mikrofluidiksystems durchgeführt. Dadurch wurde sichergestellt, dass die Bausteine auf räumlich getrennten Bereichen angebunden waren. Um eine thermisch getriebene Diffusion und damit eine Kreuzkontamination der verschiedenen Depot- und Zielbereiche zu verhindern, wurde die Ankersequenz so gewählt, dass sie thermodynamisch stabil an die komplementären Sequenzen bindet.

Die Assemblierung wurde mit einem kombinierten AFM-TIRF-Mikroskop durchgeführt. Dieses Gerät ermöglichte es, den Transport der molekularen Bausteine mit unabhängigen Messmethoden zu beobachten. Die aufgezeichneten Kraft-Abstandskurven lieferten ein exaktes Transferprotokoll, das es erlaubte, die Anzahl der platzierten Moleküle zu bestimmen. Parallel dazu konnte über Einzelmolekülfluoreszenz ebenfalls die Anzahl der Moleküle und ihr tatsächlicher Ort nanometergenau bestimmt werden. Da die Position des AFM-Piezotisches und damit die Sollposition für die Platzierung mit Nanometerpräzision einge-

stellt werden kann, ist die Abweichung der gemessenen Istposition von der Sollposition ein Maß für die Ortsunsicherheit der SMCP-Oberflächenassemblierung. Es konnte experimentell gezeigt werden, dass die Genauigkeit bei ± 11 nm liegt, wodurch die Voraussage eines theoretischen Modells bestätigt werden konnte.

Ein entscheidender Vorteil der SMCP-Oberflächenassemblierung ergibt sich dadurch, dass die Transfer-DNA mit einer Vielzahl unterschiedlicher Gruppen und *Tags* modifiziert werden kann. Dadurch ist es möglich, molekulare Bausteine variabel an die Transfer-DNA zu koppeln, d.h. das Transfersystem DNA arbeitet entkoppelt von dem zu transportierenden Baustein. Um dies zu zeigen, wurden Transfer-DNA-Moleküle mit verschiedenen Farbstoffmolekülen modifiziert und die SMCP-Oberflächenassemblierung durchgeführt. Es konnte darüber hinaus gezeigt werden, dass an biotinylierte Transfer-DNA-Moleküle Streptavidin aktivierte Moleküle und Partikel gekoppelt werden können. Dies wurde exemplarisch für verschiedene Halbleiternanopartikel und für Polypeptide gezeigt.

Kapitel 1

Einleitung

Die frühesten Anfänge des Lebens auf der Erde reichen mindestens 3,4 Milliarden Jahre zurück [1, 2]¹. Heute sind etwa 1,75 Millionen Tier- und Pflanzenarten [8] beschrieben, die zum Teil unter extremen Milieubedingungen vorzufinden sind. Archaeen wurden beispielsweise noch in Tiefen von über 1600 m unter dem Meeresboden gefunden, wo Temperaturen von bis zu 100 °C herrschen [9, 10]. Acidophile Organismen leben in den Abwässern industrieller Metallgewinnung bei pH-Werten von 1 und alkaliphile Lebensformen gedeihen bei pH-Werten von über 10. Aber nicht nur „einfache“ Organismen haben sich extremen Umwelteinflüssen angepasst, auch „höhere“ Lebewesen können unter Bedingungen leben, die an technische Geräte höchste Anforderungen stellen².

Die Eigenschaften der „mechanischen“ Komponenten, die die Natur hervorgebracht hat, sind enorm³. Aber auch in Bereichen der Informationsspeicherung und der Informationsverarbeitung stellen die Leistungen der Natur technische Lösungen in den Schatten. Die kognitiven Fähigkeiten „höherer“ Lebewesen, insbesondere des menschlichen Intellekts, sind eigentlich nicht fassbar, und es wird wohl noch lange Zeit dauern, bis „künstliche“ Intelligenz auch nur ansatzweise existiert⁴. Die komplexen Steuerungs- und Regelungsmechanismen (z. B. der Immunantwort), die „unbewußt“ in Lebewesen ablaufen und ein Leben in einer sich ständig ändernden Umwelt erst ermöglichen, sind erst ansatzweise verstanden.

Die makroskopischen Formen (z. B. das Strömungsprofil von Fischen), die Dimensionen

¹Es konnte gezeigt werden, dass die in 3,4 Milliarden Jahre alten Sediment entdeckten Organismen bereits in der Lage waren, Photosynthese zu betreiben [1]. Aus diesem Grund kann man annehmen, dass bereits wesentlich früher Urformen von Leben auf der Erde existierten. Die Frage nach der Entstehung des Lebens, ist nur schwer zu beantworten. Vieles spricht dafür, dass sich das heutige auf DNA-basierte Leben aus einer RNA-Welt [3] heraus entwickelt hat. In hydrothermalen Quellen könnten beispielsweise einfache RNA-Moleküle entstanden sein [4, 5], die in der Lage waren, Kopien von sich selbst herzustellen und Proteine zu synthetisieren [6, 7].

²Pottwale können beispielsweise über 2600 m tief tauchen, wobei die Dauer eines Tauchgangs bis zu 80 Minuten betragen kann [11].

³Spinnenseide z.B. ist, bezogen auf ihr Gewicht, viermal belastbarer als Stahl und kann um das dreifache seiner Länge gedehnt werden, ohne zu reißen [12, 13].

⁴1950 schlug Alan Turing dem nach ihm benannten Turing-Test vor, um zu entscheiden, ob eine Maschine künstliche Intelligenz besitzt [14]. Bis heute konnte keine Maschine diesen Test bestehen.

(z. B. das Verhältnis von Kopfgröße zu Halsdurchmesser) und die Lösungswege (z. B. der Fortbewegungsapparat von Bakterien) der verschiedenen Organismen sind ihrem jeweiligen Lebensraum evolutionär angepasst⁵. Die Grundprinzipien, auf denen das Leben basiert, sind Beispiele einer hochentwickelten Nanotechnologie. Deshalb ist es, gemessen an dem oben genannten Leistungsspektrum lebender Organismen, nicht weiter verwunderlich, dass die Nanotechnologie als eine der Schlüsseltechnologien des 21. Jahrhunderts angesehen wird.

Trotz der Komplexität und der Mannigfaltigkeit des Lebens ist die Anzahl der zum Aufbau verwendeten Bausteine minimal. Von den über 100 bekannten chemischen Elementen stellen die sechs Elemente Wasserstoff (H), Kohlenstoff (C), Sauerstoff (O), Stickstoff (N), Schwefel (S) und Phosphor (P) 99 % der Gesamtmasse eines Organismus. Aus diesen sechs Elementen sind die sogenannten Biomoleküle aufgebaut, die sich einteilen lassen in Lipide, Kohlenhydrate, Polypeptide, Nukleotide und Porphine. Diese fünf Stoffklassen bilden die molekularen Bausteine, aus denen lebende Materie nach den Prinzipien der molekularen Erkennung und der Selbstorganisation (*Self-assembly*) in einem *Bottom-up-Ansatz* modular aufgebaut ist.

Ähnlich wie die Natur unterliegt auch die moderne Technik einem enormen Anpassungs- und Innovationsdruck. Insbesondere die Anforderungen aufgrund knapp werdender Ressourcen und die daraus resultierenden Forderungen nach Effizienzsteigerung stellen zentrale Herausforderungen der nahen Zukunft dar. Darüber hinaus sollen technische Geräte, aber auch Medikamente immer zuverlässiger, präziser und schneller arbeiten. Diese Forderungen sind nur durch eine Steigerung der Komplexität und einer damit einhergehenden Miniaturisierung (*Top-down-Ansatz*) der beteiligten Komponenten zu erfüllen. Dabei hat die moderne Mikrosystemtechnik (*Micro-Electro-Mechanical System (MEMS)*) den Größenbereich des Mikrometers ($100 \mu\text{m} - 0,1 \mu\text{m}$) längst unterschritten und ist bis in den Nanometerbereich vorgedrungen, in dem die Prinzipien des *Downscaling* zunehmend versagen.

Aus diesem Grund werden seit einigen Jahren die Wirkungsmechanismen der biologischen Selbstorganisation und der molekularen Erkennung nicht mehr nur alleine von Biologen, sondern in zunehmendem Maße auch von Physikern, Medizinern und Chemikern in einem hochgradig interdisziplinären Umfeld untersucht. Speziell durch die Entwicklung verschiedener Einzelmolekültechniken [17, 18, 19, 20, 21] konnten neue und detaillierte Einblicke in die Welt der Biologie gewonnen werden. So konnte beispielsweise durch Einzelmolekülfluoreszenzexperimente der *Hand-over-Hand*-Fortbewegungsmechanismus von Motorproteinen aufgeklärt werden [22, 23]. Durch die Einzelmolekülkraftspektroskopie wurden die mechanischen Eigenschaften des DNA-Moleküls [19, 24, 25, 26, 27, 28, 29], die mechanische Stabilität vieler Proteine [30, 31, 32] und die Dissoziationseigenschaften vieler Rezeptor-Ligand-Systeme auf Einzelmolekülniveau untersucht und aufgeklärt [33, 34, 35].

Dem DNA-Molekül wird aufgrund seiner einzigartigen Eigenschaften ein besonders

⁵Aufgrund von zufälligen Mutationen im genetischen Code einzelner Individuen innerhalb einer Art kann es vorkommen, dass diese einen genetischen Vorteil erhalten und „positive“ Mutationen im Genotyp, also im genetischen Code gespeichert werden. Neben diesen zufälligen Mutationen können aber auch erworbenene Merkmale weitervererbt werden. Man spricht hierbei vom sogenannten epigenetischen Code [15, 16].

großes Potential bei der Herstellung nanoskaliger Elemente eingeräumt. Die einfache und doch hochselektive A-T- und G-C-Basenpaarbindung erlaubt es, beispielsweise Rezeptor-Ligand-Systeme in beliebiger Vielfalt zu „programmieren“, deren Dissoziationseigenschaften frei einstellbar sind. Auf diese Weise konnte das DNA-Molekül beispielsweise als Kraftsensor in molekularen Kraftwaagen [36, 37] eingesetzt und DNA-basierte molekulare Motoren entwickelt werden [38, 39]. Da die räumliche Struktur eines DNA-Moleküls leicht berechenbar ist, konnten komplizierte zweidimensionale Strukturen [40, 41] sowie einfache dreidimensionale Nanostrukturen [42] erzeugt werden. Es war möglich, DNA-basierte „Rechenmaschinen“ zu entwickeln, die in der Lage waren, komplexe mathematische Algorithmen auszuführen [43, 44, 45, 46]. Ein weiterer wichtiger Grund, weshalb dem DNA-Molekül eine so große Bedeutung in den Nanowissenschaften zukommt, liegt daran, dass die Natur einen umfangreichen Satz an „Werkzeugen“ (z. B. Ligasen, Nukleasen und Restriktionsendonukleasen) zur Manipulation des DNA-Moleküls zur Verfügung stellt.

Bei allen Möglichkeiten, die das DNA-Molekül aufgrund seiner Fähigkeit zur Selbstorganisation zum Aufbau von Nanostrukturen bietet, ist es jedoch für viele Anwendungen zwingend nötig, den Aufbau nanoskaliger Elemente von außen auf Einzelmolekülniveau kontrollieren zu können. Eine solche Technologie würde es zum Beispiel ermöglichen, interaktiv Prozesse zu steuern und Fehler bei der Assemblierung zu korrigieren. Im Ultrahochvakuum bei Temperaturen von ca. 4 °K gelang es den Physikern Don Eigler und Erhard Schweizer bereits 1990, einzelne Atome und Moleküle auf Oberflächen mit einem STM kontrolliert zu bewegen und zu manipulieren [47, 48, 49]. Mit Hilfe eines STMs konnten sogar Moleküle Atom für Atom zusammengebaut werden [50]. Es gelang jedoch nicht, eine Technologie zu entwickeln, mit der es möglich ist, unter physiologischen Bedingungen einzelne Moleküle auf Oberflächen kontrolliert zu platzieren.

Zielsetzung

Das Ziel dieser Arbeit war, eine Methode zu entwickeln, die es ermöglicht, aus verschiedenen molekularen Bausteinen mechanisch kontrolliert Strukturen im Baukastenprinzip aufzubauen. Um bei späteren Anwendungen auf das gesamte Repertoire der biomolekularen Nanomaschinen zurückgreifen zu können, sollte die Assemblierung unter physiologischen Bedingungen erfolgen. Aus diesem Grund war es zwingend nötig, die molekularen Bausteine in einem gut sortierten Depot stabil lagern zu können, um eine thermisch getriebene Diffusion zu verhindern. Da es auf Einzelmolekülniveau nicht möglich ist, Moleküle vollständig zu kontrollieren⁶, sollte die Methode zudem die Möglichkeit bieten, Anzahl und Ort der einzeln

⁶Auf die prinzipiellen Limitierungen eines mechanisch kontrollierten *Assemblers* wurde von Richard E. Smalley eindrucksvoll hingewiesen [51]. Insbesondere das Problem des „Klebrigen-Dicken-Fingers“ (*Fat-and-Sticky-Finger-Problem*) stellt eine grundlegende Einschränkung an die Kontrollierbarkeit der Prozessführung dar. Bisherige Vorschläge zielten meist darauf ab, die „Klebrigkeit“, also die Affinität des „Fingers“, von außen durch elektrische oder optische Signale zu steuern. Anstatt die Affinität von außen zu schalten, werden bei der SMCP-Oberflächenassemblierung die „programmierbaren“ Dissoziationseigenschaften von DNA-Duplexen verwendet, um ein hierarchisches Kraftsystem aufzubauen. Neben dem Problem des Klebrigen-Dicken-Fingers limitieren bei Raumtemperatur auch thermische Fluktuationen ($k_B T$ -Problem) die Kontrollierbarkeit der Assemblierung einzelner Moleküle.

assemblierten Bausteine in Echtzeit zu bestimmen, um indirekt größtmögliche Kontrolle über den Zusammenbau zu erhalten. Eine solche Methode - die Single-Molecule Cut-and-Paste (SMCP)-Oberflächenassemblierung wurde im Rahmen dieser Doktorarbeit entwickelt und ist Gegenstand dieser Arbeit.

Diese Dissertation wurde kumulativ verfasst. Den in den Anhängen A - E angeführten Publikationen wurden zwei einleitende Kapitel vorangestellt, in denen die beiden zentralen Techniken, nämlich die Rasterkraftspektroskopie und die Einzelmolekülfluoreszenzmikroskopie, sowie das DNA-basierte Prinzip des hierarchischen Kraftsystems beschrieben werden. Die SMCP-Technik hat den Charakter einer Basistechnologie, die viele Erweiterungs- und Anwendungsmöglichkeiten bietet. Im Kapitel 4 folgt ein kurzer Ausblick, wozu die Technik in Zukunft verwendet werden könnte. In den Anhängen F - H wurden Ergebnisse zusammengefasst, die noch nicht publiziert wurden.

Kapitel 2

Grundlagen zur Einzelmolekülkraftspektroskopie an DNA-Molekülen

In dieser Arbeit wurden einzelne molekulare Bausteine mit Hilfe eines Rasterkraftmikroskops mechanisch kontrolliert auf Oberflächen platziert. Dazu wurde ein hierarchisches Kraftsystem auf DNA-Basis entwickelt. Die Methode der Kraftspektroskopie, die Dissoziation von DNA-Molekülen unter Einfluss einer äußeren Kraft und das zugrunde liegende Kraftsystem werden in diesem Kapitel näher beschrieben.

2.1 Das Kraftmikroskop

Das Kraftmikroskop (*Atomic Force Microscope*, AFM) gehört zu den Rastersondenmikroskopen [52, 17, 53, 54] und wurde von Gerd Binnig, Calvin Quate und Christoph Gerber 1986 entwickelt [17]. Im Gegensatz zum Rastertunnelmikroskop (*Scanning Tunneling Microscope*, STM) [55, 56], das den abstandsabhängigen Tunnelstrom zwischen einer leitenden, atomar feinen Spitze und einer leitenden Oberfläche misst, dient das Kraftmikroskop zur mechanischen Abtastung von nicht leitenden Oberflächen und zur Messung atomarer Kräfte.

Messprinzip

Das Prinzip der Kraftmessung beim AFM beruht auf der mechanischen Verbiegung z_C einer mikroskopisch kleinen „weichen“ Blattfeder - dem sogenannten *Cantilever* - an dessen Ende eine als Sonde dienende scharfe Spitze sitzt (Abbildung 2.1). Unter Belastung zeigt der Cantilever entsprechend einer „Hooke’schen Feder“ mit einer Federkonstanten k_C ein linear-elastisches Verhalten und wird direkt proportional zur einwirkenden Belastung gemäß

$$F = k_C z_C \implies z_C = \frac{F}{k_C} \quad (2.1)$$

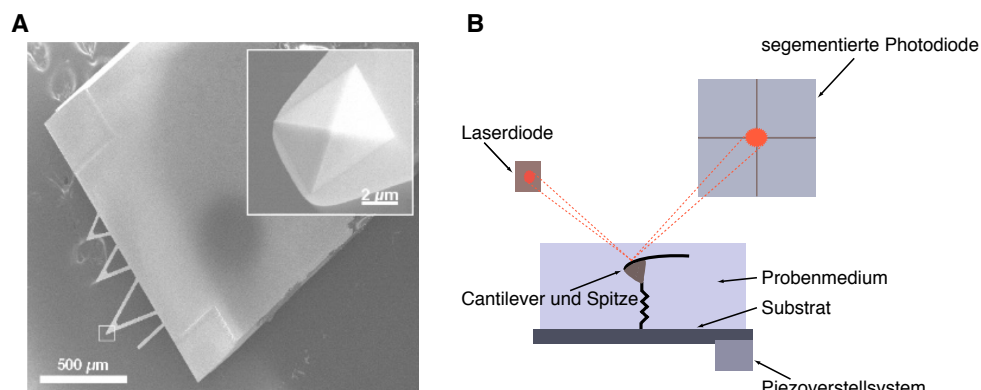


Abbildung 2.1: (A) Elektronenmikroskopische Aufnahme eines in dieser Arbeit häufig verwendeten Cantilever-Chips (MLCT-AUHW, Veeco Probes). Dieser Chip besteht aus vier Cantilivern (drei dreieckig und ein rechteckiger Cantiliver) mit unterschiedlichen Federkonstanten und Resonanzfrequenzen. Die Detailaufnahme zeigt die pyramidenförmige Spitze des größten Cantilivers. Die Spitzen sind mit Krümmungsradien von 40 nm bzw. 10 nm erhältlich. (B) Schematische Darstellung der Funktionsweise eines Kraftmikroskops. Mittels eines Piezoverstellungssystems kann die Spitze in xyz-Richtung relativ zum Substrat bewegt werden. Wirkt auf den Cantiliver eine Kraft, wird die daraus resultierende Verbiegung über die Ablenkung eines Laserstrahls mit einer segmentierten Photodiode detektiert. (Die REM-Aufnahme wurde von Ferdinand Kühner freundlicherweise zur Verfügung gestellt.)

verbogen. Diese kraftinduzierte Verbiegung wird meist optisch über die Ablenkung eines Laserstrahls mit einer segmentierten Photodiode detektiert [57]. Eine AFM-Spitze kann nun mittels piezoelektrischer Kristalle Oberflächen mit hoher Ortsauflösung abrastern und somit lokale Oberflächeneigenschaften über die kraftabhängige Verbiegung des Cantilivers messen. Das Messprinzip des AFMs erlaubt es somit auch, Proben in Flüssigkeit zu untersuchen, was für die Untersuchung biologischer Prozesse oftmals eine zwingende Voraussetzung ist.

AFM-basierte Kraftspektroskopie

Wird eine Oberfläche von einem Cantiliver im Kontaktmodus abgerastert, kann das Höhenprofil der Probe mit atomarer Auflösung durch die Verbiegung des Cantilivers ermittelt werden. Ist zusätzlich die Federkonstante¹ des verwendeten Cantilivers bekannt, kann die Verbiegung verursachende Kraft gemäß Gleichung 2.1 berechnet werden. Bei der AFM-basierten Kraftspektroskopie wird der Cantiliver der zu untersuchenden Probe angenähert, mit ihr in Kontakt gebracht und wieder zurückgezogen. Die auf den Cantiliver einwirkenden

¹Die Federkonstante wird meist über die Methode des thermischen Rauschens [58, 59, 60, 61] bestimmt. Dazu wird ein Rauschspektrum der Auslenkung $z_C(t)$ aufgenommen und fouriertransformiert. Die Federkonstante und die Resonanzfrequenz erhält man aus diesem Frequenzspektrum durch Anfitzen einer Lorenzkurve. Die Federkonstante kann mit dieser Methode mit einem Fehler von 10 % ermittelt werden.

de Kraft wird als Funktion des Abstands der Cantilever-Spitze von der Oberfläche aufgetragen. Diese als Kraft-Abstandskurven bezeichneten Funktionen erlauben es, inter- und intramolekulare Wechselwirkungen einzelner Moleküle zu untersuchen.

Kraftauflösung

Im thermischen Gleichgewicht erhält jeder Freiheitsgrad eines Systems, der quadratisch zur Gesamtenergie beiträgt und nicht „eingefroren“ ist, gemäß des Gleichverteilungssatzes eine Energie $\frac{1}{2}k_B T$. Entsprechend eines harmonischen Oszillators wird die Grundschiwingung eines Cantilevers thermisch angeregt und sein mittleres Auslenkungsquadrat ist gegeben durch:

$$\frac{1}{2}k_C \langle z_C(t)^2 \rangle = \frac{1}{2}k_B T \implies \langle z_C(t)^2 \rangle = \frac{k_B T}{k_C}. \quad (2.2)$$

Die mittlere thermisch induzierte quadratische Fluktuation der Kraft ergibt sich hieraus zu:

$$\langle F(t)^2 \rangle = k_C^2 \langle z_C(t)^2 \rangle = k_C k_B T. \quad (2.3)$$

Die Federkonstanten der in dieser Arbeit verwendeten Cantilever lagen typischerweise in der Größenordnung von $k_C \approx 6$ pN/nm, d.h. die daraus resultierende Standardabweichung der Kraftfluktuationen im Bereich von 5 pN. Eine genauere Analyse der Kraftauflösung [62, 63, 64] führt zu dem Nyquist-Theorem

$$F_{min} = \sqrt{4k_B T R B} \quad (2.4)$$

für die minimal detektierbare Kraft bei einer thermisch limitierten Messungen, wobei R die viskose Dämpfung und B die Bandbreite darstellen.

2.2 Dissoziation von DNA-Duplexen unter Einfluss einer äußeren Kraft

Aufbau und Struktur der DNA

Der molekulare „Bauplan“ aller² Lebewesen ist in Form des DNA-Moleküls „aufgeschrieben“. Trotz der unzählbar großen Anzahl verschiedener Lebensformen ist die DNA sehr einfach aufgebaut. Chemisch gesehen handelt es sich um ein fadenförmiges Makromolekül, das aus vier verschiedenen Bausteinen, nämlich den Basen Adenin (A), Thymin (T), Cytosin (C) und Guanin(G) zusammengesetzt ist. Die Basen sind über Zucker-Phosphat-Gruppen miteinander verbunden (siehe Abbildung 2.2). Die Abfolge der vier Basen bestimmt den genetischen Code eines Lebewesens.

Erwin Chargaff erkannte 1950, dass jeweils zwei der vier Basen, nämlich Guanin/Cytosin (G-C) und Adenin/Thymin (A-T), in der DNA in genau äquimolaren Mengen vorhanden sind und postulierte die Regel, dass diese Basen stets paarweise auftreten [65]. Kurze Zeit

²Lediglich einige Viren benutzen RNA als Träger ihrer Erbinformation

später erkannten Watson und Crick durch Interpretation röntgenspektrometrischer Daten den helixartigen Aufbau kristallisierter DNA-Moleküle. Nach diesem Modell ist ein DNA-Molekül aus zwei antiparallelen Nukleinsäuresträngen aufgebaut, die in einer rechtsgewundenen Spirale über Wasserstoffbrückenbindungen der zueinander komplementären Basen miteinander verbunden sind (siehe Abbildung 2.2).

Die in einer DNA-Doppelhelix verknüpften Einzelstränge lassen sich reversibel in Einzelstränge aufschmelzen. Die Rückreaktion zweier Einzelstränge zur DNA-Doppelhelix bezeichnet man als Hybridisierung.

Belastungsgeometrien

Die mechanischen Eigenschaften einer DNA-Doppelhelix lassen sich mittels Einzelmolekülkraftspektroskopie untersuchen. Insbesondere kann die mechanische Stabilität einer Doppelhelix bestimmt werden. Prinzipiell gibt es zwei Möglichkeiten, an DNA-Moleküle eine externe Kraft anzulegen (siehe Abbildung 2.3).

- unzip-Geometrie: Die Kraft wird an einem Einzelstrang am 5'-Ende und am anderen Einzelstrang am 3'-Ende angelegt. Dadurch wird die Doppelhelix Basenpaar für Basenpaar auseinander gezogen. Die Bindungsenergie von AT- bzw. GC-Basenpaaren kann auf diese Weise direkt bestimmt werden. In [26, 27, 28] wurde gezeigt, dass die Kraft zur Trennung einer in unzip-Geometrie belasteten DNA-Doppelhelix unabhängig von der Kraftladungsrate³ und von der Länge der Doppelhelix ist. Sie ist allerdings abhängig vom AT- bzw. GT-Anteil der belasteten Sequenz. AT-Basenpaare werden lediglich über zwei Wasserstoffbrücken stabilisiert, während GC-Basenpaare über drei Wasserstoffbrücken gebunden sind. Aus diesem Grund öffnen AT reiche Sequenzen schon bei einer Kraft von ca. 10 pN, während GC reiche Sequenzen erst bei ca. 25 pN geöffnet werden. Für Sequenzen mit gemischtem AT- und GC-Gehalt ergibt sich eine mittlere Kraft. Abbildung 2.4(A) zeigt eine typische Kraft-Abstandskurve einer 30 Basenpaar langen DNA-Sequenz, die in unzip-Geometrie belastet wird. Die Länge des Plateaus beträgt ca. 27 nm und stimmt gut mit der erwarteten Länge von ca. 30 nm überein. Die Kraft zum Trennen beträgt ca. 20 pN.
- shear-Geometrie: Die Kraft wird an einem Einzelstrang am 5'-Ende und am anderen Einzelstrang ebenfalls am 5'-Ende, bzw. jeweils am 3'-Ende, angelegt. Dadurch wird die Doppelhelix parallel zum Rückgrat gestreckt und die Kraft wirkt auf alle Basenpaare der Doppelhelix gleichzeitig. Die Abrisskraft ist abhängig von der Kraftladungsrate und der Länge der Sequenz [29].

³Die Kraftladungsrate ist die zeitliche Ableitung $\frac{dF}{dt}$ der angelegten Kraft beim Abriss und ein Maß dafür, mit welcher Geschwindigkeit die Kraft in der Bindung aufgebaut wird.

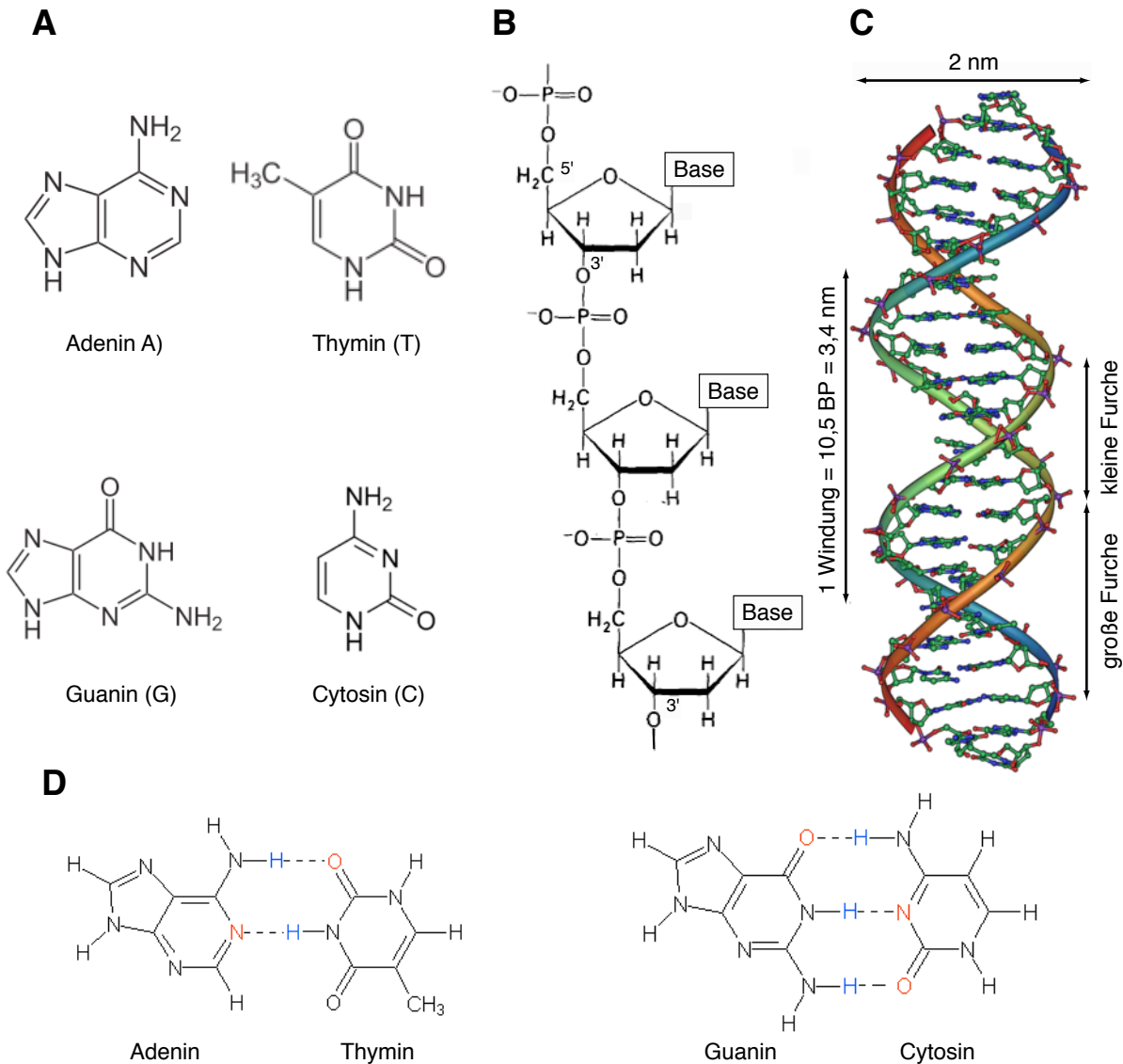


Abbildung 2.2: Aufbau und Struktur des DNA-Moleküls. (A) Die DNA ist aus den vier Basen Adenin (A), Thymin (T), Guanin (G) und Cytosin (C) modular aufgebaut. (B) Eine Base ist jeweils an ein Desoxyribosemolekül gebunden. Die Desoxyribosemoleküle sind untereinander über Phosphatgruppen verbunden, wobei die Phosphatgruppe am 5'-C und am 3'-C des Zuckers gebunden sind. (C) Die DNA-Doppelhelix ist aus zwei antiparallelen, einzelsträngigen DNA-Molekülen aufgebaut, die in einer rechtsgewundenen Spirale miteinander verbunden sind. Die Stabilisierung der Doppelhelix erfolgt über Wasserstoffbrückenbindungen der Basen. (D) Adenin und Thymin werden über zwei Wasserstoffbrücken verbunden, Guanin und Cytosin über drei. (Bilder adaptiert von <http://de.wikipedia.org>)

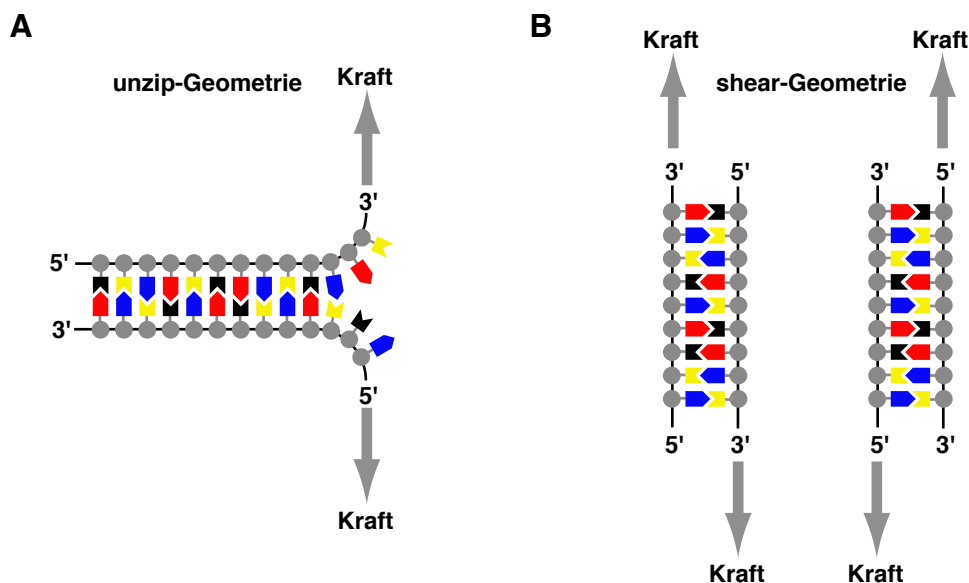


Abbildung 2.3: Belastungsgeometrien für DNA-Moleküle. (A) Wird die Kraft zum Trennen einer Doppelhelix am 5'-Ende des ersten Stranges und 3'-Ende des zweiten Stranges angelegt, werden die Basenpaare paarweise getrennt und man spricht von unzip-Geometrie. In den Kraft-Abstandskurven ergibt sich ein Plateau, dessen Länge abhängig von der Länge der Sequenz ist. Die Höhe des Plateaus ist abhängig vom AT- und GC-Gehalt. (B) Wird die Kraft an einem Strang am 5'-Ende und am anderen Einzelstrang ebenfalls 5'-Ende, bzw. jeweils am 3'-Ende, angelegt, spricht man von shear-Geometrie. Die Basenpaare werden alle gleichzeitig belastet. In den Kraft-Abstandskurven ergibt sich eine Abrisskraft, die abhängig von der Kraftladungsrate und der Länge der Sequenz ist.

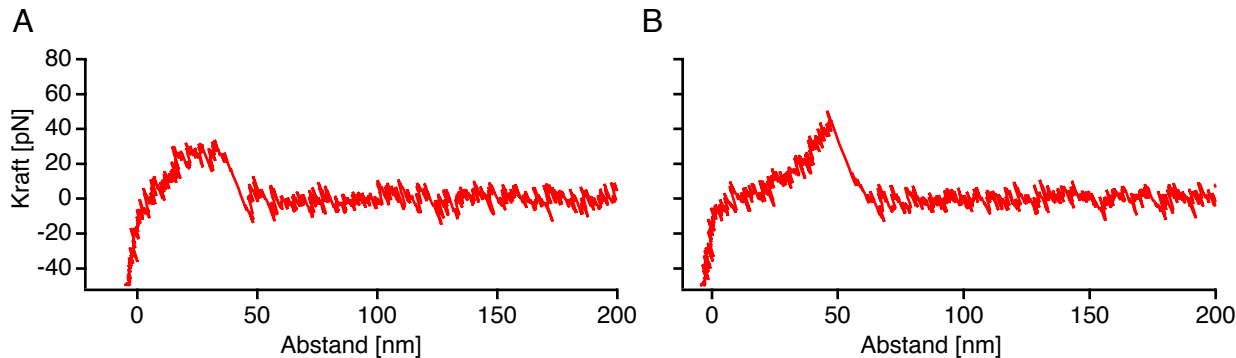


Abbildung 2.4: Typische Kraft-Abstandskurven von unzip- und shear-Geometrien. (A) Die Kraft-Abstandskurve zeigt das Öffnen einer 30 Basenpaar langen Ankersequenz, die in unzip-Geometrie vom Depot abgelöst wurde. (B) Die Kraft-Abstandskurve zeigt den Abriss einer 20 Basenpaar langen Henkelsequenz, die in shear-Geometrie im Zielbereich belastet wurde.

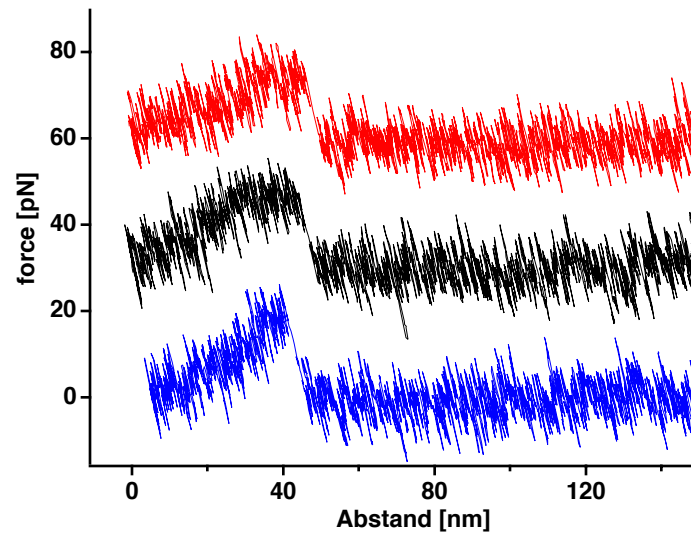


Abbildung 2.5: Aufnahme von einzelnen Transfer-DNA-Molekülen vom Depot im Nicht-Kontaktmodus. Aufgrund der Länge des PEG-DNA-Komplexes muss die Spitze nicht vollständig mit der Oberfläche in Kontakt gebracht werden, damit die Henkelsequenz mit der Cantilever-DNA hybridisieren kann. Die Kraft-Abstandskurven zeigen ebenfalls das typische entropische Dehnungsverhalten des PEG-DNA-Komplexes. Bei einer Kraft von ca. 20 pN öffnet die Ankersequenz in unzip-Geometrie.

2.3 Das Kraftsystem

Das zentrale Prinzip der SMCP-Oberflächenassemblierung beruht auf einem hierarchischen Kraftsystem auf DNA-Basis. Einzelsträngige DNA-Moleküle, die als entkoppeltes Transfersystem dienen, werden über eine 30 Basenpaar lange Ankersequenz thermodynamisch stabil⁴ an Depotbereiche angebunden. Diese Transfer-DNA besitzt zusätzlich zur 30 Basenpaar langen Ankersequenz eine 20 Basenpaar lange Henkelsequenz (siehe Abbildung 2.6). Die Ankersequenz ist komplementär zu einer einzelsträngigen DNA, die kovalent an die Spitze eines AFMs angebunden ist. Wird die Spitze mit der Depotfläche in Kontakt gebracht⁵, hybridisiert die Henkelsequenz mit der Cantilever-DNA. Beim Rückziehen der Spitze werden Anker- und Henkelsequenz gleichzeitig belastet. Obwohl die Anker- und Henkelsequenz eine vergleichbare thermodynamische Stabilität haben, ist ihr Dissoziationsverhalten unter Kraft völlig unterschiedlich (vgl. Abschnitt 2.2).

Die Transfer-DNA ist im Depotbereich derart angebunden, dass die Ankersequenz dort

⁴Die Schmelztemperatur der Ankersequenz in 1*SSC-Puffer (150 mM NaCl, 15 mM Natrium Zitrat, pH 7) beträgt 65 °C.

⁵Aufgrund der Länge des PEG-DNA-Komplexes muss die Spitze nicht vollständig mit der Oberfläche in Kontakt gebracht werden. In Abbildung 2.5 sind Kraft-Abstandskurven während der Aufnahme einer Transfer-DNA vom Depot gezeigt, wobei die Spitze jeweils einige Nanometer von der Oberfläche entfernt war. Man erhält ebenfalls die typischen unzip-Kurven des Depots. Dies zeigt, dass die DNA-Moleküle nicht unspezifisch vom Cantilever aufgenommen werden.

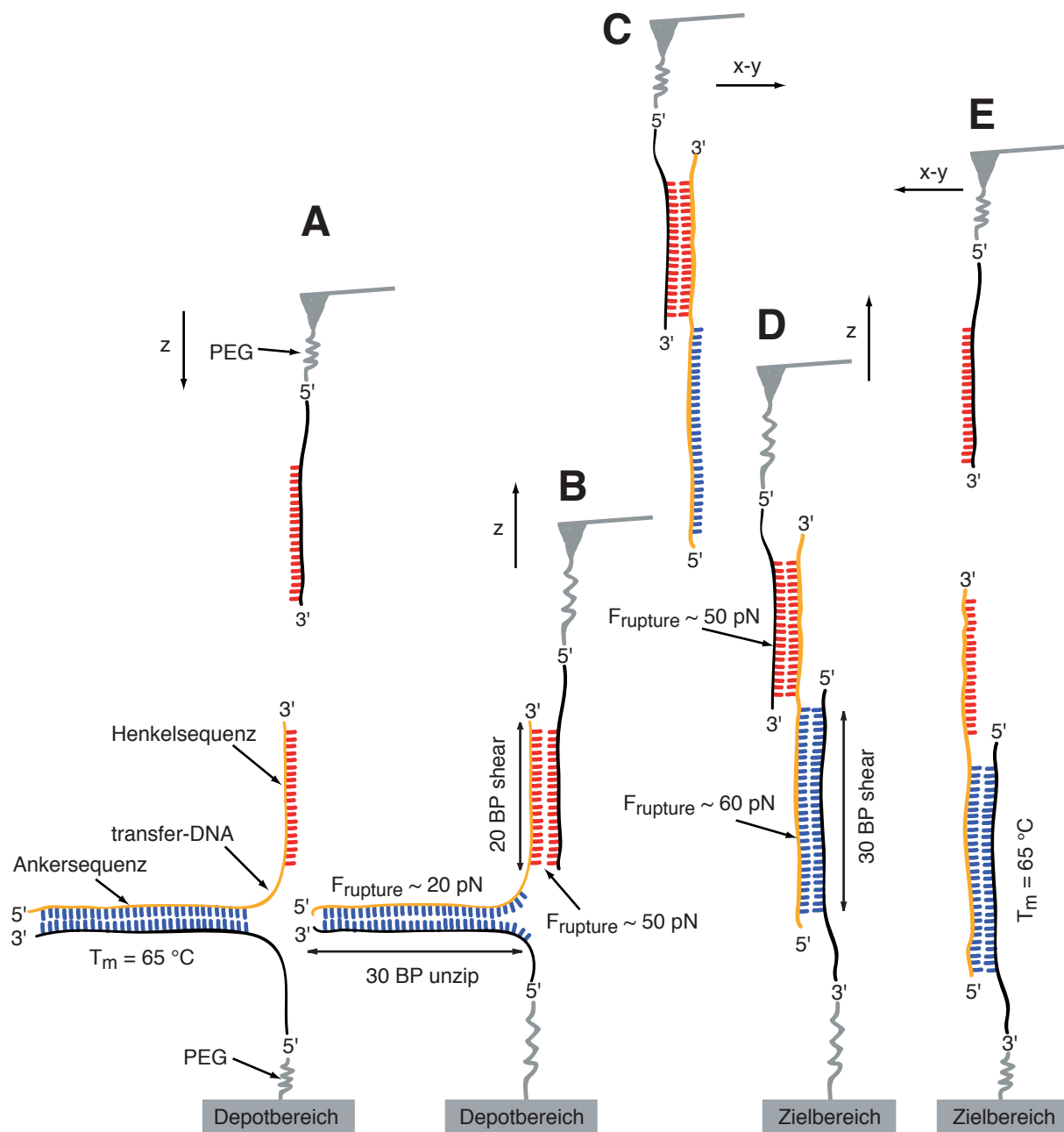


Abbildung 2.6: Das hierarchische Kraftsystem. (A) Die Transfer-DNA besitzt eine 30 Basenpaar lange Anker- und eine 20 Basenpaar lange Henkelsequenz. Sie wird über die Ankersequenz in unzipped-Geometrie an das Depot gebunden. Die AFM-Spitze ist mit einer 20 Basenpaar langen, zur Henkelsequenz komplementären DNA kovalent modifiziert. (B) Wird die Spitze in Kontakt mit der Depotfläche gebracht, hybridisiert die Henkelsequenz der Transfer-DNA in shear-Geometrie mit der Cantilever-DNA. Unter mechanischer Belastung öffnet die Ankersequenz vor der Henkelsequenz und die Transfer-DNA wird von der Spitze aufgenommen. (C) Die Transfer-DNA wird an die Zielstelle transportiert und bindet dort über die 30 Basenpaar lange Ankersequenz in shear-Geometrie an den Zielbereich. (D) Unter Belastung öffnet die 20 Basenpaar lange Henkelsequenz vor der 30 Basenpaar langen Ankersequenz. (E) Die AFM-Spitze ist wieder im Anfangszustand und der nächste Transferzyklus kann durchgeführt werden.

in unzip-Geometrie belastet wird, während die Henkelsequenz in shear-Geometrie belastet wird (Abbildung 2.6(A und B)). Erreicht die angelegte Kraft einen Wert von ca. 20 pN, wird die Ankersequenz Basenpaar für Basenpaar auseinander gezogen. Die Transfer-DNA, die von der AFM-Spitze aufgenommen wurde, kann nun in den Zielbereich transportiert werden (Abbildung 2.6(C)). Dort hybridisiert die 30 Basenpaar lange Ankersequenz mit einer kovalent an das Ziel angebundenen komplementären DNA. Im Unterschied zum Depot bindet die Transfer-DNA ans Ziel in shear-Geometrie (Abbildung 2.6(D)). Unter mechanischer Belastung reißt die 20 Basenpaar lange Henkelsequenz vor der 30 Basenpaar langen Ankersequenz. Die Spitze ist jetzt wieder im Anfangszustand und kann weitere molekulare Bausteine aus den Depotbereichen in die Zielbereiche transportieren (Abbildung 2.6(E)).

Kapitel 3

Grundlagen zur Einzelmolekülfluoreszenzspektroskopie

In diesem Kapitel werden die Grundlagen der Einzelmolekülfluoreszenzspektroskopie besprochen. Ferner wird über das Auflösungsvermögen eines optischen Systems und über Techniken zur Verbesserung dieses Auflösungsvermögens diskutiert.

3.1 Das Rayleigh Kriterium - das beugungslimitierte Objekt und seine Position

Das Auflösungsvermögen eines optischen Systems

Das Auflösungsvermögen eines optischen Systems ist aufgrund der Wellennatur des Lichtes durch Beugungsphänomene begrenzt. Das Bild einer Punktquelle, das von einem optischen System erzeugt wird, ist nicht wieder ein Lichtpunkt, sondern ein Beugungsscheibchen umgeben von konzentrischen Beugungsringsen. Anschaulich können zwei räumlich getrennte Punktlichtquellen nur dann als zwei Objekte wahr genommen werden, wenn ihr Abstand größer als der Radius des zentralen Beugungsrings ist. Das Bild einer Punktlichtquelle lässt sich mit Hilfe der sogenannten Point-Spread-Funktion (PSF)

$$PSF(r) = \left(\frac{2J_1(ra)}{r} \right)^2 \quad (3.1)$$

des verwendeten Objektivs berechnen [66]. Der Parameter a ist gegeben durch:

$$a = \frac{2\pi NA}{\lambda}. \quad (3.2)$$

NA ist die Numerische Apertur des Objektivs, λ die Wellenlänge des detektierten Lichts und J_1 die Besselfunktion 1. Ordnung. Die erste Nullstelle der Point-Spread-Funktion:

$$PSF(r) = \left(\frac{2J_1(ra)}{r} \right)^2 \stackrel{!}{=} 0 \implies J_1 \left(\frac{r2\pi NA}{\lambda} \right) = 0 \quad (3.3)$$

liefert den Radius des zentralen Beugungsscheibchens. Mit $J_1(x) = 0$ für $x \approx 3,8$ ergibt sich das bekannte Rayleigh Kriterium

$$r = 0.61 \frac{\lambda}{NA}. \quad (3.4)$$

Punktlichtquellen mit einem kleineren Abstand lassen sich nicht als räumlich getrennte Objekte wahrnehmen.

Ortsbestimmung eines Objekts

Obwohl Punktlichtquellen nicht punktförmig, sondern in Form von Airy-Scheibchen abgebildet werden, lässt sich für „helle“ Objekte das Intensitätsmaximum ihres Airy-Scheibchen sehr genau bestimmen [67]. Die einfachste Möglichkeit besteht darin, eine zwei-dimensionale Gaussfunktion

$$f(x, y) = z_0 + Ae^{\left(\frac{x-x_0}{\sigma_x} + \frac{y-y_0}{\sigma_y}\right)} \quad (3.5)$$

an das gemessene Intensitätsprofil zu fitten. Sofern Polarisierungseffekte keine Rolle spielen, bestimmt das Zentrum der Gaussfunktion (x_0, y_0) den Ort der Punktlichtquelle [68]. Die Genauigkeit der Lokalisation ist jedoch stark abhängig vom gemessenen Intensitätsprofil. Die Minimalanforderung an das Intensitätsprofil, die erfüllt sein muss, folgt aus dem Nyquist-Shannonsche-Abtasttheorem¹ [69, 70]. Dem Theorem folgend ist die Rekonstruktion eines Bildes aus den ortsdiskreten Signalen (Pixel) nur dann möglich, wenn die Intensität des ersten Beugungsscheibchens auf mindestens vier Pixel verteilt wird [71]. Die in dieser Arbeit verwendeten Fluoreszenzfarbstoffe hatten Emissionswellenlängen zwischen 509 nm und 705 nm. Die Numerische Apertur des Objektivs betrug 1.49. Damit folgt nach Gleichung 3.4 für den Durchmesser des Beugungsscheibchens $d \approx 400$ nm. Um das Nyquist-Shannonsche-Abtasttheorem zu erfüllen, muss die Vergrößerung so gewählt werden, dass die Pixelgröße höchstens 200 nm beträgt.

Neben der Größe der Pixel ist für die Genauigkeit der Lokalisation eines einzelnen Farbstoffes das Verhältnis zwischen Signal zu Rauschen

$$\frac{S}{N} = \frac{I_0 - I_B}{\sigma}, \quad (3.6)$$

wobei I_0 die Intensität des Objekts, I_B die Intensität des Hintergrunds und σ die Standardabweichung der Hintergrundintensität ist [66], entscheidend. Für $\frac{S}{N} \leq 4$ ist eine Lokalisierung mit einer Genauigkeit unterhalb der Pixelgröße nicht möglich [66]. In Anhang D wurden die Positionen einzelner Cy3 Farbstoffe mit einer Genauigkeit von bis zu ± 1.4 nm bestimmt.

¹Das Abtasttheorem besagt, dass ein kontinuierliches, bandbegrenzttes Signal mit einer Minimalfrequenz von 0 Hz und einer Maximalfrequenz f_{max} , mit einer Frequenz größer als $2f_{max}$ abgetastet werden muss, damit aus dem so erhaltenen zeitdiskreten Signal das Ursprungssignal ohne Informationsverlust exakt rekonstruiert und beliebig genau approximiert werden kann.

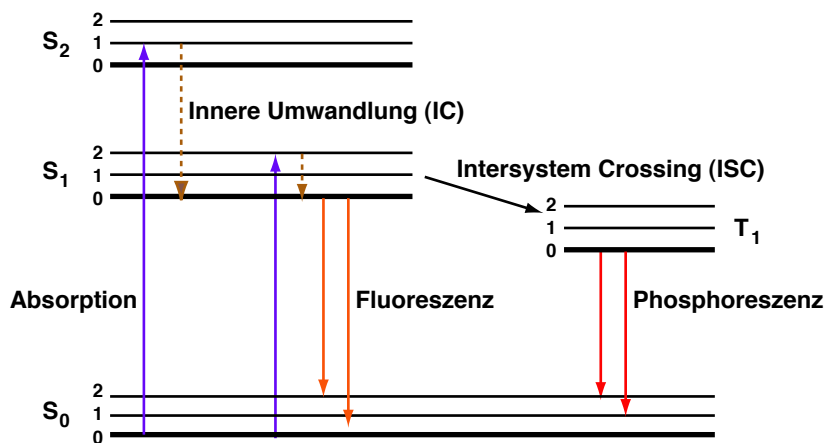


Abbildung 3.1: Jablonski Diagramm. S_0 , S_1 und S_2 bezeichnen die Singlet-Zustände des Grundzustandes und des 1. und 2. angeregten Zustandes. Für jedes elektronische Level existieren mehrere Schwingungszustände, die mit 0, 1 und 2 nummeriert sind. Die Übergänge zwischen den Zuständen sind durch vertikale Pfeile dargestellt. Durch Innere Umwandlung relaxiert das Elektron in den 0. Schwingungszustand des S_1 -Zustandes. Aus den S_1 -Zustand kann das angeregte Elektron durch Intersystem Crossing in den Triplet-Zustand T_1 gelangen.

3.2 Fluoreszenzspektroskopie

Lumineszenz - Fluoreszenz - Phosphoreszenz

Allgemein wird die Emission von Licht aus elektronisch angeregten Zuständen als Lumineszenz bezeichnet. Formal wird die Lumineszenz, abhängig von der Art des angeregten Zustandes, in zwei Klassen eingeteilt [72]:

- **Fluoreszenz:** Ist der angeregte Zustand ein Singlet-Zustand, d.h. das Elektron im angeregten Zustand und das zweite Elektron im Grundzustand haben einen unterschiedlichen Spin, spricht man von Fluoreszenz. In diesem Fall ist ein Übergang vom angeregten Zustand in den Grundzustand erlaubt, wobei die Emissionsraten typischerweise 10^8 s^{-1} und damit die Fluoreszenzlebensdauern 10 ns betragen.
- **Phosphoreszenz:** Ist der angeregte Zustand ein Triplet-Zustand, d.h. das Elektron im angeregten Zustand hat den gleichen Spin wie das Elektron im Grundzustand, spricht man von Phosphoreszenz. Ein Übergang in den Grundzustand ist verboten und die Emissionsraten liegen typischerweise im Bereich von $10^3 - 10^0 \text{ s}^{-1}$. In Lösung bei Raumtemperatur tritt Phosphoreszenz gewöhnlich nicht auf, da dort viele Deaktivierungsprozesse mit der Emission konkurrieren.

Die Prozesse, die zwischen Absorption und Emission von Licht auftreten, werden üblicherweise in Form von Jablonski-Diagrammen dargestellt (siehe Abbildung 3.1). Die Singlet-

Zustände sind mit S_0 , S_1 und S_2 bezeichnet. T_1 ist ein Triplet-Zustand. Für jedes elektronische Niveau existieren mehrere Schwingungszustände, die mit 0, 1 und 2 nummeriert sind. Bei Raumtemperatur reicht die thermische Energie nicht aus, um angeregte Schwingungszustände zu besetzen. Aus diesem Grund erfolgt die Absorption eines Photons aus den S_0 -Zustand und endet in einem der Schwingungszustände eines angeregten Zustandes. Durch innere Umwandlung relaxiert das Elektron in den 0. Schwingungszustand des S_1 -Zustandes. Dieser Prozess wird als „Innere Umwandlung“ bezeichnet und erfolgt üblicherweise in weniger als 10^{-12} s. Da die Fluoreszenzlebensdauer typischerweise 10^{-8} s beträgt, erfolgt die Fluoreszenz üblicherweise aus den 0. Schwingungszustand des S_1 -Zustandes. Aus den S_1 -Zustand kann das angeregte Elektron durch Intersystem Crossing in den Triplet-Zustand T_1 gelangen und durch Phosphoreszenz in den S_0 -Zustand gelangen.

Aus den Jablonski-Diagrammen erkennt man, dass die Energie der Emission üblicherweise niedriger als die Energie der Absorption ist, d.h. die Frequenz des emittierten Lichts ist rotverschoben. Diese Verschiebung wird als Stokes-Shift bezeichnet und erlaubt es, das Anregungslicht durch geeignete Filter vom Emissionslicht zu trennen. Durch Verwendung „schmaler“ Filter kann auf diese Weise das Verhältnis zwischen Signal zu Rauschen stark erhöht werden.

Einzelmolekülfluoreszenzspektroskopie

Der erste erfolgreiche Fluoreszenznachweis eines einzelnen Moleküls in Lösung wurde von Hirschfeld 1976 durchgeführt [73, 74]. Grundvoraussetzung für die Detektion des Fluoreszenzsignals einzelner Farbstoffe ist neben einer starken Verdünnung der Farbstoffe ein möglichst kleines Anregungsvolumen. Bei der Fluoreszenz-Korrelations-Spektroskopie (FCS) wird das beispielsweise durch Verwendung eines konfokalen Mikroskops erreicht [75]. In dieser Arbeit erfolgte die Fluoreszenzanregung durch ein Total-Internes-Reflexions (TIR) Mikroskops. Da die Eindringtiefe des evaneszenten Feldes lediglich ca. 100 nm betrug, konnte auf diese Weise das Anregungsvolumen ebenfalls stark verringert werden.

Da die Intensität eines einzelnen Farbstoffes sehr gering ist, müssen effektive Detektoren verwendet werden, um die schwachen Signale detektieren zu können. Meist werden dazu Photomultiplier (*Photomultiplier Tubes*, PMT), Lawinen-Photodioden (*Avalanche Photo Diodes*, APD) oder CCD-Kameras (*Charge Coupled Device*) verwendet.

3.3 Hochauflösende Mikroskopiemethoden

Wie in Kapitel 3.1 gezeigt wurde, ist aufgrund der Welleneigenschaft des Lichts, das Auflösungsvermögen eines optischen System nach Gleichung 3.4 beugungsbeschränkt. Punktlichtquellen mit einem Abstand kleiner als den durch Gleichung 3.4 gegebenen Radius lassen sich nicht als räumlich getrennte Objekte wahrnehmen. Die Positionen einzelner Farbstoffe können jedoch unter gewissen Voraussetzungen mit Nanometerpräzision bestimmt werden [67, 22]. Lassen sich die Intensitätsbeiträge mehrerer Punktlichtquellen, die einen Abstand unterhalb der Auflösungsgrenze haben, trennen, ist es deshalb möglich, die Posi-

tionen der einzelnen Emitter zu bestimmen. In den letzten Jahren wurden einige Verfahren zur Trennung der Intensitätsbeiträge entwickelt [54, 76, 77, 78, 79, 80, 81]. Eine einfache Methode die Beiträge zu trennen besteht darin, die Intensitätsverteilung zeitlich aufgelöst aufzunehmen. Abbildung 3.2(A) zeigt beispielsweise das Intensitätsprofil eines einzelnen Cy3 Farbstoffmoleküls. Die Größe der Pixel beträgt 125 nm. Die Integrationszeit betrug 100 ms, d.h. es wurden pro Sekunde 10 Bilder aufgenommen. Abbildung 3.2(B) zeigt die zeitliche Entwicklung der mittleren Intensität des 3x3-Pixel großen Beugungsscheibchen. Wie für einzelne Farbstoffmoleküle üblich, bleicht das Molekül in einem einzelnen Schritt. Während der Lebenszeit des Farbstoffes kann seine Position, wie in Abschnitt 3.1 beschrieben, durch Anfitzen von 2D-Gausfunktionen bestimmt werden. In Anhang D wurde auf diese Weise die Position eines einzelnen Cy3 Moleküls, das mittels SMCS platziert wurde, bestimmt.

Das Photobleichen eines Farbstoffes ist ein stochastischer Prozess, d.h. für eine bestimmte Sorte von Farbstoffmolekülen, die eine mittlere Lebensdauer T besitzen, sind die Lebensdauern für die einzelnen Farbstoffe unterschiedlich. Sind in einem beugungsbegrenzten Bereich nur wenige Farbstoffe vorhanden, die zu unterschiedlichen Zeiten bleichen, kann man die Beiträge der einzelnen Farbstoffe trennen [79, 78]. Abbildung 3.2(C) zeigt beispielsweise die zeitliche Entwicklung der mittleren Intensität eines 3x3-Pixel großen Beugungsscheibchens. In dem Bereich wurden mittels SMCP mehrere Moleküle platziert. Die Anzahl der diskreten Bleichschritte erlaubt es, die Anzahl der transportierten Moleküle zu bestimmen. Falls die Bleichstufen der einzelnen Farbstoffe zeitlich auflösbar sind, kann man die Positionen bestimmen². Im Anhang D wird diese Methode im Detail erklärt und verwendet, um ein mittels SMCP geschriebenes Muster hochaufgelöst zu detektieren.

²Die Anzahl an Farbstoffen innerhalb eines beugungslimitierten Bereichs, die sich auf diese Weise lokalisieren lassen, ist allerdings begrenzt. Zum einen steigt mit zunehmender Anzahl an Molekülen N die Wahrscheinlichkeit, dass die Bleichstufen zeitlich überlappen. Man könnte zwar die Samplingrate erhöhen, dadurch verschlechtert sich allerdings das $\frac{S}{N}$ und damit die Genauigkeit der Lokalisierung. Zum anderen nimmt mit zunehmender Anzahl an detektierten Photonen N_P das absolute Rauschen mit $\sqrt{N_P}$ zu. Bezeichnet N die Anzahl an Farbstoffen und n_P die Anzahl Photonen, die ein einzelner Farbstoff pro Zeitintervall emittiert, ist für $4\sqrt{N_P} = 4\sqrt{N n_P} \stackrel{!}{=} n_P$, also für $N = \frac{n_P}{16}$ an Molekülen das $\frac{S}{N} = 4$. Erhöht man die Anzahl an Farbstoffen weiter, ist das $\frac{S}{N} \leq 4$ und eine Positionsbestimmung mit Subpixelauflösung nicht mehr möglich. Typische Zählraten für einen einzelnen Fluorophor liegen bei 100 Photonen pro 100 ms, d.h. mehr als $\frac{100}{16} \approx 6$ Moleküle lassen sich auf diese Weise bei einer Samplingrate von 10 Hz nicht lokalisieren.

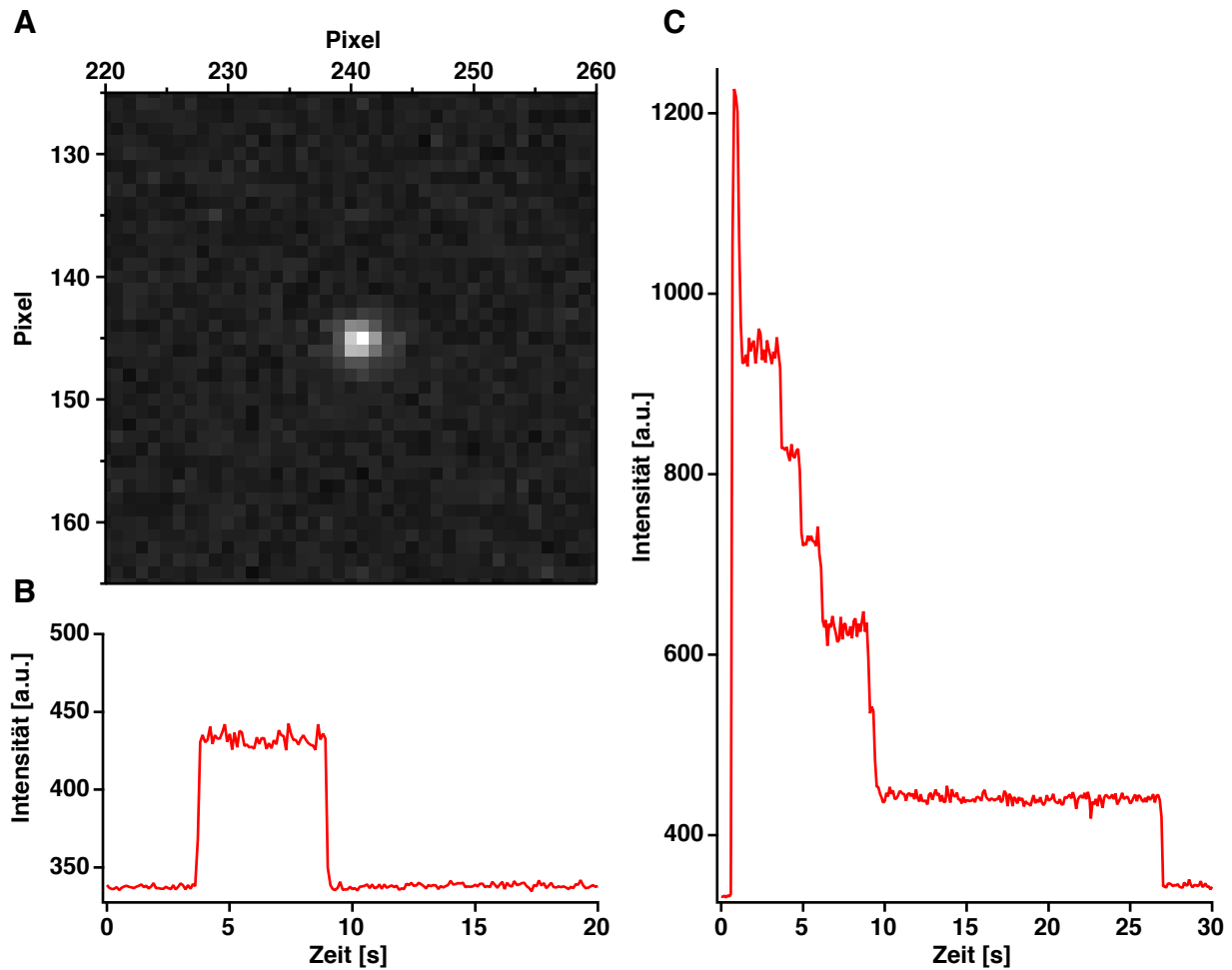


Abbildung 3.2: (A) Intensitätsprofil eines einzelnen Farbstoffes. Die Integrationszeit betrug 100 ms. Die Pixelgröße entspricht 125 nm. (B) Der Fluorophor in (A) hatte eine Lebenszeit von 5,1 s, d.h. es konnten 51 Intensitätsbilder aufgezeichnet werden. (C) Zeitliche Entwicklung der Intensität eines Beugungsscheibchens, in dem mehrere Fluorophore mittels SMCP platziert wurden. Die Höhe einer Bleichstufe beträgt ca. 100 [a.u.]. Zur Zeit $t = 0$ beträgt die Intensität aller Farbstoffe 880 [a.u.], d.h. es sind 8-9 Fluorophore vorhanden. Die ersten 2-3 Bleichstufen lassen sich zeitlich nicht trennen.

Kapitel 4

Ausblick

Durch die Entwicklung der SMCP-Oberflächenassemblierung ist eine neue Basistechnologie für die Nanotechnologie entstanden. Die Methode ermöglicht erstmals die Durchführung einer Reihe neuartiger Experimente, von denen einige im Folgenden kurz skizziert werden.

Kombination von SMCP mit DNA-Origami - Superresolution Cut-and-Paste

Die Ortsunsicherheit der Assemblierung beim SMCP wurde im Anhang D theoretisch und experimentell betrachtet. Dabei stellte man fest, dass die Genauigkeit abhängig

- von der Anzahl von DNA-Molekülen an der Spitze ist. Im Idealfall ist der unterste Bereich der Spitze mit genau einem DNA-Molekül, welches dann als mechanischer „Manipulatorarm“ dient, kovalent aktiviert. Die Anzahl der DNA-Moleküle kann durch Ausdünnen der zur kovalenten Modifikation verwendeten Maleimid-Gruppen oder durch Verringerung der DNA-Konzentration bei der kovalenten Anbindung eingestellt werden. Eine einfache Möglichkeit, die Anzahl von DNA-Molekülen zu verringern, besteht in der Verwendung von geschärften Spitzen mit nur wenigen Nanometer großen Krümmungsradien.
- von der xy-Wiederholgenauigkeit des verwendeten Piezosystems ist. Abhängig vom verwendeten Feedback-System ist diese im Subnanometerbereich und stellt keine Limitierung dar.
- vom End-zu-End-Abstand des PEG-DNA-DNA Komplexes an der Spitze ist. Dieser Abstand kann durch die Verwendung kürzerer PEG-Spacer und durch ein optimiertes Kraftsystem verkürzt werden.
- von der Dichte der Ankerpunkte im Zielbereich ist. Wird die Spitze in Kontakt mit der Zielfläche gebracht, „sucht“ die Ankersequenz der Transfer-DNA die Oberfläche solange ab, bis ein Bindungspartner gefunden ist. Im Grenzfall eines Kontinuums an Bindungsstellen ist die Ortsunsicherheit durch den mittleren End-zu-End-Abstand des PEG-DNA-DNA Komplexes gegeben.

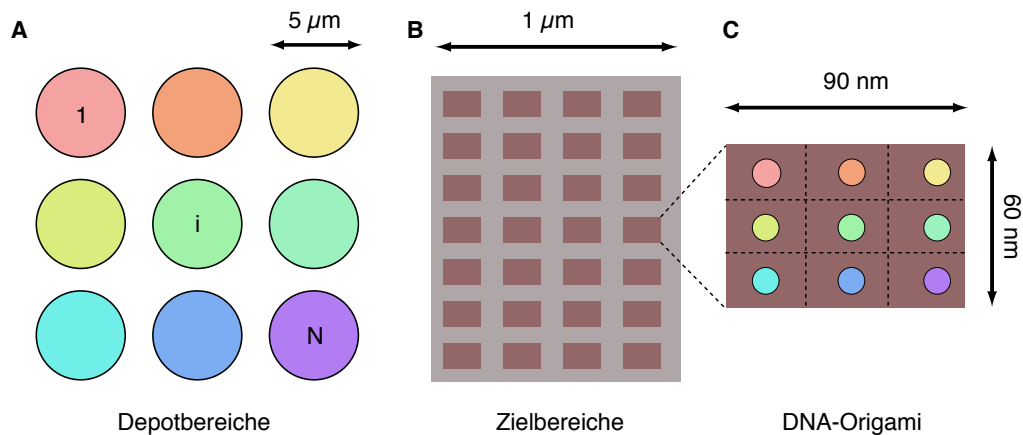


Abbildung 4.1: (A) Molekulare Bausteine werden auf räumlich getrennten Depotbereichen über verschiedene Ankersequenzen angebonden. (B) Im Zielbereich sind die zunächst identischen DNA-Origami gebunden. (C) Jedes Origami trägt an wohldefinierten Stellen verschiedene Ankersequenzen, wobei jede Sequenz nur einmal pro Origami vorkommt. Mittels SMCP kann ein molekularer Baustein mit seiner jeweiligen Ankersequenz aus dem Depot geholt und auf dem Ziel-Origami mit Subnanometerpräzision assembliert werden. Es ist dadurch möglich, jedes Origami individuell zu kodieren.

Eine Kombination von SMCP mit der Methode des DNA-Origami [41, 82] würde eine entscheidende Erweiterung des SMCP darstellen, da die oben aufgelisteten Limitierungen hierbei keine Rolle mehr spielen. In [82] wurde gezeigt, dass ein DNA-Origami mit verschiedenen Bindungsstellen bestückt und für Hybridisierungs-Assays benützt werden kann. Da die Hybridisierung als *Self-assembly*-Prozess abläuft, ist eine individuelle Bestückung der Origami jedoch nicht möglich. SMCP würde dies erlauben. In Abbildung 4.1 ist das Prinzip des SMCP-DNA-Origami schematisch dargestellt. Die Ankerpunkte im Zielbereich sind durch feste Positionen in einem DNA-Origami mit Subnanometergenauigkeit vorgegeben. Da die Ankerpunkte auf den Origami mit verschiedenen Ankersequenzen bestückt werden können, besteht die Möglichkeit, jede der verschiedenen Ankersequenzen nur einmal pro Origami vorkommen zu lassen. Wird eine Transfer-DNA mit einer bestimmten Ankersequenz dem Origami angeboten, kann diese nur an der durch das Origami vorgegebenen Stelle binden. Da das „Beschreiben“ des Origami mechanisch kontrolliert über SMCP erfolgt, ist jedes Origami individuell kodierbar.

Erzeugung kovalenter Oberflächenstrukturierungen mit SMCP

Die Assemblierung von molekularen Bausteinen im Zielbereich erfolgt über die Hybridisierung der 32 Basenpaar langen Ankersequenz. Die Schmelztemperatur dieser Sequenz in $1\times\text{SSC}$ beträgt 65°C . Für Anwendungen, bei denen beispielsweise der Puffer nach dem SMCP-Prozess gegen einen denaturierenden Puffer ausgetauscht werden muss, ist es dennoch zwingend nötig, eine kovalente Anbindung zu erreichen. Strategien dazu wären:

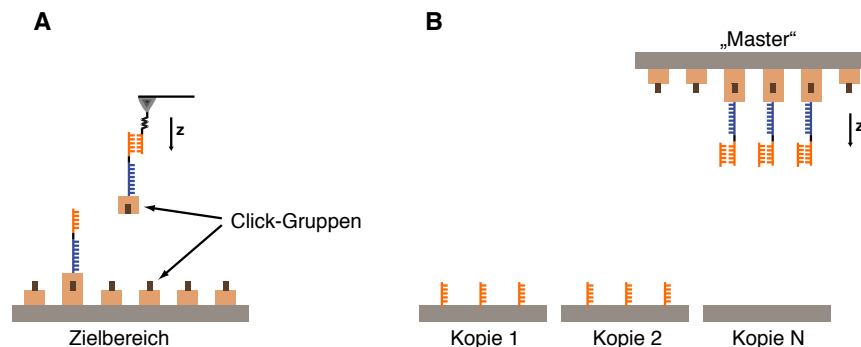


Abbildung 4.2: (A) Die Transfer-DNA ist mit einer Click-Gruppe modifiziert und wird mittels SMCP aus den Depotbereichen in den Zielbereich transportiert. Der Zielbereich ist mit dem passenden Click-Partner aktiviert. Beim Absetzen der Transfer-DNA binden die beiden Click-Gruppen kovalent aneinander und die Transfer-DNA wird irreversibel angebonden. (B) Eine auf diese Weise strukturierte Zielfläche kann als „Master“ verwendet werden. Dazu werden vor jedem Kopierschritt komplementäre DNA-Oligomere an den Master hybridisiert und anschließend auf eine Oberfläche gestempelt.

- Click-Chemie: Das Konzept der Click-Chemie wurde 2001 von K. Barry Sharpless [83] eingeführt. Man versteht darunter exotherme Reaktionen, die unter milden Bedingungen in Wasser ablaufen und molekulare Bausteine kovalent miteinander verbinden. Ein typisches Beispiel für eine Click-Reaktion ist die Alkin-Azid (3+2)-Cycloaddition unter Bildung von 1,2,3-Triazolen. Azide und Alkine sind unter physiologischen Bedingungen inert und lassen sich leicht an Biomoleküle wie DNA oder Polypeptide binden. In [84] wurde gezeigt, dass man Alkin-modifizierte DNA irreversibel mittels Mikrokontakt-Stempeln an Azid-aktivierte Oberflächen koppeln kann. Diese Methode kann mit der SMCP-Oberflächenassemblierung verknüpft werden. Dazu werden die Transfer-DNA-Oligomere mit Alkin-Gruppen modifiziert und mittels der Ankersequenz in das Depot gebunden. Die Zielfläche wird mit Azid-Gruppen aktiviert. Mit dem Cantilever werden die DNA-Moleküle vom Depot aufgenommen und an die Zielstelle transportiert, wo die beiden Click-Gruppen eine kovalente Verbindung eingehen (Abbildung 4.2(A)). Eine auf diese Weise kovalent strukturierte Zielfläche kann als „Master“ verwendet und beliebig oft kopiert werden (Abbildung 4.2(B)).
- Suicide-Koppler: Im Anhang B wird die Methode der enzymatischen Kopplung des menschlichen DNA-Reparaturenzyms hAGT an ein sogenanntes „*Suicide-Substrat*“ (Benzylguanin BG) benützt, rekombinate Proteine gerichtet, selektiv und kovalent an Festkörperoberflächen zu binden. Ferner wird im Anhang G auf die Möglichkeit hingewiesen, BG modifizierte DNA zu benützen, kovalent hAGT-Fusionsproteine an Transfer-DNA Moleküle zu koppeln. Eine Kombination dieser beiden Techniken kann zur Erzeugung kovalenter Oberflächenstrukturen eingesetzt werden. Beispielsweise

können BG-aktivierte Zielbereiche benützt werden, hAGT-Fusionsproteine, die mit SMCP in den Zielbereich transportiert werden, kovalent an die Oberfläche zu binden, bzw. können mit hAGT aktivierte Zielbereiche zur kovalenten Anbindung von BG-modifizierter Transfer-DNA dienen.

Funktionale Nanoassemblierung

In bisherigen SMCP-Experimenten wurden mit verschiedenen funktionalen Einheiten modifizierte Transfer-DNA-Moleküle aus gut sortierten Depotbereichen einzeln in den Zielbereich transportiert und dort kontrolliert assembliert. Die Funktion der jeweiligen molekularen Einheit wurde dabei nicht abgeändert. In zukünftigen Arbeiten wird diese kontrollierte Modifikation der Funktion jedoch eine zentrale Rolle spielen. Beispiele hierfür wären:

- Lokale Feldverstärkung - Hot Spots: Im Anhang E wurden mittels SMCP Strukturen aus Halbleiternanokristallen in beliebigen Mustern und Größen erzeugt. In [85] wurde gezeigt, dass Goldnanopartikel zur lokalen Feldverstärkung eingesetzt werden können. Dieser Strategie folgend können mit SMCP ebenfalls solche *Hot Spots* erzeugt werden. In einem zweiten Schritt können verschiedene molekulare Bausteine relativ zu den *Hot Spots* positioniert und durch die starke lokale Feldverstärkung untersucht werden.
Halbleiternanokristalle lassen sich über einen weiten Wellenlängenbereich anregen, emittieren jedoch abhängig von ihrer Größe in einem schmalen Wellenlängenbereich. Durch die Assemblierung verschiedenfarbiger Halbleiternanokristalle können lokal Anregungsfelder erzeugt werden und zur spektroskopischen Untersuchung von Molekülen eingesetzt werden [86].
- Enzymkaskaden: Wie in Anhang G gezeigt, ermöglicht die SMCP-Oberflächenassemblierung auch den Transport von Polypeptiden. Dadurch können im Zielbereich Enzymkaskaden aufgebaut und ihr enzymatischer Reaktionsweg auf Einzelmolekülbasis studiert werden.
- Split-Enzym: Eine weitere interessante Anwendung besteht in dem kontrollierten Zusammenbau von einzelnen, enzymatisch aktiven Polypeptiden. Wie in [87] gezeigt wurde, können solche Komplementierungsreaktionen in vitro durchgeführt werden.

Anhang A

Modular multichannel surface plasmon spectrometer

Gregor Neuert, Stefan K. Kufer, Martin Benoit and Hermann E. Gaub

Review of Scientific Instruments 76, 054303, 22 April 2005

In dieser Veröffentlichung wird ein modular aufgebautes Mehrkanal-Oberflächenplasmonenresonanz-Spektrometer (SPR) beschrieben. Die Basis dieses Gerätes bilden kommerziell erhältliche SPR-Sensoren. Aufgrund der Modularität ist dieses Spektrometer kostengünstig, einfach zu bedienen und kann schnell an wechselnde experimentelle Bedingungen angepasst werden. Durch eine effektive thermische Kopplung der individuellen SPR-Sensoren wird eine hohe Temperaturstabilität erreicht. Die Leistungsfähigkeit des Gerätes wurde mit mehreren Standardtechniken getestet. Die Anbindungskinetik einer Cystein-Monolage, sowie die Wechselwirkung von Biotin mit Streptavidin wurde untersucht.

Im weiteren Verlauf der Doktorarbeit wurde dieses SPR-Spektrometer dazu verwendet, um verschiedene Oberflächenpassivierungen zu testen bzw. zu optimieren. In der im Anhang B angeführten Veröffentlichung wurde das SPR-Spektrometer benützt, um die selektive Bindung von hAGT-Fusionsproteinen an BG-aktivierte Oberflächen zu zeigen.

Modular multichannel surface plasmon spectrometer

G. Neuert,^{a)} S. Kufer, M. Benoit, and H. E. Gaub
*Lehrstuhl für Angewandte Physik & Center for Nanoscience, Ludwig-Maximilians Universität,
Amalienstrasse 54, 80799 München, Germany*

(Received 3 December 2004; accepted 6 March 2005; published online 22 April 2005)

We have developed a modular multichannel surface plasmon resonance (SPR) spectrometer on the basis of a commercially available hybrid sensor chip. Due to its modularity this inexpensive and easy to use setup can readily be adapted to different experimental environments. High temperature stability is achieved through efficient thermal coupling of individual SPR units. With standard systems the performance of the multichannel instrument was evaluated. The absorption kinetics of a cysteamine monolayer, as well as the concentration dependence of the specific receptor-ligand interaction between biotin and streptavidin was measured. © 2005 American Institute of Physics. [DOI: 10.1063/1.1899503]

I. INTRODUCTION

Receptor ligand interactions are the hallmark of life. Surface plasmon resonance (SPR) spectroscopy was established in recent years as a standard method for the quantification of such interactions. This optical technique uses an evanescent wave to measure changes in the refractive index at a metal—typically gold—surface. One of the binding partners is immobilized at this metal surface. Binding of the other partner results in an increase of the surface concentration, and as a consequence, in a change of the refractive index. Such measurements are performed in real time and the amount of bound ligand as well as association and dissociation rates are determined.¹

Several commercial instruments are available,² which may be operated with little training on day to day basis with acceptable throughput.³ However, these instruments can hardly be modified to suite the needs in a combined experimental setup, e.g., in combination with an atomic force microscope (AFM) or a second optical device accessing the same metal surface. The SPREETA-sensor from Texas Instruments (Dallas, Texas) is a fully integrated one-chip surface plasmon device.⁴ As such it is easy to modify and may therefore be used for a wide range of application.⁵ Furthermore it is inexpensive compared to the established standard systems.

Here we describe the design of a multichannel SPR spectrometer based on such sensor chips. This spectrometer is modular and the entire half space above the gold surface is available for additional experiments. The performance of our instrument is demonstrated with binding assays of different standard systems.

II. DESCRIPTION OF THE EXPERIMENT

A. SPR-sensor chip

The basis of this SPR system is the SPREETA-Sensor from Texas Instruments^{4,5} (Fig. 1). This sensor consists of a

light-emitting diode (LED) whose light is reflected from the gold film onto a linear camera. The camera signal is digitized with 12-bit resolution by a digital signal processor (DSP) (Normadics, Stillwater, Oklahoma) and transferred via a serial interface to a personal computer. The initiation and data collection is controlled with EVM software (Normadics, Stillwater, Oklahoma).

The sensor is initially covered by a gold layer, which was removed by dipping the sensor into solution out of 3/4 hydrochloric acid and 1/4 nitric acid. Afterwards, it was rinsed extensively with double deionized water (ddH₂O). The sensor was now cast with an epoxy resin (Robnor Resins, UK) into an aluminium block. Multiples of these units are combined to form a multichannel block. For multichannel operation each chip was operated by its own DSP controller, and analyzed in multiple windows of EVM software.

B. Gold-coated cover slips and surface functionalization

In order to allow for the sensor to be reused also with different surfaces, the initial single-use gold surface of the sensor was removed. Instead gold-coated glass cover slips were optically coupled with index matching oil to the surface of the sensor. These gold-coated cover slips are prepared as follows: cover slips (Roth, Karlsruhe, Germany) were cleaned once in 2% Helmanex-solution (Helma, Germany) for 15 min. and then two times for 15 min. in ddH₂O. All steps were performed in an ultrasonic bath. Afterward, the cleaned cover slips were dried in an oven at 75 °C overnight. The clean and dry glass cover slips were covered with 10 Å chrome/nickel (80% Cr / 20% Ni, GoodFellow, GB) as adhesive layer and 500 Å gold (99,99% pure, Leybold Optics, Germany) by thermal evaporation.

For surface functionalization the coated glass slips were transferred immediately after evaporation into a ddH₂O solution containing 20 mM cysteamine (2-aminoethanethiol, Sigma-Aldrich) stored overnight to allow a self-assembled monolayer (SAM) to form onto the gold surface.^{3,6-8} After 12 h of incubation (as can be seen later on in Fig. 2, already

^{a)}Electronic mail: gregor.neuert@physik.uni-muenchen.de

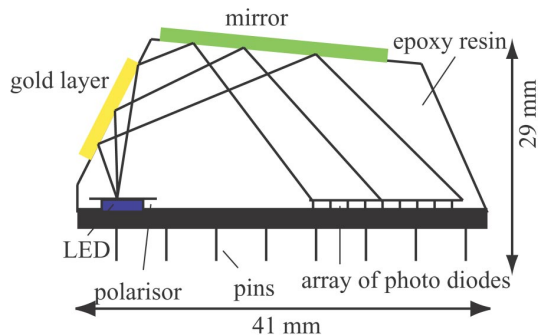


FIG. 1. (Color online) Schematics of the SPREETA sensor. A LED emits light at 840 nm, which passes a polarizer, illuminating the whole sensor surface. The reflected light is mirrored onto the array of photo diodes.

an incubation time of one hour would be sufficient), the SAM-coated cover slips were washed extensively with ddH₂O and placed into 1 M NaOH for 5 min to deprotonate the NH³⁺ groups of the SAM. Afterwards, the cover slips were washed with ddH₂O, dried in a stream of N₂ and processed immediately.

As a result of this procedure the gold-coated cover slips have a high density of NH₂ at the surface, which are used to couple carboxymethyl cellulose (CMC, Sigma).³ A CMC solution was prepared and added to the solid form of 1-ethyl-3-(3-dimethylaminopropyl) carbodiimide hydrochlorid (EDC, Sigma)/N-hydroxysuccinimid (NHS, Sigma) to reach a final concentration of 5% CMC with 50 mM EDC/NHS in 10 mM hepes. 200 μ l of this solution was pipette onto one cysteamine coated gold slide and covered by a second cysteamine coated gold slide in a sandwich like structure. Previous AFM studies had shown that a covalent attachment of the polymer to the gold surface is achieved this way.⁹ These slips were then stored in an incubation chamber with a ddH₂O atmosphere at room temperature for 2 h. After the CMC coupling, the cover slips were washed extensively with ddH₂O and stored in ddH₂O for later use. Before use, the functionalized slips were well dried in a N₂ stream.

C. Fluid cell

The flow chambers were made from poly (dimethylsiloxane) (PDMS, Sylgard 184, Dow Corning) a fluid silicon

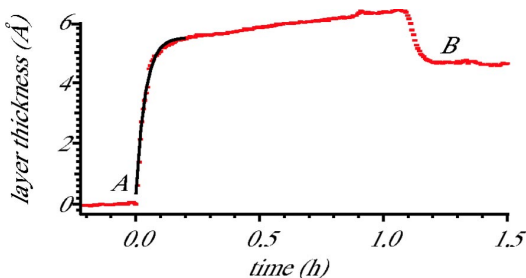


FIG. 2. (Color online) Binding kinetics of cysteamine layer on gold. (A) Start of the absorption. (B) Rinse with PBS. The thickness of $d=4.8$ Å is measured between points (A) and (B). The index of refraction of the cysteamine layer was assumed to be $n=1.525$. The black line is a guide for the eye.

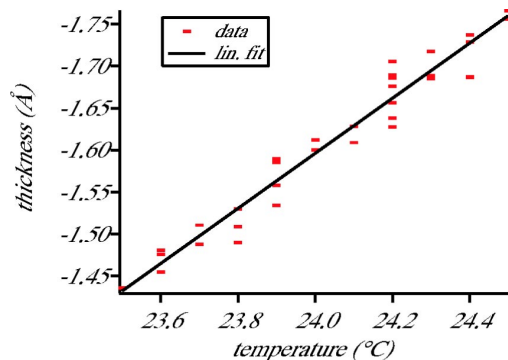


FIG. 3. (Color online) Linear drift of the surface plasmon plotted as thickness change ($n=1.5$ in water $n=1.33$) dependent on the temperature ($^{\circ}$ C) over a time period of 5.5 h. Linear least-squares line fit results in an average thickness error of 0.33 Å per $^{\circ}$ C. Red dots: measured data, black line: linear fit.

elastomer.⁵ After mixing the elastomer with a catalyst, the mixture was degassed and cast into a special form. The silicon tubes, which later on allow the fluid exchange of the sample are already inserted and polymerized into the elastomer. The polymer was cured for 24 h at 60 $^{\circ}$ C. The approximately 2 mm thick fluid chambers were finished by cutting a 10 mm \times 3 mm sample volume out of the PDMS. Before each measurement, the fluid chambers were cleaned with Helmanex, ddH₂O, ultra pure ethanol, and dried in a stream of N₂. The fluid chambers were then placed on top of the coated cover slip and sealed with a microscope slide. This assembly was fixed with a metal bar from the top.

To ensure a continuous flow of the buffer, the fluid cell was connected to a peristaltic pump. It is also possible to introduce sample liquid via a valve [Fig. 4(a)]. The flow was controlled down to values as low as 30 μ l/min. This allows measurements of sample volume as small as 100 μ l per channel in a stop flow manner. Before each measurement, the sensor was calibrated in air and buffer.

D. Cysteamine monolayer adsorption

The quantification of the online adsorption of cysteamine onto a freshly evaporated glass cover slip was the first proof of reliable operation of the instrument as shown in Fig. 2. The gold cover slip was prepared and placed into the instrument as described above. As a running buffer we used (PBS). After equilibration of the instrument, we switched to the sample liquid system that contained a 10 mM cysteamine solution dissolved in PBS and inject it into the fluid chamber. The thickness of the adsorbed layer in units of angstroms as a function of time in hours is plotted. The index of refraction n is set to $n=1.525$. The adsorption of the cysteamine starts at $t=0$ h (A) and rises rapidly, indicating the strong adsorption of the mercapto group to the gold surface. After 15 min. a plateau was reached which indicates a saturation of the gold surface with cysteamine. After one hour no significant increase of the signal was observed any longer, so that the adsorption of the cysteamine was stopped (B) by switching to the running buffer. The latter washed away unbound cysteamine, which resulted in a baseline shift of 4.8 Å,

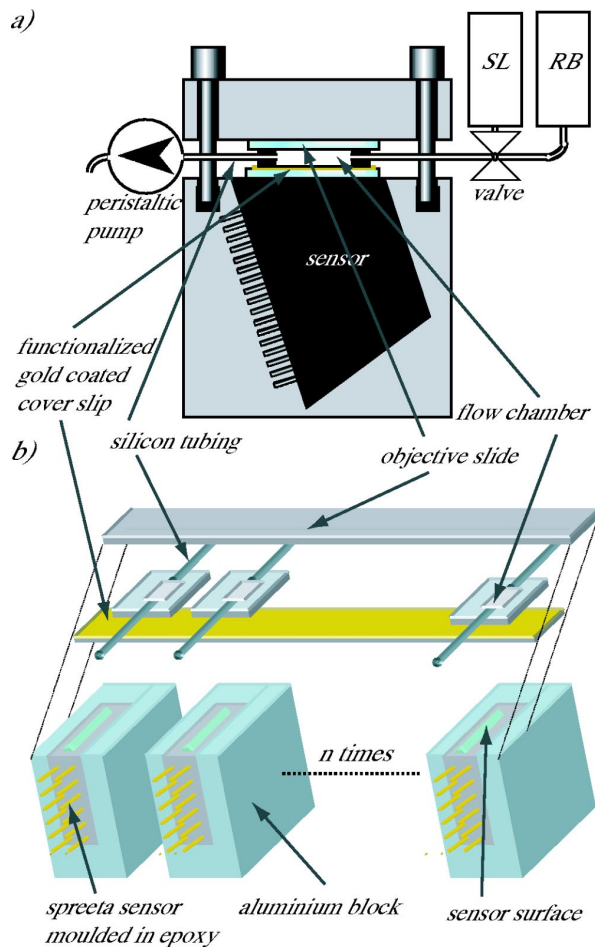


FIG. 4. (Color online) (a) Compiled setup contains the molded sensor with functionalized gold coated glass cover slip and fluid cell. The fluid cell is connected via a valve to the sample liquid (SL) or the running buffer (RB). To ensure a continuous flow of the buffer, the fluid cell was connected to a peristaltic pump. (b) The factory-made gold surface of the SPREETA sensors was removed with nitro hydrochloric acid. The bare sensor was molded with epoxy resin into an aluminium block. A cover slip, which was evaporated with 15 \AA CrNi and 500 \AA gold was optically coupled with index matching oil to the glass surface of the sensor. A flow chamber, made of PDMS, was placed onto the active sensing region of the sensor and sealed with a microscope slide.

which corresponds to a dense monolayer of cysteamine. This is in very good agreement with the theoretical value of 4.83 \AA .

E. Temperature dependence of the sensor signal

Surface plasmons are very sensitive to temperature. Therefore we measured the temperature dependence of the plasmon resonance after encapsulation into the aluminium block (Fig. 3). The experiment was performed in ddH_2O . Plotted is the resonance angle in values of the thickness of a hypothetical film with a refractive index of $n=1.5$ in water ($n=1.33$) as a function of the temperature. This measurement was taken over 5.5 h and shows a linear thickness drift of $0.33 \text{ \AA per } ^\circ\text{C}$.

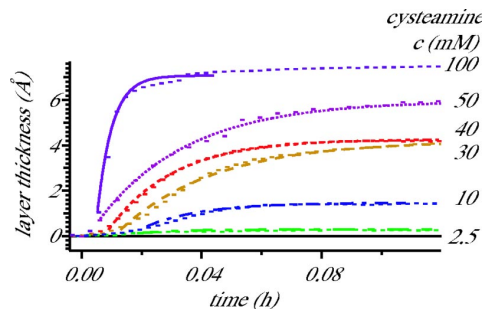


FIG. 5. (Color online) Simultaneous multichannel SPR measurements of the absorption of cysteamine onto the gold surface. Concentrations in PBS ranged between 100 and 2.5 mM. Thickness was measured based on an refractive index of $n=1.5$. Solid lines are first order exponential fits of the measured data.

III. MULTICHANNEL OPERATION

Because of this pronounced dependence of the surface plasmon resonance on the temperature we coupled several sensor units together to form a solid block [Figs. 4(a) and 4(b)]. This solid block connects all sensors thermally, ensuring the same temperature for each sensor. Having the same temperature at all sensors, it is therefore possible to use one sensor as a reference for the others. The temperature dependence can later be subtracted from the other sensor signals.

Another benefit of arranging single sensor units in parallel is the possibility to build a modular multichannel SPR device [Fig. 4(b)]. In our experimental setup it is possible to cover six SPR sensors at the same time with one gold slide. To demonstrate the ability of multichannel operation, we measured the absorption kinetic for cysteamine in a concentrations range between 2.5 and 100 mM.

In Fig. 5 the layer thickness is plotted as a function of absorption time in hours for six different channels in parallel. The cysteamine was solved and diluted in PBS. After the instrument was thermally equilibrated, we injected several solutions of cysteamine at different concentrations (2.5, 10, 30, 40, 50, and 100 mM) in the six flow channels. The measured concentration dependence in the absorption kinetic in the different channels is a convincing demonstration of the stable, reliable, and parallel operation of the instrument.

To explore the potential range of applications of this instrument in biophysical research we investigated the interaction of biotin with streptavidin as shown in Fig. 6. For this experiment we used a CMC surface as described before, which provides a carboxyl functionalized surface. All measurements in this experiment were performed in degassed 10 mM hepes buffer (Sigma) under a constant flow rate of $30 \mu\text{l/min}$. After equilibration of the experiment 10 mM biotin-hydrazid (Sigma-Aldrich) was mixed with an equal volume of 10 mM hepes with 100 mM EDC / NHS (channel 1,2). In channel 3 only biotinhydrazid without EDC/NHS was injected into the fluid system (A). The strong increase in signal is related to the large change of the refractive index related to EDC/NHS. By switching all three channels to hepes buffer after 32 min of incubation (B), we washed unbound biotin-hydrazid and EDC/NHS away. This resulted in a strong decrease of the signal until a new baseline was reached. We

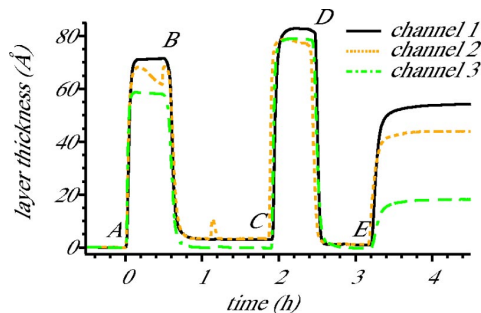


FIG. 6. (Color online) Competitive binding assay for streptavidin to biotinhydrazid. (A) Immobilization of biotinhydrazid with EDC/NHS (channel 1,2) and without EDC/NHS (channel 3); (B) rinse with 10 mM hepes; (C) deactivation of the remaining activated carboxyl groups with 1 M ethanolamine; (D) rinse with 10 mM hepes; (E) channel (1,3) streptavidin (0.1 mg/ml), channel 2: streptavidin 0.1 mg/ml preincubated with 1:25 biotinhydrazid.

then deactivated the surface by injecting a solution of 1 M ethanolamine (Sigma) (channel 1–3) (C) for 30 min. Since not all the EDC/NHS activated carboxyl groups have reacted with biotinhydrazid it is necessary to deactivate the remaining activated carboxyl groups with an excess of ethanolamine, so that no protein binds covalently to the surface, later on.

Afterward, we washed again with 10 mM hepes (D) until a stable baseline was reached. At point (E) we injected 0.1 mg/ml streptavidin in 10 mM hepes (channel 1,3). Preincubated streptavidin (0.1 mg/ml) with a 25-fold molar excess of biotinhydrazid was injected in channel 2 until saturation was reached. It can be clearly seen that the strongest interaction occurs between the biotin functionalized surface and streptavidin in channel 1. The coverage decreased for the preincubate streptavidin (channel 2). This was to be expected because the majority of the binding sites of streptavidin were blocked with free biotinhydrazid and binding of streptavidin to the surface is thus largely suppressed. For the surface that was not activated before (channel 3) the interaction of the streptavidin bound only non-specifically at much lower levels.

IV. DISCUSSION

Three major benefits helped this instrument to become a workhorse in our laboratory: multichannel operation, free access to the active gold surface with other techniques, and ease of operation. High end commercial instruments like the Biacore have a better thickness resolution but the accuracy of 1% of a protein monolayer, reached with our setup is more than sufficient for most applications. Also the option to design, test, and implement new surface functionalization protocols on the gold films with great ease and moderate costs has helped to standardize surface chemistry in our lab.

Having multiple channels running in parallel not only speeds up screening steps. Since all traces run on the same chip with the same history and chemistry, standard deviations between the traces came down drastically. Being able to design the fluid chamber, e.g., with an optical window to the upper side has allowed to combine SPR measurements with optical excitation and light induced chemistry. The integration of an AFM became possible and initiated a different set of experiments not reported here. The block design helped markedly to increase the temperature stability of the setup. An additional external thermostat, also controlling the sample fluids may help to improve this stability further if needed.

ACKNOWLEDGMENTS

The authors thank E. K. Sinner, Ch. Albrecht, K. Blank, T. Nickolaus, and E. Sackmann for helpful discussions. Financial support by the Deutsche Forschungs Gemeinschaft (SFB 486) is gratefully acknowledged.

- ¹W. Knoll, *Annu. Rev. Phys. Chem.* **49**, 569 (1998); E. K. Sinner *et al.*, *Anal. Biochem.* **333**, 216 (2004); E. L. Florin and H. E. G. Gaub, *Biophys. J.* **64**, 375 (1993).
- ²W. M. Mullett, E. P. C. Lai, and J. M. Yeung, *Methods* **22**, 77 (2000).
- ³B. Johnson, S. Löfås, and G. Lindquist, *Anal. Biochem.* **198**, 268 (1991).
- ⁴J. Meléndez *et al.*, *Sens. Actuators B* **35–36**, 212 (1996).
- ⁵A. R. Wheeler *et al.*, *Sens. Actuators B* **98**, 208 (2004).
- ⁶C. D. Bain *et al.*, *J. Am. Chem. Soc.* **111**, 321 (1989).
- ⁷S. Löfås *et al.*, *Sens. Actuators B* **5**, 79 (1991).
- ⁸G. Brink *et al.*, *Biochim. Biophys. Acta* **1196** (2), 227 (1994).
- ⁹M. Grandbois *et al.*, *Science* **283**, 1727 (1999).

Anhang B

Covalent immobilization of recombinant fusion proteins with hAGT for single molecule force spectroscopy

Stefan K. Kufer, Hendrik Dietz, Christian Albrecht, Kerstin Blank, Angelika Kardinal, Matthias Rief and Hermann E. Gaub

European Biophysics Journal, Vol 35, 72-78, 14. September 2005

In dieser Veröffentlichung wurde eine genetisch veränderte Variante des menschlichen DNA-Reparaturproteins *O*⁶-Alkylguanin-DNA-Alkyltransferase (hAGT) verwendet, um verschiedene rekombinante Proteine gerichtet, selektiv und kovalent an Festkörperoberflächen zu binden. Diese neuartige Konjugationsmethode beruht auf der irreversiblen und kovalenten Bindung der hAGT an Benzylguanin-Substrate. Die Konjugation wurde mit mehreren, zueinander komplementären Messverfahren (Oberflächenplasmonenresonanz-, Fluoreszenz- und AFM-basierter Kraftspektroskopie) nachgewiesen.

Die in dieser Veröffentlichung verwendete Methode der irreversiblen Anbindung von Proteinen an Festkörperoberflächen mittels hAGT, ist eine vielversprechende Strategie zur Erzeugung kovalenter SMCP-Muster.

Stefan K. Kufer · Hendrik Dietz · Christian Albrecht
Kerstin Blank · Angelika Kardinal
Matthias Rief · Hermann E. Gaub

Covalent immobilization of recombinant fusion proteins with hAGT for single molecule force spectroscopy

Received: 1 April 2005 / Revised: 5 July 2005 / Accepted: 18 July 2005
© EBSA 2005

Abstract A genetically modified form of the human DNA repair protein O⁶-alkylguanine-DNA-alkyltransferase (hAGT) was used to immobilize different recombinant hAGT fusion proteins covalently and selectively on gold and glass surfaces. Fusion proteins of hAGT with Glutathione S-Transferase and with tandem repeats of Titin Ig-domains, were produced and anchored via amino-polyethylene glycol benzylguanine. Anchoring was characterized and quantified with surface plasmon resonance, atomic force microscope and fluorescence measurements. Individual fusion proteins were unfolded by single molecule force spectroscopy corroborating the selectivity of the covalent attachment.

Keywords Molecular recognition · SPR · AFM · Suicide coupler · hAGT · SNAP-tag

Abbreviations hAGT: O⁶-alkylguanine-DNA-alkyltransferase · GST: Glutathione S-Transferase · PEG: Polyethylene glycol · BG: Benzylguanine · SPR: Surface plasmon resonance · AFM: Atomic force microscope · EDC: 1-ethyl-3-(3-diaminopropyl) carbodiimide hydrochloride · NHS: *N*-hydroxy succinimide · GST: Glutathione S-transferase · CMC: Carboxymethylcellulose

Introduction

Various areas of modern biotechnology are in great demand for strategies and protocols to attach recombinant proteins permanently, selectively and in a defined manner to solid surfaces. Especially in the field of single molecule biophysics the need for such techniques is emerging. For a broad range of conventional binding studies at surfaces, physisorption of, e.g. a capture antibody in an ELISA, is sufficient as long as the spontaneous off-rate is slower than the one of the target molecule, a covalent attachment is essential for the rapidly growing number of experiments, where forces are measured between molecules. In such experiments the weakest of the bonds in series ruptures first and it must not be the attachment. However, since the force required to rupture a bio-molecular complex is not directly correlated to the binding energy, physisorption, although thermally stable is in many cases insufficient. Various strategies for a covalent attachment have therefore been investigated and established, most of them based on covalently binding the protein of choice either via amines or the thiol group of a cysteine. Besides the limited lifetime due to hydrolysis, the low selectivity and the limited yield of these coupling reactions motivate the search for alternative strategies. Here, we investigated the possibility of using fusion proteins with a mutant of O⁶-alkylguanine-DNA-alkyltransferase (hAGT) also known as SNAP-tag in combination with its substrate polyethylene glycol (PEG)-benzylguanine (BG) as a promising strategy for the covalent and directed attachment of proteins for single molecule force spectroscopy.

The natural role of hAGT is the repair of alkylation damage of the DNA at the O⁶-position of guanine in a unique, stoichiometric reaction (Daniels and Tainer 2000). Since hAGT also accepts free O⁶-benzylguanine as a substrate it is possible to inactivate hAGT irreversibly with this small molecule (Pegg et al. 1993). Interestingly, oligonucleotides containing derivatives of O⁶-benzylguanine with substituted benzyl rings are also accepted as

S. K. Kufer · C. Albrecht · K. Blank · A. Kardinal
H. E. Gaub (✉)
Lehrstuhl für Angewandte Physik, Sektion Physik,
Ludwig-Maximilians-Universität München
and Center for NanoScience, Amalienstrasse 54,
80799 Munich, Germany
E-mail: Hermann.Gaub@physik.uni-muenchen.de
Fax: + 49-89-21802050

H. Dietz · M. Rief
Physik-Department E22, Technische Universität München,
James-Franck-Strasse, 85747 Garching, Germany

substrates of hAGT (Damoiseaux et al. 2001). As a consequence, various derivatives of BG were used to label hAGT fusion proteins with small molecules in vivo (Keppler et al. 2003). A BG-PEG-amino derivative, covalently attached to carboxy dextran gold surfaces (Biacore) via EDC/NHS chemistry, was used in a previous study to immobilize GST-hAGT fusion proteins on these BG activated slides (Kindermann et al. 2003).

Here we used the same BG-PEG-amino derivative as an anchor (Fig. 1) and verified the immobilization of Gluthathione S-Transferase (GST)-hAGT fusion proteins on gold surfaces. In the next step, Titin-GFP-hAGT fusion proteins (Fig. 2) were anchored on gold and glass surfaces and were investigated with surface plasmon resonance (SPR), fluorescence and single molecule measurements.

Materials and methods

If not stated otherwise, all chemicals used for the functionalization of surfaces were of analytical standard and

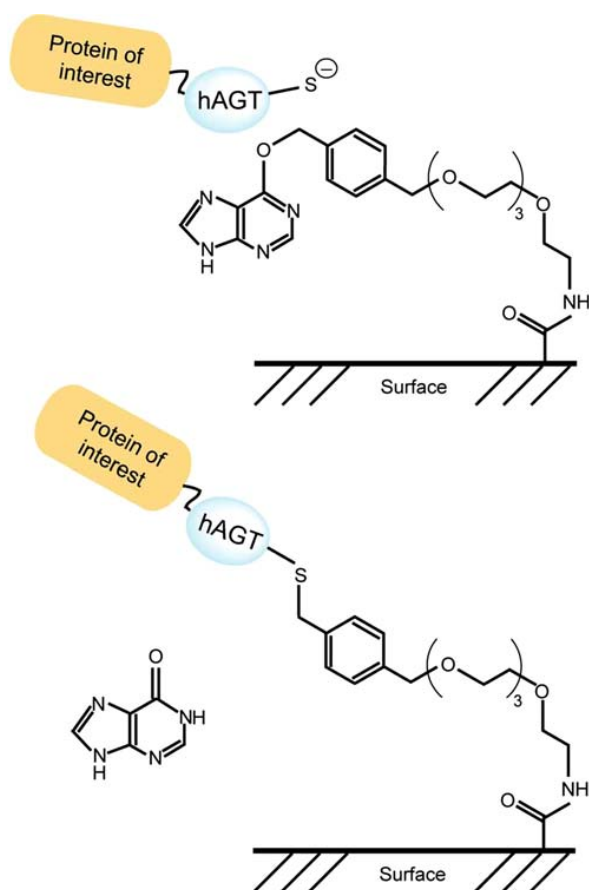


Fig. 1 Immobilization principle of hAGT fusion proteins. The BG-PEG-amino derivative is attached to carboxylized gold and glass surfaces via EDC/NHS chemistry. The hAGT protein accepts BG as a substrate and connects itself to the surface

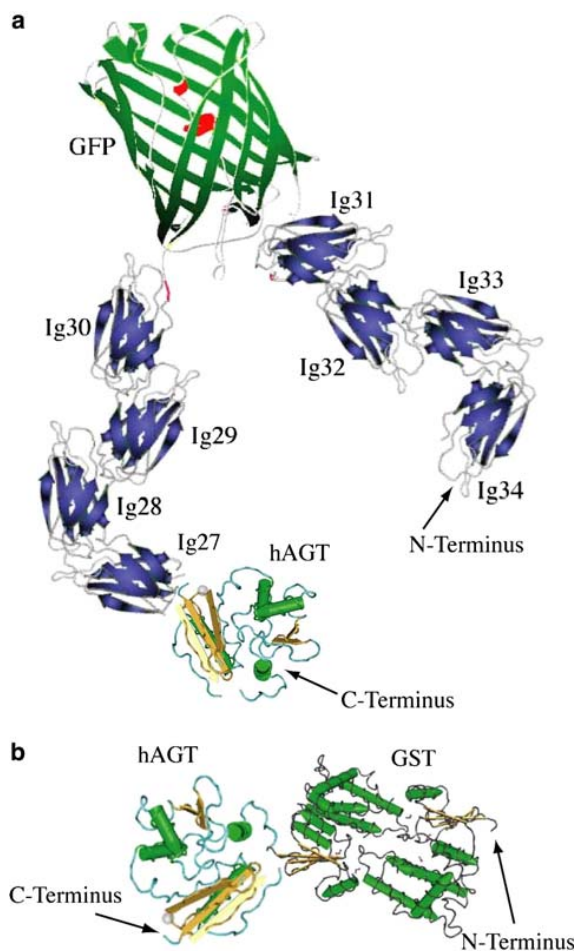


Fig. 2 O⁶-alkylguanine-DNA-alkyltransferase fusion proteins used for the immobilization experiments. **a** Titin-GFP-hAGT fusion protein. Molecular weight about 100 kDa. GFP serves as a fluorescence marker, the eight Ig-domains as molecular rulers for unfolding forces and segment lengths. **b** GST-hAGT fusion protein. Molecular weight about 45 kDa

purchased by Sigma (Taufkirchen, Germany). PBS (10 mM PBS, 150 mM NaCl, pH 7.4) and MES (10 mM MES, 150 mM NaCl, pH 6.3) were used as buffer solutions. For the hAGT fusion proteins, we used a genetically modified form of the wild type form of hAGT, that has a 20-fold increased activity against BG (Juillerat et al. 2003). In addition, the DNA binding site was mutated (Gendreizig et al. 2003) and cysteine 62 was exchanged to alanine (unpublished data). The DNA sequence of this hAGT mutant was C-terminally fused to the sequences of GST and Titin-GFP using standard molecular biology protocols. The recombinant proteins were expressed in *E. coli*. The GST-hAGT fusion protein was expressed following the protocol in Kindermann et al. (2003) and purified with a GST affinity column following the instructions of the affinity medium (Amersham Biosciences, Freiburg, Germany). Purified GST-hAGT fusion proteins were stored in PBS or MES

at 4°C. The Titin-GFP-hAGT fusion protein was expressed exactly as described for Titin-GFP fusion proteins (Dietz and Rief 2004b). The Titin-GFP-hAGT fusion proteins were immobilized without prior purification. Therefore BG functionalized slides were incubated directly with crude extracts of *E. coli* cells expressing this fusion protein.

Surface plasmon resonance measurements

To investigate the binding of hAGT fusion proteins on gold-slides, we used a homebuilt multi-channel SPR device that consists of several commercially available SPR-sensor chips (Neuert et al. 2004). Spreeta Evaluation Module software (version 5.21) was used to analyse the SPR curves. All SPR experiments were performed at constant room temperature with thoroughly degassed PBS or MES buffer solutions at a constant flow-rate of 0.03 ml/min.

Cover slides were evaporated at a pressure of $1-2 \times 10^{-6}$ mbar with 1 nm chrome/nickel (GoodFellow, GB) as adhesive layer and 50 nm high-purity gold (purity degree: 99.99%, Leybold Optics, Germany). Afterwards, the slides were incubated with cysteamine (20 mM) for 12 h to obtain a cysteamine monolayer. Carboxymethylcellulose (CMC) was bound to these amino groups using standard EDC protocols to obtain carboxylized gold surfaces. In addition to CMC surfaces, sulphur-PEG-COOH ($M=20$ kd) (Rapp Polymere GmbH, Tübingen, Germany) gold coated surfaces were prepared. For this purpose S-PEG-COOH molecules were solved in H₂O (3 mM). The COOH groups of that polymers were activated in solution with EDC (100 mM) and *N*-hydroxysuccinimide (NHS) (50 mM). Those activated polymers were incubated with BG (5 mM) for 12 h. All non-reacted COOH groups were quenched with ethanolamine (1 M) for 30 min. Gold coated cover slides were incubated with the BG activated PEG for 4 h. The control sample was treated identically except for the BG activation, which was omitted.

These gold slides were optically coupled to the SPR sensors using index matching oil (518 C, Zeiss, Germany).

Fluorescence binding measurements

To verify the specific anchoring of Titin-GFP-hAGT fusion proteins using the auto-fluorescence properties of GFP, Titin-GFP-hAGT proteins were immobilised on aldehyde-functionalised glass slides (Quantifoil Micro Tools GmbH, Germany). The aldehyde groups were oxidised with potassium permanganate to carboxyl groups. After that, spots of BG (3 mM) were attached to these groups using standard EDC/NHS protocols. All non-reacted NHS groups were blocked with 1 M ethanolamine. Following this, the Titin-GFP-hAGT fusion proteins were coupled to this surface by incubating the whole slide with the crude extract of hAGT-expressing *E. coli* cells. After an incubation time of 45 min all un-

bound proteins from the cell extract were removed by extensive washing with PBS.

A fluorescence-scanner (LS100, Tecan, Austria) was used to determine the amount of bound fusion proteins. GFP was excited with a 488 nm laser and the emitted light was filtered with a 500–570 nm band-pass filter. The spatial resolution was 20 μ m. Mean fluorescence as well as background intensity was determined by using NIH IMAGE software (National Institutes of Health, Bethesda).

Single molecule force spectroscopy

All single molecule force measurements were performed with a custom-built atomic force microscope (AFM) (Oesterhelt et al. 1999). Cantilevers were calibrated in solution using the equipartition theorem (Butt and Jaschke 1995; Florin et al. 1995). This method provides a resolution, in force, of roughly 10%. Two types of gold-coated cantilevers (Bio-Levers, Olympus, Japan) with spring constants and resonance frequencies of 30 pN/nm and 8.5 kHz or 6 pN/nm and 1.5 kHz, respectively, were used. The force curves of the Titin-GFP-hAGT construct were collected at pulling speeds ranging around 300 nm/s. All experiments were conducted at room temperature in PBS buffer.

Titin-GFP-hAGT fusion proteins were immobilised on BG activated aldehyde-functionalised glass slides as described before (see fluorescence binding measurements).

Results and discussion

Binding studies with surface plasmon resonance

In the beginning we describe an experiment on CMC functionalized cover slides. The CMC layer in channel 1 was activated with BG (Covalys Biosciences AG, Switzerland) using standard EDC/NHS protocols. As a control for specific immobilisation of the fusion proteins in channel 2 no BG, but also EDC/NHS was added. The attachment of the BG-PEG-amino derivative causes an increase of layer thickness of about 6 Å in channel 1 (Fig. 3). After blocking all non-reacted NHS groups from both channels with 1 M ethanolamine, each channel was incubated with GST-hAGT fusion protein. The sensor response of channel 1 (BG activated) was about four times higher than the response of channel 2 (non-activated with BG) (Fig. 4).

The SPR measurements show that a protein layer of the same thickness as a GST-hAGT monolayer is bound only to the BG activated surface. The result of this immobilisation experiment is in good accordance with literature values (Kindermann et al. 2003).

With the anchoring protocol established for GST, in the second experiment we now immobilised a Titin-GFP-hAGT fusion protein on a S-PEG-COOH coated

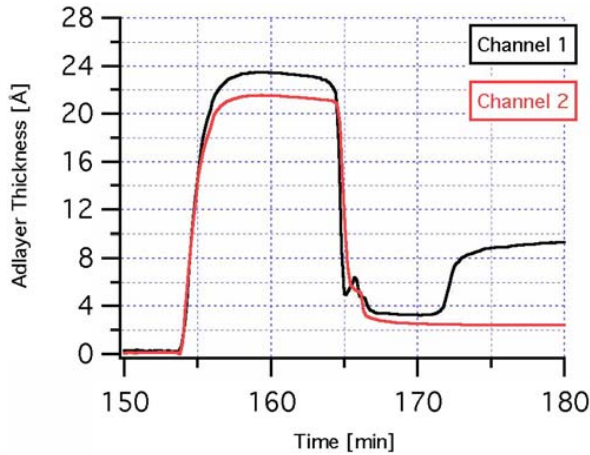


Fig. 3 Surface plasmon resonance signal of the BG-PEG-amino anchor. Carboxylized gold surfaces were activated with EDC/NHS ($t=154$ min). After a short washing step with H_2O (Millipore, Germany) ($t=164$ min) the BG-PEG-amino derivative was anchored to the surface of channel 1. The immobilization of the BG anchor causes an increase in layer thickness of about 6 Å

gold surface. The PEG of channel 1 was activated with BG and the PEG of channel 2 was not. First the surfaces were equilibrated in MES buffer. After 10 min the surfaces of both channels were incubated with crude cell extract of Titin-GFP-hAGT expressing bacteria resuspended in MES buffer. We observed a sizable increase (about 12 Å) in the measured adlayer thickness, which we attribute to the high density of the cell content (Fig. 5). The thickness of the surface in channel 2 slightly decreased in time to drop to nearly zero after

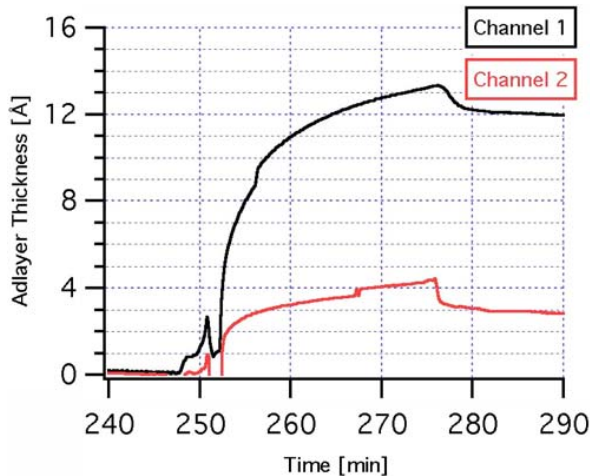


Fig. 4 Surface plasmon resonance signal of GST-hAGT fusions proteins. Surface of channel 1 was activated with BG. Surface of channel 2 was not activated with BG. At time $t=248$ min the surfaces of both channels were incubated with GST-hAGT fusion proteins. After an incubation time of about 30 min all unbound proteins were washed away with PBS buffer ($t=276$ min). The SPR response of channel 1 was about four times higher than that of channel 2

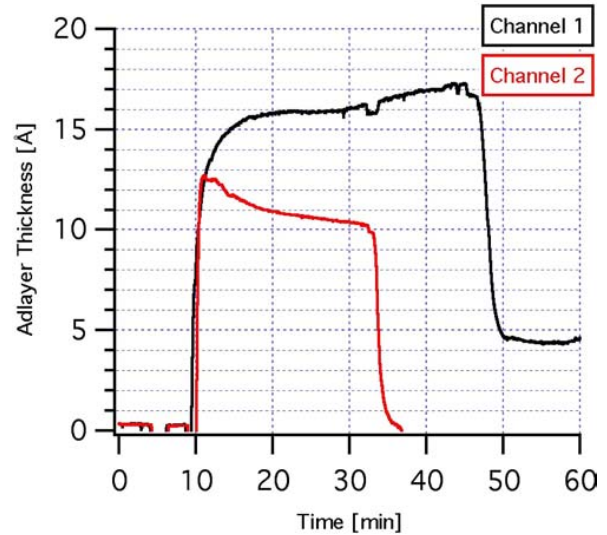


Fig. 5 Surface plasmon resonance signal of Titin-GFP-hAGT fusion proteins. The surface of channel 1 was activated with BG. The surface of channel 2; Å was not activated with BG. At time $t=10$ min the surfaces of both channels were incubated with crude cell extract of Titin-GFP-hAGT expression bacteria. After an incubation time of about 35 min all unbound proteins were washed away with MES buffer ($t=45$ min, channel 1; $t=35$ min channel 2). On the surface of channel 2 no protein was bound whereas in channel 1 a film thickness of 4.5 Å remained

extensive rinsing with MES buffer. The thickness in channel 1, however, slightly increased with time. After rinsing, a final thickness increase of 4.5 Å remained.

Verification of anchoring with fluorescence measurements

The specific binding of Titin-GFP-hAGT fusion proteins on BG coated surfaces was verified by spotting BG on EDC/NHS activated slides. Titin-GFP-hAGT fusion proteins were anchored to these slides as described above. The amount of bound fusion proteins was detected by fluorescence measurements. The result is shown in Fig. 6.

The result of the fluorescence-binding assay clearly shows that Titin-GFP-hAGT fusion proteins are only bound to BG activated spots of the glass slide. It also proves the high selectivity of this immobilisation technique since the anchoring was carried out with crude cell lysate.

Single molecule force spectroscopy on anchored proteins

The selectivity of the attachment of hAGT fusion proteins was also investigated by single molecule force spectroscopy. This method is complementary to SPR and fluorescence measurements. Single proteins anchored between surface and AFM cantilever tip can be

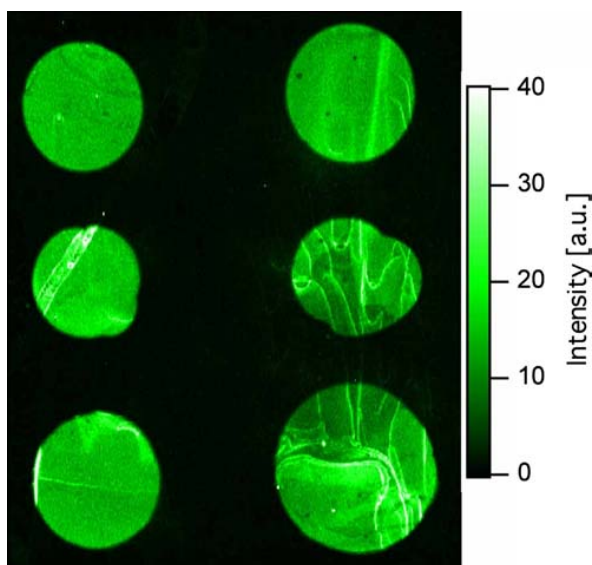


Fig. 6 Fluorescence signal of immobilized Titin-GFP-hAGT fusion proteins. The whole area was activated with EDC/NHS and six spots of BG were coupled to this surface. After blocking all non-reacted NHS groups with 1 M ethanolamine the whole area was incubated with Titin-GFP-hAGT fusion proteins. The fluorescence signal between BG activated areas to non-activated areas was typically 17:1

identified via their specific mechanical unfolding pattern (Rief et al. 1997). Recently, the mechanical unfolding of single Titin-GFP proteins (lacking the hAGT domain) has been investigated and their specific mechanical unfolding pattern has been identified (Dietz and Rief 2004b). Those experiments were performed with unspecific adsorbed proteins. Here we anchored hAGT-Titin-GFP fusion proteins with BG on a glass slide in a site-directed manner. For this purpose, one spot (upper spot Fig. 7b) on the glass slide was activated with BG while the other spot was not activated. Both spots were incubated for 45 min with *E. coli* crude extract and afterwards extensively rinsed with PBS buffer to remove all unbound molecules.

Figure 7a shows typical force-extension traces collected at the BG activated spot. They exhibit the typical saw-tooth pattern due to sequential domain unfolding in single Titin and Titin-GFP molecules as described before (Dietz and Rief 2004b; Rief et al. 1997). At extensions below 100 nm all traces exhibit complicated force patterns, which are most probably due to multiple molecule interactions. Then, at higher extensions the force gradually increases according to polypeptide elasticity until one of the contained Titin domains unfolds. This leads to a quasi-instantaneous increase in the contour length of the polypeptide and the force drops rapidly. Then, subsequent stretching of the lengthened molecule takes place until the next Titin domain unfolds. These unfolding events are equidistant since the Titin domains are identical in size. Then ultimately, the whole

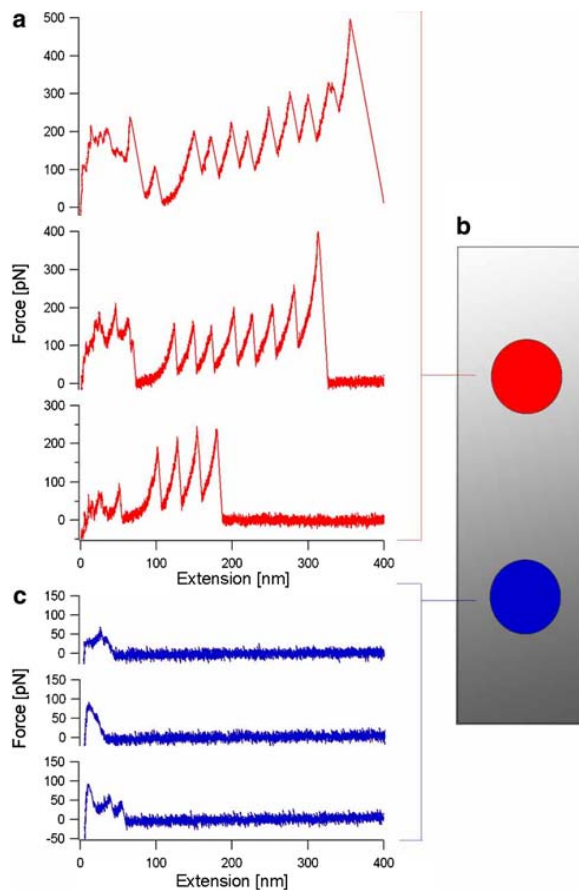
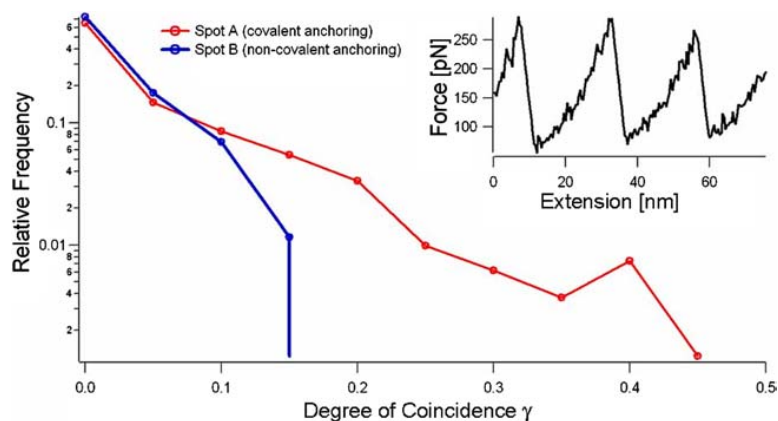


Fig. 7 Atomic force microscope experiments on immobilized hAGT-Titin fusion proteins. The upper spot of the slide was activated with the BG anchor while the lower spot was not activated (b). Both spots were incubated with Titin-GFP-hAGT fusion proteins. Before the AFM experiments, all unbound proteins were washed away with PBS buffer. a Typical force-extension traces collected at the BG activated spot. c Typical force-extension traces collected at the non-activated spot

molecule ruptures from the cantilever (reflected by the last force peak in each trace) and the force drops to zero.

Titin domains exhibit a much higher unfolding force than GFP and thus GFP unfolding always occurs at small extensions. Therefore, this unfolding event will be often masked by non-specific interactions (Dietz and Rief 2004a). This can also be seen in our data—especially in the two topmost traces in Fig. 7a. There we note at least seven Titin domain unfolding events and therefore, also expect a detected GFP unfolding event. However, this event is obviously masked by the multiple molecule interactions below 100 nm extension. The same will most probably be true for the hAGT domain contained in the investigated molecules. In our data we could not find clear indication for an additional event reflecting the unfolding of the hAGT domain. This also supports the notion that hAGT loses partly its structural integrity when it binds to its target BG (Daniels et al.

Fig. 8 Results of the search for Titin domain unfolding events on the activated and on the non-activated spot with a pattern recognition algorithm. We searched all force-distance curves from both areas for the typical Titin fingerprint (inset). It is clearly visible that at the BG activated spot the frequency of partial ($\gamma > 0.2$) and good matching ($\gamma > 0.35$) with the three Titin domain-unfolding pattern is by far higher than at the non-activated spot



2000). The mechanical contribution of the amino-polyethylene glycol linker to the force-extension curves should be negligible, since the PEG linker consists of only three monomers. It will be an important task for the future to further characterise the mechanical properties of this enzyme.

However, the traces in Fig. 7a clearly demonstrate on the single molecule level the successful anchoring of the Titin-GFP-hAGT molecules. In contrast, the traces collected at spot B (Fig. 7c) exhibit only unspecific low-force interaction patterns, which cannot be attributed to the unfolding of modules contained in the Titin-GFP-hAGT molecule.

To compare quantitatively the yield of force-extension traces exhibiting Titin unfolding patterns collected on both spots, we performed an analysis based on pattern recognition techniques as described in Dietz and Rief (2004a). This method involves first definition of a test pattern, then identification of the best matching section with the test pattern in each force trace and finally calculation of a degree of coincidence γ with the pattern as defined in equation 10 in Dietz and Rief (2004a). As a test pattern we chose a section of a measured single molecule force-extension trace exhibiting three Titin domain-unfolding events (Fig. 8, inset). The graph shows the distribution of the degrees of coincidence with the given pattern as they have been assigned to each force trace contained in the data sets collected at the BG activated spot and at the non-activated spot. It is clearly visible that at the BG activated spot the frequency of partial ($\gamma > 0.2$) and good matching ($\gamma > 0.35$) with the three Titin domain-unfolding pattern is by far higher than at the non-activated spot. This testifies again that proteins containing Titin domains are selectively immobilised only on the BG activated spot.

We therefore conclude that the anchoring is indeed performed via the hAGT-BG coupling mechanism. However, from our single molecule experiments we cannot infer directly if the binding is covalent since the forces at which the molecules rupture from the cantilever are compromised by the fact that the connection

between the stretched molecules and the cantilever was still unspecific. It will be necessary to anchor single proteins selectively and specifically on both the substrate and cantilever. Then, from the rupture forces one would be able to infer if the nature of the binding is covalent, since rupture forces should then reach into the nN regime (Grandbois et al. 1999).

Conclusion

Our study clearly shows that anchoring of fusion proteins via hAGT to BG activated surfaces is a suitable technique for single molecule force spectroscopy. The results show that the hAGT in the fusion acts as an anchor for the coupling and that it does not influence the unfolding behaviour of the molecule of interest. This technique offers several advantages: the first one lies in the gentle coupling procedure (in particular no drying required). There is no need for any (chemical) modification on the protein of interest making it possible to investigate the protein under native conditions. The possibility to use different functionalized surfaces (here CMC and S-PEG-COOH coated surfaces) is another advantage especially in terms of investigations with the AFM. The highly specific, self-searching coupling mechanism, which relies on biological recognition, allows the implementation of patterning experiments; hAGT will direct the protein of interest to the desired positions and anchor it on the surface covalently. Furthermore, time-consuming purification steps could be avoided and proteins can be coupled directly from crude cell extract onto the BG coated surfaces. Due to the high fidelity of this coupling method, covalent attachment of recombinant proteins out of single cells expressing hAGT fusion proteins should be possible.

Acknowledgements We thank Martin Benoit for advise and help. Special thank also to Jan Barnikow and Kai Johnsson from Cov-alyz Switzerland who provided the BG-anchor and the hAGT vector. This work was supported by the DFG.

References

- Butt HJ, Jaschke M (1995) Calculation of thermal noise in atomic force microscopy. *Nanotechnology* 6:1–7
- Damoiseaux R, Keppler A, Johnsson K (2001) Synthesis and applications of chemical probes for human O6-alkylguanine-DNA alkyltransferase. *Chembiochem* 2:285–287
- Daniels DS, Tainer JA (2000) Conserved structural motifs governing the stoichiometric repair of alkylated DNA by O(6)-alkylguanine-DNA alkyltransferase. *Mutat Res* 460:151–163
- Daniels DS, Mol CD, Arvai AS, Kanugula S, Pegg AE, Tainer JA (2000) Active and alkylated human AGT structures: a novel zinc site, inhibitor and extrahelical base binding. *Embo J* 19:1719–1730
- Dietz H, Rief M (2004a) Single molecule force spectroscopy of proteins. In: *Proceedings of NATO ASI and SUSSP 59th. Soft condens Matter Phys Mol cell Biol* (in press)
- Dietz H, Rief M (2004b) Exploring the energy landscape of green fluorescent protein by single molecule mechanical experiments. *PNAS* 101:16192–16197
- Florin E-L, Rief M, Lehmann M, Ludwig M, Dornmair C, Moy T, Gaub HE (1995) Sensing specific molecular interactions with the atomic force microscope. *Biosensors Bioelectronics* 10:895–901
- Gendreizig S, Kindermann M, Johnsson K (2003) Induced protein dimerization in vivo through covalent labeling. *J Am Chem Soc* 125:14970–14971
- Grandbois M, Beyer M, Rief M, Clausen-Schaumann H, Gaub HE (1999) How strong is a covalent bond?. *Science* 283:1727–1730
- Juillerat A, Gronemeyer T, Keppler A, Gendreizig S, Pick H, Vogel H, Johnsson K (2003) Directed evolution of O6-alkylguanine-DNA alkyltransferase for efficient labeling of fusion proteins with small molecules in vivo. *Chem Biol* 10:313–317
- Keppler A, Gendreizig S, Gronemeyer T, Pick H, Vogel H, Johnsson K (2003) A general method for the covalent labeling of fusion proteins with small molecules in vivo. *Nat Biotechnol* 21:86–89
- Kindermann M, George N, Johnsson N, Johnsson K (2003) Covalent and selective immobilization of fusion proteins. *J Am Chem Soc* 125:7810–7811
- Neuert G, Kufer SK, Benoit M, Gaub HE (2004) Modular multichannel surface plasmon spectrometer. *Review of Scientific Instruments* (in press)
- Oesterhelt F, Rief M, Gaub HE (1999) Single molecule force spectroscopy by AFM indicates helical structure of poly(ethylene-glycol) in water. *New J Phys*, pp 6.1–6.11
- Pegg AE, Boosalis M, Samson L, Moschel RC, Byers TL, Swenn K, Dolan ME (1993) Mechanism of inactivation of human O6-alkylguanine-DNA alkyltransferase by O6-benzylguanine. *Biochemistry* 32:11998–12006
- Rief M, Gautel M, Oesterhelt F, Fernandez JM, Gaub HE (1997) Reversible unfolding of individual titin immunoglobulin domains by AFM. *Science* 276:1109–1112

Anhang C

Single-Molecule Cut-and-Paste Surface Assembly

Stefan K. Kufer, Elias M. Puchner, Hermann Gump, Tim Liedl and Hermann E. Gaub

Science, Vol 319, 594-596, 1 Februar 2008

In dieser Veröffentlichung wird eine Methode für die bottom-up Assemblierung von biomolekularen Strukturen eingeführt, welche die Präzision eines AFMs mit der Selektivität der DNA-Hybridisierung kombiniert. Funktionale Einheiten wurden an DNA-Oligomere gekoppelt und von einem Depot mit einem komplementären DNA-Strang, der an die Spitze eines AFMs gebunden war, aufgenommen. Die Einheiten wurden zu einer Zielfläche transferiert und dort deponiert. Jedes der Single-Molecule Cut-and-Paste (SMCP) Ereignisse wurde mit Einzelmolekülkraftspektroskopie charakterisiert. Die resultierenden Kraft-Abstandskurven liefern ein präzises Protokoll zur Evaluierung der Assemblierung. Unter Verwendung einer einzigen Spitze konnte der Transport und die Deponierung von mehr als 5000 Einheiten gezeigt werden, wobei die Transfereffizienz während des Transports um weniger als 10 % abnahm.



Single-Molecule Cut-and-Paste Surface Assembly

S. K. Kufer, *et al.*
Science **319**, 594 (2008);
DOI: 10.1126/science.1151424

The following resources related to this article are available online at www.sciencemag.org (this information is current as of January 31, 2008):

Updated information and services, including high-resolution figures, can be found in the online version of this article at:

<http://www.sciencemag.org/cgi/content/full/319/5863/594>

This article **cites 33 articles**, 16 of which can be accessed for free:

<http://www.sciencemag.org/cgi/content/full/319/5863/594#otherarticles>

This article appears in the following **subject collections**:

Chemistry

<http://www.sciencemag.org/cgi/collection/chemistry>

Information about obtaining **reprints** of this article or about obtaining **permission to reproduce this article** in whole or in part can be found at:

<http://www.sciencemag.org/about/permissions.dtl>

19. V. Reinke, I. S. Gil, S. Ward, K. Kazmer, *Development* **131**, 311 (2004).
20. H. Browning, S. Strome, *Development* **122**, 391 (1996).
21. R. W. Beeman, K. S. Friesen, R. E. Denell, *Science* **256**, 89 (1992).
22. G. D. Hurst, J. H. Werren, *Nat. Rev. Genet.* **2**, 597 (2001).
23. A. Atlan, H. Mercot, C. Landre, C. Montchamp-Moreau, *Evol. Int. J. Org. Evol.* **51**, 1886 (1997).
24. R. W. Beeman, K. S. Friesen, *Heredity* **82**, 529 (1999).
25. L. Fishman, J. H. Willis, *Genetics* **169**, 347 (2005).
26. H. A. Orr, S. Irving, *Genetics* **169**, 671 (2005).
27. F. A. Reed, R. G. Reeves, C. F. Aquadro, *Evol. Int. J. Org. Evol.* **59**, 1280 (2005).
28. E. A. Stahl, G. Dwyer, R. Mauricio, M. Kreitman, J. Bergelson, *Nature* **400**, 667 (1999).
29. D. Tian, H. Araki, E. Stahl, J. Bergelson, M. Kreitman, *Proc. Natl. Acad. Sci. U.S.A.* **99**, 11525 (2002).
30. M. Shapira *et al.*, *Proc. Natl. Acad. Sci. U.S.A.* **103**, 14086 (2006).
31. J. H. Thomas, *Genome Res.* **16**, 1017 (2006).
32. J. H. Thomas, *Genetics* **172**, 127 (2006).
33. H. A. Orr, D. C. Presgraves, *Bioessays* **22**, 1085 (2000).
34. K. A. Frazer, L. Pachter, A. Poliakov, E. M. Rubin, I. Dubchak, *Nucleic Acids Res.* **32**, W273 (2004).
35. Z. Yang, *Comput. Appl. Biosci.* **13**, 555 (1997).
36. We thank the *Caenorhabditis* Genetics Center, the National Bioresource Project of Japan, the NemaGENETAG Consortium, M.-A. Félix, A. Barrière, E. Dolgin, and H. Van Epps for strains; R. Maruyama and A. Singson for advice; S. Skrovaneck for lab assistance; and H. Collier, A. Cutter, D. Gresham, R. Gosh, L. Moyle, J. Shapiro, and E. Smith for comments on the manuscript. Supported by a National Defense Science and Engineering Graduate fellowship to H.S.S., a Jane Coffin Childs Fellowship to M.V.R., NIH grants R37 MH059520 and R01 HG004321 and a James S. McDonnell Foundation Centennial Fellowship to L.K., and NIH grant GM071508 to the Lewis-Sigler Institute. GenBank sequence accession numbers are EU163897 to EU163940.

Supporting Online Material
www.sciencemag.org/cgi/content/full/1151107/DC1
SOM Text
Fig. S1
Tables S1 to S7
References

28 September 2007; accepted 17 December 2007
Published online 10 January 2008;
10.1126/science.1151107
Include this information when citing this paper.

REPORTS

Single-Molecule Cut-and-Paste Surface Assembly

S. K. Kufer,¹ E. M. Puchner,¹ H. Gump, H. Liedl,² H. E. Gaub¹

We introduce a method for the bottom-up assembly of biomolecular structures that combines the precision of the atomic force microscope (AFM) with the selectivity of DNA hybridization. Functional units coupled to DNA oligomers were picked up from a depot area by means of a complementary DNA strand bound to an AFM tip. These units were transferred to and deposited on a target area to create basic geometrical structures, assembled from units with different functions. Each of these cut-and-paste events was characterized by single-molecule force spectroscopy and single-molecule fluorescence microscopy. Transport and deposition of more than 5000 units were achieved, with less than 10% loss in transfer efficiency.

Functional biomolecular assembly aims to create structures from a large variety of biomolecular building blocks in a geometrically well-defined manner in order to create new functions (1, 2), such as artificial signaling cascades or synergetic combinations of enzymes. Hybrid devices could include quantum dots co-assembled with dye molecules, or gold particles assembled as plasmon hot spots with a sample protein positioned into the focus (3). One way to assemble such molecular devices would be to physically pick up the different units needed with a scanning probe tip, translocate these units to a different location, and deposit them with high spatial precision (4–6). The entire process would also have to be carried out in an aqueous environment.

For the translocation of nanoscale objects, we used atomic force microscopy, which has been used in this context for mechanical single-molecule experiments (7–12) or lithography (13, 14); however, previously suggested devices include the use of molecular pliers at the end of atomic force microscope (AFM) cantilevers that could grab and release the building blocks, triggered by an

external signal of either electrical or optical nature (15). We report a simpler and robust solution based on DNA hybridization and hierarchical bonds defined by different unbinding forces.

A well-sorted “depot,” with a large variety of molecular species, stably stored in well-defined loci, is a prerequisite for the assembly of a multi-component device. DNA chips offer a freely programmable pattern of oligomers that are commercially available and have spot sizes in the submicrometer range (16). Niemeyer *et al.* (17) converted such a DNA pattern into a protein pattern by binding a DNA-labeled protein to its corresponding spot on a DNA chip. The length of the oligomers can be chosen so that after incubation and stringent washing, a thermodynamically stable pattern of proteins is obtained. Given the known sequence map of the DNA chip, different molecular species can be stored in a known position on the depot chip. Alternatively, when only a limited variety of building blocks is needed, microfluidic elastomer channels may be used to create patterns (18–20) of building blocks, which after removal of the elastomer may be manipulated with the AFM tip (fig. S3).

We used this approach to store our functional units and also extended the DNA oligomers to fulfill a second function; namely, to serve as a handle (Fig. 1). This additional stretch of DNA

can hybridize to a complementary DNA covalently attached to an AFM tip. We chose the duplexes to be comparable in length and binding free energy, but we selected the sequences so that the anchor hybridizes in the so-called “unzip” geometry and the handle hybridizes in the “shear” geometry [Fig. 1 and (21)]. These two duplex geometries differ substantially in that, upon forced unbinding, the zipper duplex is opened up base pair by base pair, whereas in the shear geometry, all base pairs are loaded in parallel (Fig. 2 and fig. S1). Although the thermodynamic stability and the spontaneous off rate of both geometries are comparable, their rupture forces differ dramatically (22), as has been shown experimentally and was validated theoretically in several studies (21, 23–27). Thus, upon retraction of the AFM tip, the anchor duplex will break open and the functional unit will be bound to the tip.

As can be seen in Fig. 2C, these force distance curves provide a characteristic fingerprint and serve as a robust criterion to decide whether a molecule was picked up from the depot. To avoid multiple transfers, we chose the density of the anchors on the tip to be low enough that in 35% of the attempts, only one unit was picked up, and in 20% of the attempts, just two units. In 20% of all attempts, we recorded traces like the lower two in Fig. 2C, which showed that we had not picked up any unit (fig. S5D). Because we recorded such a force distance curve for every pickup, we knew exactly how many units were transferred to the tip. The pickup process can be corrected online by either picking up more units or by dropping excess units in a “trash can” on the target area.

Once a unit is transferred to the tip, it can be moved to its new position on the target area. The target area had surface chemistry similar to that of the depot area, but the anchor oligomers were chosen so that when the tip was lowered, they bound to the transfer DNA in shear geometry and formed a duplex, which was longer than the handle duplex. Although the AFM tip can be positioned with subnanometer reproducibility, the precision with which the units can be

¹Center for Nanoscience and Department of Physics, University of Munich, Amalienstrasse 54, 80799 Munich, Germany.
²Department of Biological Chemistry and Molecular Pharmacology, Harvard Medical School, and Department of Cancer Biology, Dana-Farber Cancer Institute, Boston, MA 02115, USA.

deposited is limited by the lateral density of the anchor oligomers and their spacer length (presently in the 10-nm range).

Upon retraction of the tip from the surface, the force in the two DNA duplexes in series gradually increases until the weaker of the two

complexes ruptures. The upper traces in Fig. 2D show examples of this process, which differs considerably in its signature from the unzipping shown in Fig. 2C (28, 29). It was shown (21) that a length difference of 10 base pairs (bp) is sufficient to make the rupture of the shorter handle duplex more likely by one order of magnitude than the rupture of the longer anchor duplex. As was the case during pickup, no bond rupture was detected in certain cases (Fig. 2D, lower traces). Here the hybridization with the target anchor oligomer had failed, although a functional unit was offered. In the majority of cases, a second or third attempt made a few nanometers away from the originally planned target spot was successful. Again, a protocol with a characteristic force distance curve (for brevity referred to as a transfer protocol) was recorded for each transfer event. After delivery of the functional unit to the target, the oligomer covalently attached to the AFM tip was free again to hybridize with another handle sequence in the depot area.

For simplicity, we transferred only functional units of the same species but created patterns from single units with multiple functions instead. As functional units, we used molecular constructs consisting of a fluorophore (rhodamine green), a generic small ligand (biotin), and a DNA with extra overlap (which allows further docking of other units to the assembly in a later step) (Fig. 2 shows the schematics). The units were picked up

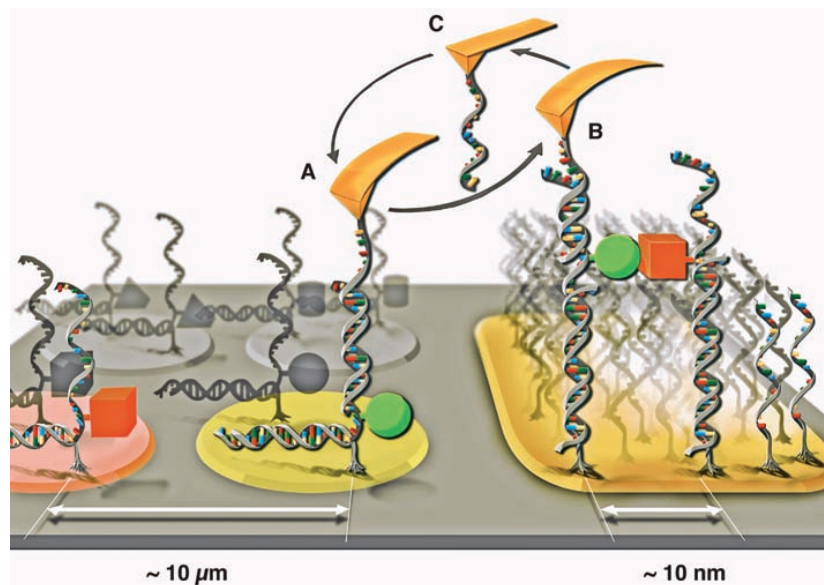
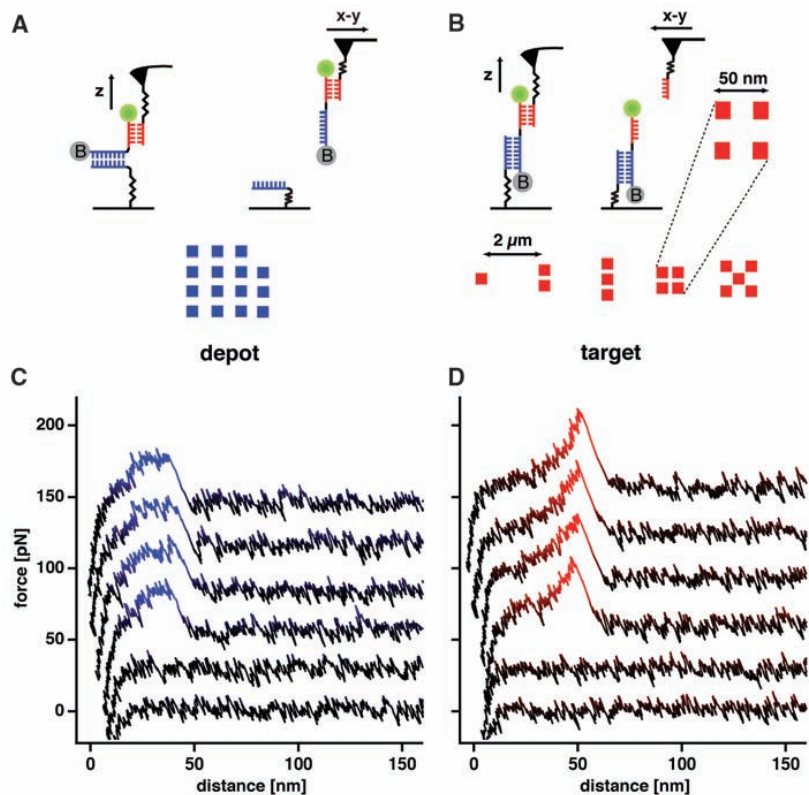


Fig. 1. Cartoon of the single-molecule cut-and-paste process. (A) Individual nanosized objects are picked up from discrete storage sites with a DNA oligomer at the tip of an AFM cantilever and transferred to a target site, where they are deposited with high spatial precision (B). (C) The length and binding geometry of the oligomers, which are used as an anchor or a handle, are chosen so that a hierarchy of unbinding forces allows the repetition of this process over and over again.

Fig. 2. Design of the assembled pattern with typical transfer protocols. (A) Individual functional units stored on the depot were picked up one at a time and transferred to the target area. The functional units consisted of a DNA oligomer with anchor and handle sequences, one fluorophore, one biotin, and an additional DNA binding site. (B) Five different patterns with different geometries were assembled on spots, which were 2 μm apart. In the first spot, we deposited one unit; in the second spot, two units with a lateral spacing of 50 nm; in the third spot, three units, and so forth. The lateral precision of the closed-loop feedback was ±6 nm. Force distance curves were recorded in every cycle as transfer protocols recording successful pickup and deposition. (C) Typical force distance curves measured during the pickup of functional units from the depot. At low extensions, the cantilever acts against the entropic force of the polyethylene glycol–DNA complex. When the force reaches about 20 pN, the anchor sequence is pulled open in a zipperlike mode, resulting in a plateau ~20 nm long. (D) Typical force distance curves recorded during the deposition of a single unit to the target area. The shape, with its sudden drop in force at about 50 pN, is characteristic of a rupture of a 20-bp DNA handle duplex loaded in shear geometry. The lower two force distance curves in (C) and (D) show attempts, where no transfer had occurred.



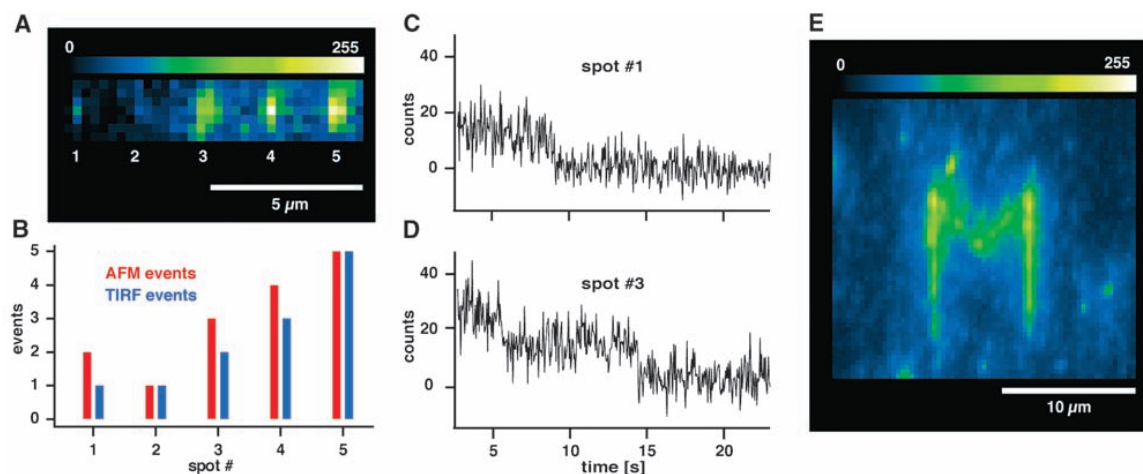


Fig. 3. (A) Fluorescence micrograph of the assembled pattern described in Fig. 2, imaged with TIRF excitation. The image was averaged over 440 frames, with 50 ms of integration time each. Because of the diffraction limit, individual fluorophores cannot be resolved spatially but can be resolved temporally. (C) and (D) show time traces of the two diffraction-limited 3×3 -pixel-sized spots 1 and 3, exhibiting the typical stepwise bleaching of one and two single fluorophores, respectively. (B) Correlation analysis of the number of success-

fully transferred units as judged by the AFM transfer protocols and the number of bleaching steps in the fluorescence. (E) The capital letter M written by transporting 400 molecules from the depot area to defined positions at the target area. It was assembled with a tip that had already been used to transport more than 5000 molecules from the depot to the target area. These results demonstrate the long-term stability of the tip functionalization and the possibility of assembling extended constructs.

from a 100-nm-square pattern (Fig. 2A) and transferred to the target area. A pattern, as sketched in Fig. 2B, was assembled where we deposited a single unit in the first spot, a pair in the second spot, a triplet in the third, and so on. The transfer protocols always documented the actual number of transferred units.

After the assembly was completed, total internal reflection fluorescence (TIRF) imaging (30) showed discrete spots at the predicted positions (Fig. 3A). Because of the limited optical resolution, no details of the assemblies are resolved, but larger assemblies appear brighter. Time traces (Fig. 3, C and D) exhibited well-pronounced steps that were a clear indication of bleaching of individual fluorophores (31, 32) (movie S1). On the spot in the first column, we recorded a single step only, and the fluorophore was bleached after 9 s. The spot in the third column exhibited only two steps, although our transfer protocol reported the deposition of three functional units. Either one of the fluorophores was inactive from the beginning or it was bleached during the first 2 s of the illumination and not recorded because of background fluorescence. A direct correlation between the number of deposited units as judged by the transfer protocol and the number of bleaching steps is given in Fig. 3B. Both independent experiments are in excellent agreement, which indicates that we lost only a minor fraction of fluorophores in the transfer process.

In order to demonstrate the formation of larger constructs, we assembled the capital letter M shown in Fig. 3E. It consists of 400 units and was written with a tip that had already been used to transport more than 5000 functional units from the depot to the target area. All of the data shown

here and in the supporting online material were recorded with one cantilever. Because the pickup probability dropped by only 10% toward the end of the experiment, the lifetime of the tip functionalization was adequate. The pattern was assembled at an average rate of 7 s per transfer. This slow transfer rate was limited by the rather large distance between depot and target area of 15 μm and the closed-loop feedback of the translational stages of the instrument. The online analysis of the transfer protocols was also not optimized. The physical limits are given by the resonance frequency of the piezo stage, and so improvements of several orders of magnitude are possible (33). With the development of massively parallel-operating AFM cantilevers (34), molecule-by-molecule assembly based on hierarchical forces may evolve into a versatile technology.

References and Notes

- B. A. Grzybowski, H. A. Stone, G. M. Whitesides, *Nature* **405**, 1033 (2000).
- T. Pellegrino *et al.*, *Small* **1**, 48 (2005).
- M. Ringle *et al.*, *Nano Lett.* **7**, 2753 (2007).
- D. M. Egler, E. K. Schweizer, *Nature* **344**, 524 (1990).
- M. T. Cuberes, R. R. Schlittler, J. K. Gimzewski, *Appl. Phys. Lett.* **69**, 3016 (1996).
- S. J. Greissl *et al.*, *J. Phys. Chem. B* **108**, 11556 (2004).
- G. Binnig, H. Rohrer, C. Gerber, E. Weibel, *Phys. Rev. Lett.* **49**, 57 (1982).
- G. Binnig, C. F. Quate, C. Gerber, *Phys. Rev. Lett.* **56**, 930 (1986).
- P. K. Hansma, V. B. Elings, O. Marti, C. E. Bracker, *Science* **242**, 209 (1988).
- M. Radmacher, R. W. Tillmann, M. Fritz, H. E. Gaub, *Science* **257**, 1900 (1992).
- P. E. Marszalek *et al.*, *Nature* **402**, 100 (1999).
- D. Fotiadis *et al.*, *Curr. Opin. Struct. Biol.* **16**, 252 (2006).
- M. Jaschke *et al.*, *Biosens. Bioelectron.* **11**, 601 (1996).
- R. D. Piner, J. Zhu, F. Xu, S. Hong, C. A. Mirkin, *Science* **283**, 661 (1999).
- C. P. Collier *et al.*, *Science* **289**, 1172 (2000).
- S. P. Fodor *et al.*, *Science* **251**, 767 (1991).
- C. M. Niemeyer, T. Sano, C. L. Smith, C. R. Cantor, *Nucleic Acids Res.* **22**, 5530 (1994).
- E. Delamarche, A. Bernard, H. Schmid, B. Michel, H. Biebuyck, *Science* **276**, 779 (1997).
- S. R. Quake, A. Scherer, *Science* **290**, 1536 (2000).
- D. C. Duffy, J. C. McDonald, O. J. A. Schueller, G. M. Whitesides, *Anal. Chem.* **70**, 4974 (1998).
- C. Albrecht *et al.*, *Science* **301**, 367 (2003).
- A hand-waving argument: Upon separation, the binding energy is overcome in the shear geometry within a much shorter distance than in the unzip geometry, therefore the force to overcome the energy barrier is much lower in the unzip geometry. Because the forced unbinding of the oligomer in shear geometry is a nonequilibrium process, its unbinding force is rate-dependent. In all experiments shown here, the duplexes were loaded with a rate of 3000 pN/s.
- G. I. Bell, *Science* **200**, 618 (1978).
- S. B. Smith, Y. J. Cui, C. Bustamante, *Science* **271**, 795 (1996).
- B. Essevaz-Roulet, U. Bockelmann, F. Heslot, *Proc. Natl. Acad. Sci. U.S.A.* **94**, 11935 (1997).
- M. Rief, H. Clausen-Schaumann, H. E. Gaub, *Nat. Struct. Biol.* **6**, 346 (1999).
- G. Neuert, C. H. Albrecht, H. E. Gaub, *Biophys. J.* **93**, 1215 (2007).
- J. Morfill *et al.*, *Biophys. J.* **93**, 2400 (2007).
- T. Strunz, K. Oroszlan, R. Schafer, H. J. Guntherodt, *Proc. Natl. Acad. Sci. U.S.A.* **96**, 11277 (1999).
- R. D. Vale *et al.*, *Nature* **380**, 451 (1996).
- G. Seisenberger *et al.*, *Science* **294**, 1929 (2001).
- P. Tinnefeld, M. Sauer, *Angew. Chem. Int. Ed.* **44**, 2642 (2005).
- G. Schitter *et al.*, *IEEE Trans. Control Syst. Technol.* **15**, 906 (2007).
- P. Vettiger *et al.*, *IBM J. Res. Devel.* **44**, 323 (2000).
- Helpful discussions with P. Hansma, G. M. Whitesides, J. Fernandez, H. Heus, P. Tinnefeld, J. Morfill, C. Albrecht, and L. Whetton are gratefully acknowledged. Supported by the German Science Foundation and the Nanosystems Initiative Munich.

Supporting Online Material

www.sciencemag.org/cgi/content/full/319/5863/594/DC1

Materials and Methods

Figs. S1 to S5

References

Movie S1

9 October 2007; accepted 18 December 2007

10.1126/science.1151424



www.sciencemag.org/cgi/content/full/319/5863/594/DC1

Supporting Online Material for
Single-Molecule Cut-and-Paste Surface Assembly

S. K. Kufer, E. M. Puchner, H. Gump, T. Liedl, H. E. Gaub

Published 1 February 2008, *Science* **319**, 594 (2008)
DOI: 10.1126/science.1151424

This PDF file includes:

Materials and Methods
Figs. S1 to S5
References

Other Supporting Online Material for this manuscript includes the following: (available at www.sciencemag.org/cgi/content/full/319/5863/594/DC1)

Movie S1

Supporting online material

Single-Molecule, Cut-and-Paste Surface Assembly

S. K. Kufer¹, E. M. Puchner¹, H. Gump¹, T. Liedl², H. E. Gaub¹

Materials and Methods

General:

In this report, DNA oligomers were employed as anchors and handles for pick-up and delivery of nanosized objects (e.g. fluorophores) with an AFM. The oligomers were chosen such that they form duplexes, which under load unbind at different forces. They define a hierarchical set of unbinding forces. Upon pick-up, the force at which the anchor releases the object from the depot must be smaller than the force that binds it to the tip. Upon delivery, however, the force at which the object is released from the tip must be smaller than the force that anchors the object at the target site. This is achieved by choosing both length and unbinding geometries of the duplexes accordingly. A schematic of the molecular constructs employed is shown in Fig. S1. The sequences of the oligomers are given in Fig. S2.

Preparation of cover slips:

Cover slips were cleaned through a 15 min supersonic treatment in a mixture (1:1 (v/v)) of ethanol and H₂O (Millipore water with a conductance of 0.054 μ S), rinsed with H₂O and dried in a nitrogen stream. After 10 min of activation using a UV-ozone cleaning system (UVOH 150 LAB, FHR Anlagenbau GmbH, Ottendorf-Okrilla, Germany) the cover slips were functionalized with a solution of 2 % 3-aminopropyltrimethoxysilane, 88 % ethanol and 10 % H₂O for 30 min at room temperature. Cover slips were again rinsed with ethanol and H₂O and dried in a nitrogen stream. After 30 min of curing at 80 °C the amino modified cover slips were immersed for 1 h in sodium borate (SB) buffer (50 mM, pH 8.5) to deprotonate the amino groups. Then NHS-PEG-maleimide was dissolved in a concentration of 50 mM in SB buffer and incubated on the amino modified cover slips for 1 h. After rinsing with H₂O a PDMS flow chamber (fabrication and features are described below) was mounted on one of the cover slips. Both channels were connected to a peristaltic pump (Minipuls3, Gilson International B.V. Bad Camberg, Germany) that was operated at a flow rate of 1 μ l/min. The anchor oligomers for the depot and target area (Fig. S2) were reduced using TCEP beads in order to generate free mercaptans. The left channel (depot area) was rinsed for 1 h with a 10- μ M solution of depot anchor oligomers and the right one (target area) with a 10- μ M solution of target anchor oligomers. Afterwards both channels were rinsed with H₂O to remove all non-covalently bound oligomers. The left channel (depot area) was rinsed with a 1- μ M solution of transfer-DNA

¹Center for Nanoscience & Physics Department, University Munich, Amalienstr. 54, 80799 Munich

²Department of Biological Chemistry and Molecular Pharmacology, Harvard Medical School & Department of Cancer Biology, Dana-Farber Cancer Institute, Boston, MA 02115, USA

(dissolved in 5*saline sodium citrate buffer (SSC) buffer) for 1 h. After rinsing both channels for 5 min with 1*SSC buffer to remove all non-hybridized transfer-DNA from the depot channel, the PDMS flow chamber was removed and the cover slip was dried in a nitrogen stream. Finally the cover slip was mounted to the AFM-TIRF sample holder (Fig. S4) and immersed in 2*SSC buffer.

Preparation of cantilevers:

Cantilevers (Bio-lever, Olympus, Tokyo, Japan) were activated by a 10 min UV-ozone cleaning treatment and modified with 3-aminopropyltrimethyl-ethoxysilane as described in (1, 2). Afterwards they were rinsed with SB buffer for 1 h to deprotonate the amino groups. NHS-PEG-maleimide was dissolved in a concentration of 50 mM in SB buffer and incubated for 1 h on the amino modified cantilevers. After washing with H₂O, the cantilevers were incubated for 1 h with a 10- μ M solution of reduced cantilever oligomers. Finally, the cantilevers were rinsed with H₂O to remove all non-covalently bound oligomers and stored in an argon atmosphere until use.

To prepare cantilevers with reduced functionalization densities the NHS-PEG-maleimide and therefore the binding sites for the mercaptans were diluted with NHS-PEG-methoxy. An ideally prepared cantilever has only one binding site for the handle sequence and therefore the optimal ratio between the NHS-PEG-maleimide and NHS-PEG-methoxy depends on the area of the apex and varies from cantilever to cantilever. During many cut-and-paste experiments, a ratio between the NHS-PEG-maleimide and NHS-PEG-methoxy of 1:5 (m/m) dissolved in SB buffer with a final concentration of 50 mM was determined as an optimal mixture for cantilevers with low functionalization densities.

Fabrication of PDMS microfluidic channels:

PDMS siloxane elastomer and curing reagent were mixed at a ratio of 10:1 (m/m) and poured onto a lithographically prepared microstructured silicon wafer (master) shown schematically in Fig. S3A. After incubation for 1 h at 60 °C, the polymer was removed from the master and a 1.5 cm x 1.5 cm piece was cut out with a scalpel. An inlet and outlet were pierced in both channels using a canula with a diameter of 0.8 mm. Then the PDMS flow chamber was placed on a NHS-PEG-maleimide activated cover slip and cured again for 10 min at 60 °C to seal the flow channels. The two resulting flow channels run parallel and were separated by a 15- μ m PDMS wall. Each channel was 100 μ m broad, 20 μ m high and 2 cm long. Fig. S3B shows a TIRF image of the depot and target area and the 15- μ m gap between them. To make not only the depot area but also the target area visible both regions were activated here with fluorescently labeled DNA. Fig. S3C shows a typical fluorescence image of a functionalized cover slip used for the experiments. The depot area is visible due to fluorescently labeled DNA. No fluorescence signal is detectable on the target area, which clearly shows that crosstalk between both channels is negligible. The fluorescence image was recorded with a confocal laser scanner (LS 300 Scanner, Tecan Deutschland GmbH, Crailsheim, Germany). The fluorescence signal is equivalent to a surface density of 15 fmol/mm² and therefore the mean distance between the anchor oligomers is roughly 10 nm.

AFM measurements:

All single-molecule cut-and-paste experiments were performed with a custom built AFM (3) at room temperature in 2* SSC (Fig. S4). The spring constant of the DNA modified

cantilever was calibrated in solution using the equipartition theorem (4, 5). This method provides an accuracy of roughly 10% and yielded a spring constant of 4.2 pN/nm and a resonance frequency of 1.6 kHz for the cantilever used in this study.

The protocol for the single-molecule cut-and-paste as well as the data recording was programmed using Igor Pro (Wave Metrics) and an Asylum Research controller, which provides ACD and DAC channels as well as a DSP board for setting up feedback loops. Cantilever positioning for pick-up and delivery was controlled in closed-loop operation. Usually the precision was set to ± 6 nm. For the letter "M" in Fig. 3E, the precision of the feedback was reduced in order to speed up the cut-and-paste protocol. In this case the experimental deviation from the given positions amounts ± 50 nm. Once this position was reached within an accuracy of 10 nm, the cantilever approached the surface with closed-loop control until the repulsion reached 50 pN within an error of 5 pN. The tip was then withdrawn from the surface at a speed of 1200 nm/s, and the force was recorded at a sampling rate of 10 kHz. The resulting force distance curve characterizes the cut-and-paste process and allows determination of the number of molecules that were picked up and delivered (Fig. S5). The timing of the process is roughly as follows: approach ~ 1 s, dwell time for pick up ~ 0.5 s, retract ~ 1 s, approach new position ~ 0.5 -2 s (depending on precision of the closed-loop) approach ~ 1 s, dwell time for contact ~ 0.5 s, retract and reposition ~ 1 s, resulting in a total time of ~ 7 s for one cut-and-paste cycle.

The functionalization density on the tip was chosen in a compromise between no pick-up (Fig. S5A) and multiple pick-ups, as shown in Fig. S5C. In cases where multiple units were picked up, they were either "dropped" in the "trash can" (we deposited them in an area next to the structure to be assembled) or we deposited multiples like we did when we assembled the capital letter "M". The traces in Fig. S5, E-G were recorded from these transfers. Under the category "others" in Fig. S5, D and H, we collected all traces, which resulted from higher multiples we were unable to quantify precisely.

Fluorescence microscopy:

Single-molecule fluorescence microscopy was carried out in TIRF excitation. Fluorescence excitation of the rhodamine green dyes is performed by a 472 nm, 80 mW DPSS laser (Viasho Technology Co., Ltd., Beijing, China) through a 100x/1.45 oil immersion objective lens (alpha Plan-Fluar, Zeiss, Oberkochen, Germany), where the collimated laser beam is focused in the back focal plane of the objective lens such that the beam is totally reflected at the cover slip (6). The focus is controlled with a piezo (Mipos 100, Piezosystemjena, Jena, Germany). The emitted light is detected by a 128 x 128 pixel back-illuminated EMCCD camera (DU-860, Andor, Belfast, Ireland). Time series were recorded in frame-transfer mode with an integration time of 50 ms per frame. The peltier-cooled CCD chip was typically operated at a temperature of -60°C and an electron multiplication gain of 200x was used.

The movie M1 of the supplement shows the step-wise bleaching of individual fluorophores, which were deposited as displayed in the first frame of this movie. The six bright spots constituting the uppermost row were written by performing 9 transfer cycles whereas all other spots were written in single approaches. The content of the tip was deposited regardless of the number of units that were picked up. As was to be expected from the statistics in Fig. S4, the single dots are predominantly single units, and some spots

remained empty. As can be seen in the movie, under our experimental conditions, the average lifetime of one rhodamine green fluorophore is about 10 s. As it becomes clear in this movie, the closely spaced molecules in the first row cannot be resolved optically. However, the accurate positions of individual fluorophores can in principle be determined by taking advantage of the time domain. This, however, remains to be shown in future studies.

Materials:

- H₂O with a conductance of 0.054 μ S (Millipore, Eschborn, Germany)
- Water-for-chromatography (Merck KGaA, Darmstadt, Germany)
- Ethanol 99,8 % (Carl Roth GmbH + Co. KG, Karlsruhe, Germany)
- Argon (AIRLIQUIDE Deutschland GmbH, Düsseldorf, Germany)
- Cover slips (Marienfeld, Lauda-Königshofen, Germany)
- Sylgard184TM polydimethylsiloxane (PDMS), (Dow Corning, Wiesbaden, Germany)
- 3-Aminopropyltrimethoxysilane (ABCR, Karlsruhe, Germany)
- Oligomers (IBA GmbH, Göttingen, Germany)
- N-hydroxy-succinimide-ester-polyethylenglycol-maleimide (NHS-PEG-Maleimide), MW 5000 g/mol (Nektar, Huntsville, Alabama, USA)
- N-hydroxy-succinimide-ester-polyethylenglycol-methoxy (NHS-PEG-Methoxy), MW 5000 g/mol (Rapp Polymere GmbH, Tübingen, Germany)
- 20*Saline sodium citrate buffer (SSC) (Sigma, Taufkirchen, Germany)
- 5*SSC buffer were prepared by diluting 20*SSC with H₂O
- 2*SSC buffer were prepared by diluting 20*SSC with water-for-chromatography
- Sodium borate buffer (SB) (50 mM, pH 8.5)
- TCEP beads (Perbio Science, Bonn, Germany)
- Canula (Sterican, 0,80 x 22 mm, Carl Roth GmbH + Co, Karlsruhe, Germany)

Figures

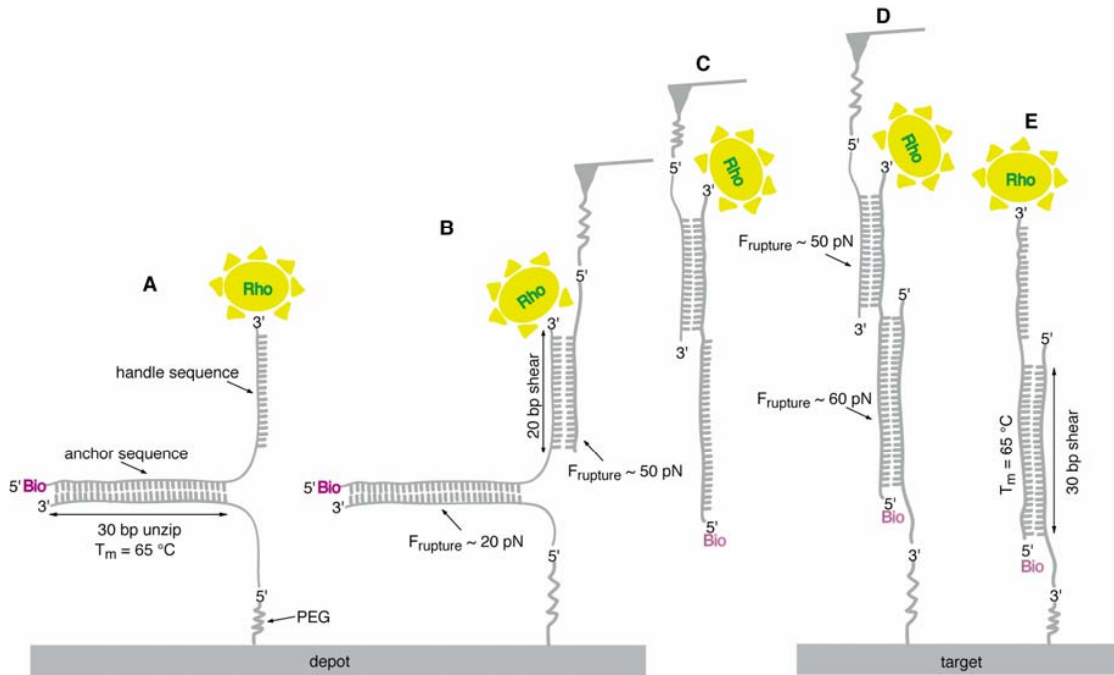


Fig. S1. Schematic of the pick-up and delivery system based on DNA duplexes with hierarchical unbinding forces. (A) The 5' end of the depot anchor oligomer is covalently attached to a cover slip via a PEG spacer. Upon incubation, the transfer-DNA with the functional unit hybridizes to the 30-bp anchor in the depot area. The remaining 20 nucleotides long sequence was chosen to be complementary to the cantilever oligomer and serves as a molecular handle. (B) The cantilever oligomer is covalently bound via a PEG spacer with the 5' end to the AFM tip. Upon approaching the depot area, the handle sequence of the transfer-DNA and the cantilever oligomer hybridize. By retracting the tip from the substrate, both duplexes are loaded in series and thus equally, however, in different geometries. The anchor duplex is loaded in unzip geometry whereas the handle duplex is loaded in shear geometry. Despite the fact that the anchor duplex is longer than the handle duplex, it unbinds at lower forces and as a result the transfer-DNA goes along with the tip (C). It may now be transferred to the target area. The target anchor oligomer has the same sequence as the depot anchor oligomer but it is attached to the target surface with its 3' end. Therefore it hybridizes with the transfer-DNA in shear geometry (D). When the tip is withdrawn from the target surface both duplexes are loaded in shear geometry. Since the shorter of the duplexes opens first, the transfer-DNA with its functional unit remains at the target site (E). The tip is in its initial state and the cycle may start over again.

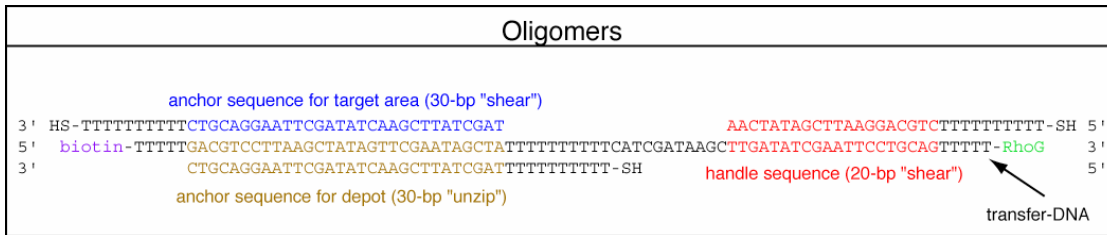


Fig. S2. Sequences of the handle, transfer and anchor oligomers. All oligomers were synthesized and purified (HPLC-grade) form IBA (IBA GmbH, Göttingen, Germany).

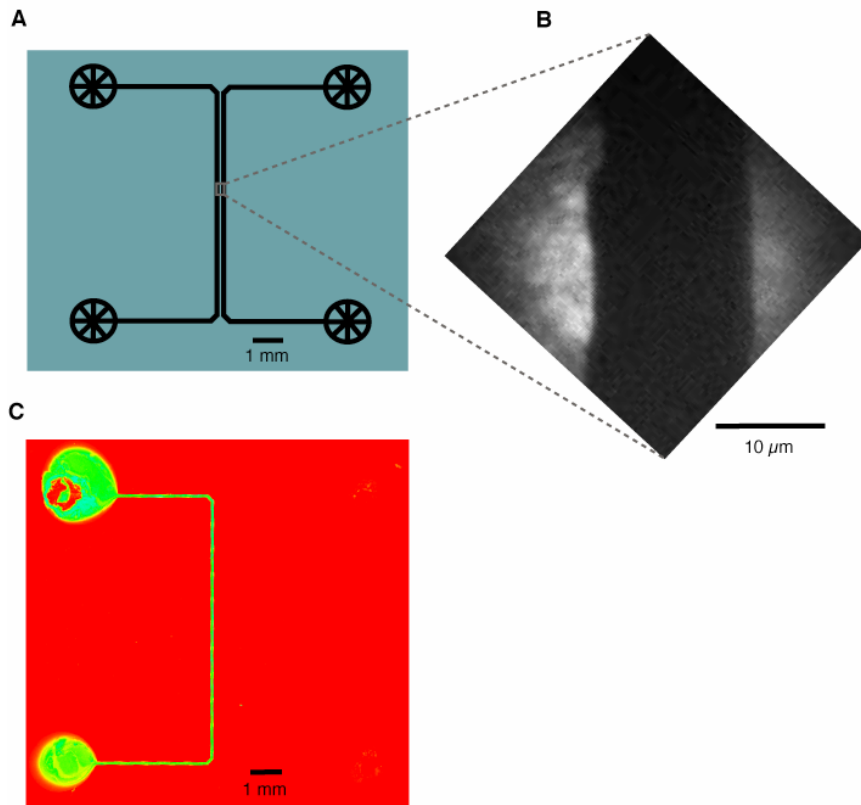


Fig. S3. Surface functionalization by means of PDMS flow channels. (A) Schematic illustration of the microstructured silicon wafer used as a mold for the PDMS elastomer. Each channel was 100 μm wide, 20 μm high, 2 cm long and separated by a 15- μm gap. Round microstructures were at both ends of each channel, where an inlet and outlet could be pierced into the cured PDMS flow channels. (B) TIRF image of the depot and target area and the 15- μm gap between them. The left channel serves as depot and the right as target area. For this image both areas were functionalized with fluorescently labeled DNA to make them visible. (C) Fluorescence image of a functionalized cover slip used for a typical cut-and-paste experiment.

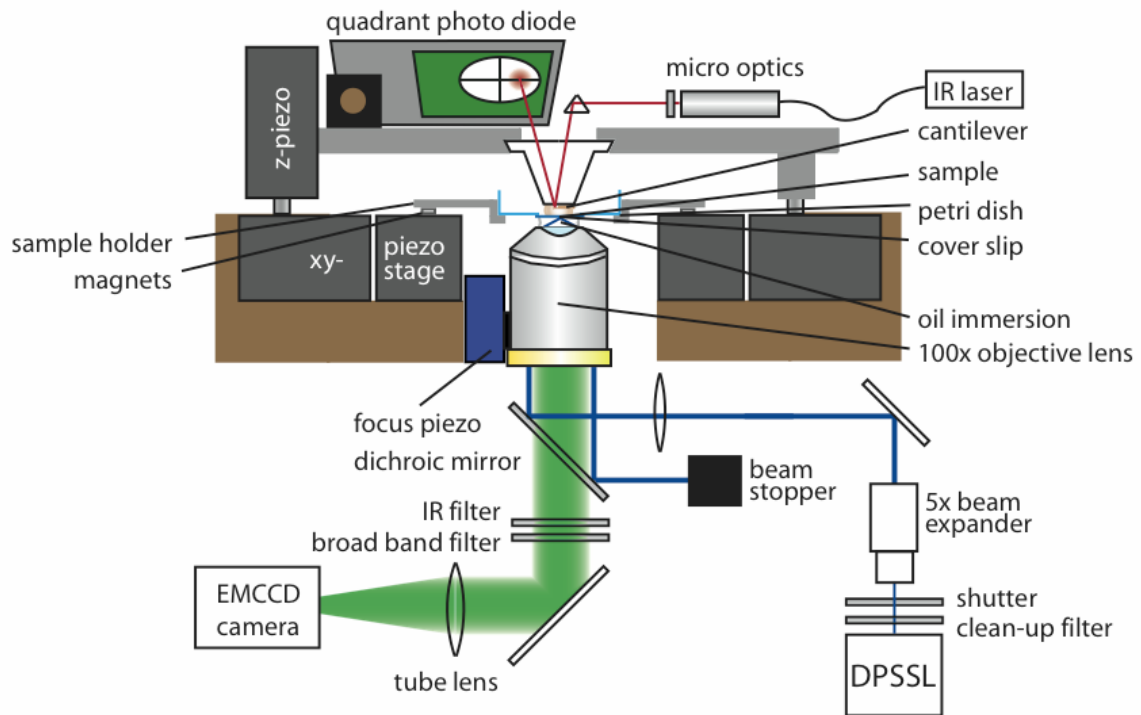


Fig. S4. Experimental setup. The combined TIRF-AFM setup comprises an inverted microscope for objective-type wide-field TIRF excitation and a custom built AFM installed on an x-y piezo scanning stage. The sample is situated on a cover slip glued into a drilled petri dish, which is mounted into a steel vessel that can be moved by the piezo scanner.

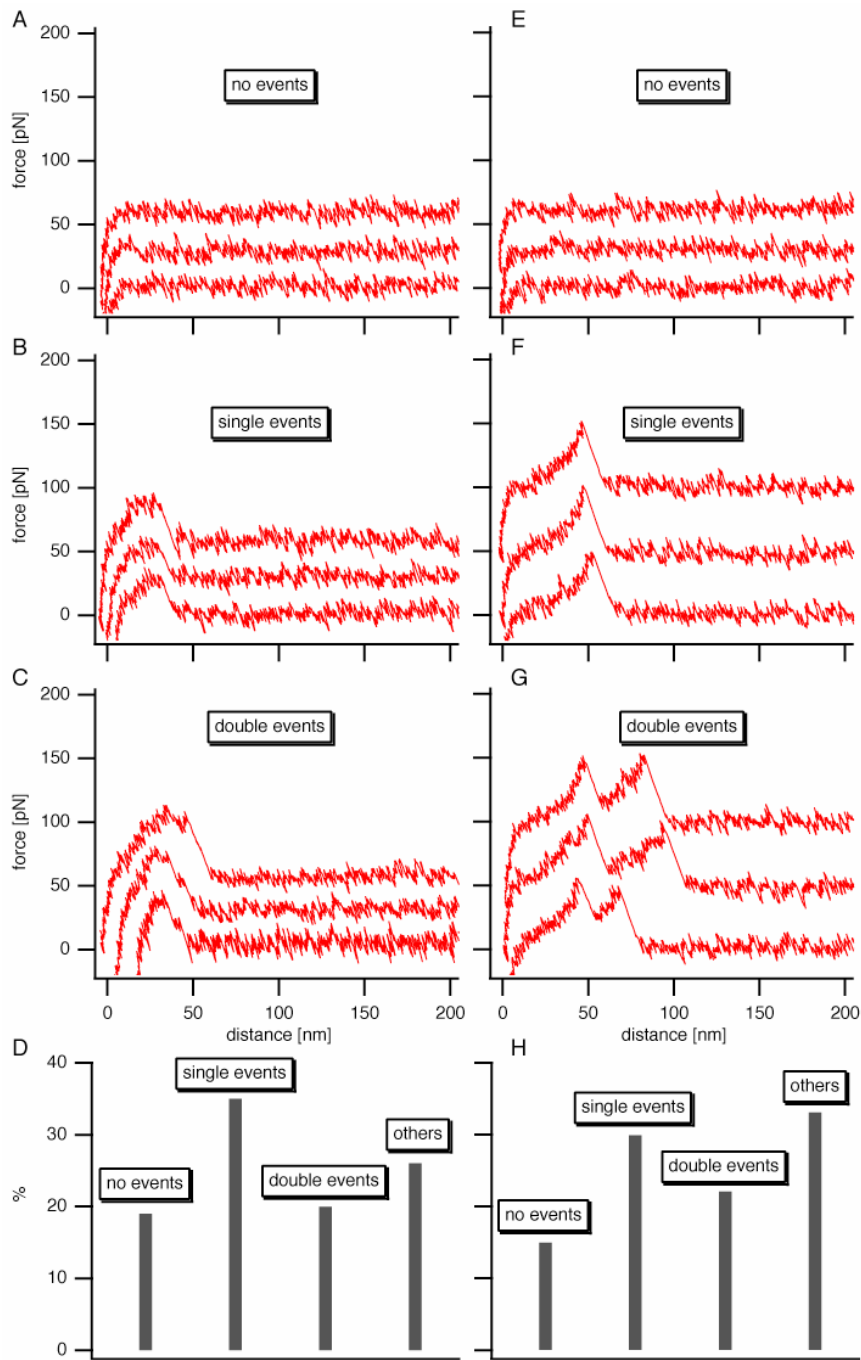


Fig. S5. Typical single-molecule force distance transfer protocols of the individual steps of the pick-up (A-C) and the delivery (E-G) and their statistical analysis (D) and (H). Double events are clearly distinguishable from single pick-ups or deliveries by the doubled height of the plateau or the multiple rupture peaks, respectively.

References

1. G. Neuert, C. Albrecht, E. Pamir, H. E. Gaub, *FEBS letters* **580**, 505 (2006).
2. J. Morfill *et al.*, *Biophys. J.* (June 8, 2007).
3. F. Kühner, R. Lugmaier, S. Mihatsch, H. E. Gaub, *Rev. Sci. Instrum.* **78** (2007).
4. H. J. Butt, M. Jaschke, *Nanotechnology* **6**, 1 (1995).
5. E.-L. Florin *et al.*, *Biosensors and Bioelectronics* **10**, 895 (1995).
6. T. Funatsu, Y. Harada, M. Tokunaga, K. Saito, T. Yanagida, *Nature* **374**, 555 (1995).

Anhang D

Super-Resolution Imaging of Fluorophore Patterns Deposited by Single-Molecule Cut-and-Paste

Stefan K. Kufer, Mathias Strackharn, Stefan W. Stahl, Hermann Gump, Elias M.
Puchner and Hermann E. Gaub

Nature Nanotechnology, eingereicht

In dieser Veröffentlichung wurde die Methode der SMCP-Oberflächenassemblierung verwendet, um mittels Einzelmolekülfluoreszenzmikroskopie die mechanisch kontrollierte Deposition einzelner Farbstoffmoleküle Schritt für Schritt zu beobachten. Die Positionen der einzeln deponierten Farbstoffmoleküle konnten durch Anfitten von zweidimensionalen Gaußkurven an die Intensitätsprofile mit Nanometerpräzision bestimmt werden. Dadurch war es möglich, die Ortsunsicherheit bei der SMCP-Oberflächenassemblierung zu bestimmen. Der experimentell bestimmte Wert von ca. ± 11 nm stimmt sehr gut mit dem theoretisch errechneten Wert überein. Zudem wurden Strukturen aus mehreren einzelnen Fluorophoren erzeugt, deren Größe weit unterhalb der optischen Auflösungsgrenze liegt. Durch eine Kombination von Schwerpunktsbestimmung und Photobleichen konnten die Positionen der individuellen Fluorophore trotzdem bestimmt werden.

Super-Resolution Imaging of a Fluorophore Pattern Assembled by Single-Molecule Cut-and-Paste

Stefan K. Kufer¹, Mathias Strackharn¹, Stefan W. Stahl¹, Hermann Gumpf¹, Elias M. Puchner¹ and Hermann E. Gaub^{1*}

¹Center for Nanoscience & Physics Department, University Munich, Amalienstr. 54, 80799 Munich

*E-mail: Gaub@LMU.de

submitted to Nature Nanotechnology

Super-resolution imaging¹⁻¹⁰ of a diffraction limited spot consisting of multiple fluorophores was demonstrated on randomly adsorbed DNA duplexes carrying several dye molecules⁶⁻⁹. We used single-molecule cut-and-paste surface assembly¹¹ for the controlled deposition of individual fluorophores in well-defined nanometer sized patterns. Although the size of the pattern is far beyond the Abbe limit, the individual dyes could be identified by centroid localization combined with photobleaching. A hybrid TIRF-AFM setup allowed to monitor the deposition process of single fluorophores in real time and to determine their position with nanometer precision.

Objects smaller than the diffraction limit of an imaging system are projected as blurry spots with the size of a Rayleigh disc. Nonetheless the center position of these spots can be determined with an accuracy far beyond the Abbe limit^{12, 13}, and the precision is only limited by the number of photons collected from this object¹⁴. This way individual fluorophores can be localized with nanometer precision¹⁵. Multiple emitters within a diffraction limited spot may also be localized if their individual contributions to the overall signal can be discriminated either spectrally or by other means. In recent years various techniques, subsumed under the expression super-resolution imaging (SRI), have been developed, which use different methods to extract one high-resolution image from a series of low-resolution images^{6, 7, 9, 10, 16}. Such attempts may be employed to first separate the contributions of the individual molecules and then to reconstruct the ensemble. Several methods were suggested to create image sequences of single-fluorophores and to reconstruct the position of these fluorophores using different localization algorithms^{13, 14}.

Impressive proof of principle experiments for super-resolution imaging were reported in the literature, where samples were designed with different fluorophores on defined positions⁶⁻⁹. Predominantly DNA duplexes with modified bases were employed as molecular rulers for this purpose. This however limits the potential pattern to a linear arrangement of the dyes. We recently introduced a new means to assemble individual nanoscale functional units called single-molecule cut-and-paste (SMCP). It combines the precision of the atomic force microscope (AFM) with the selectivity of DNA hybridization. Here we employed this technique to assemble two-dimensional (2d) patterns of individual fluorophores, which we then subsequently localized by SRI.

The SMCP system used here uses a transfer DNA with an anchor and a handle sequence carrying a single Cy3 dye molecule. The anchor sequence provides a thermodynamically stable attachment of the transfer DNA in both the depot and the target area. The handle sequence allows pick up of the transfer DNA with the AFM tip and movement of the transfer DNA from the depot to the target. Binding geometry and overlap length of the oligomers were chosen such that this cut-and-paste process may be operated in cycles. Details of the underlying hierarchical system of unbinding forces are described in the supplement.

In Fig. 1 the deposition of a single fluorophore, which had previously been picked up from the depot area, is shown step by step. When the tip is lowered towards the target site (Fig. 1a black curve), the anchor sequence hybridizes with a complementary strand. When the tip is withdrawn from the surface, both sequences are loaded in shear mode but the shorter handle sequence ruptures first, and the transfer system remains at the target site (Fig. 1b). As a force distance curve of the deposition process is recorded, the paste process can be validated with this characteristic AFM fingerprint (Fig. 1a).

Advantageously the combined AFM-TIRF setup allows monitoring of the deposition process simultaneously with single-molecule fluorescence microscopy. As can be seen in Fig. 1c only a very low background signal is detected when the tip is far away from the surface. When the tip penetrates the evanescence excitation field, a strong fluorescence signal from the dye molecule is detected in the green channel of the camera. As the tip inelastically scatters light over a wide range of wavelengths¹⁷ the tip is visible in both, the red and the green detection channels. When the tip is withdrawn, the signal from the tip vanishes, but the dye emits photons at a constant rate until it suddenly bleaches in a single step. The movie M1 in the supplementary shows this deposition event in detail. The intensity time trace in Fig. 1d clearly shows the deposition of a single-molecule. The finding that this bleaching step size in fluorescence intensity remains the same throughout a large number of experiments together with the clear signature in the single-molecule force scans during deposition unambiguously shows that SMCP allows exquisite control of the deposition of individual fluorophores.

The position of this single-molecule can now be located by fitting Gaussians to the intensity images. The image sequence is collected

LETTERS

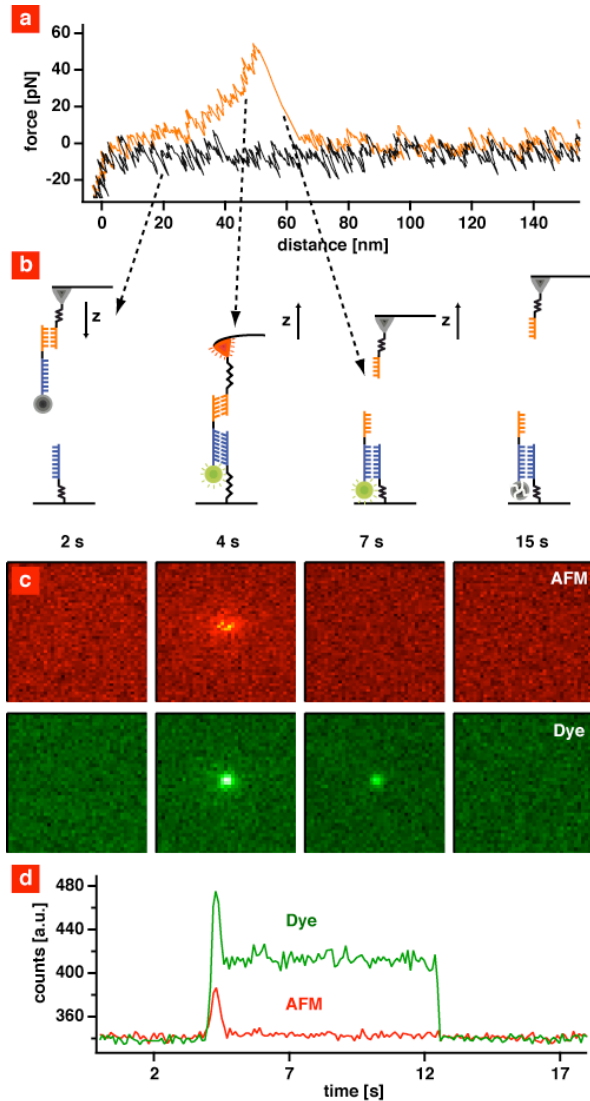


Figure. 1 Deposition of a single-molecule monitored simultaneously by AFM and TIRF microscopy. (a) Typical force distance curve of the deposition process. The transfer DNA is picked up from a depot and bound via a 20 bp DNA duplex to the tip. At the deposition site the tip was lowered until it contacts the surface (black curve) and a 30 bp DNA duplex in shear geometry is formed. By retracting the tip from the surface, the force acting on the polyethylene glycol–DNA complex gradually increases until the weakest bond in series ruptures (red curve). (b and c) Since the transfer DNA has a green fluorescence label and the tip inelastically scatters light over a broad range of wavelengths, it is possible to monitor the deposition process also with single-molecule fluorescence microscopy. As long as the tip is far away from the surface (2 s), no fluorescence is detectable in both channels. As soon as the tip penetrates the evanescent excitation field (4 s), a strong signal is detected in both channels. When the cantilever is retracted (7 s), the fluorescence from the tip vanishes whereas the fluorescently labeled transfer DNA remains anchored and emits photons at a constant rate. Finally the fluorophore photobleaches in a single step. (d) Intensity time traces at the deposition site. The red trace results solely from the tip, the green from the deposited fluorophore and inelastically scattered light from the tip. The position of this fluorophore is shown in Fig. 2.

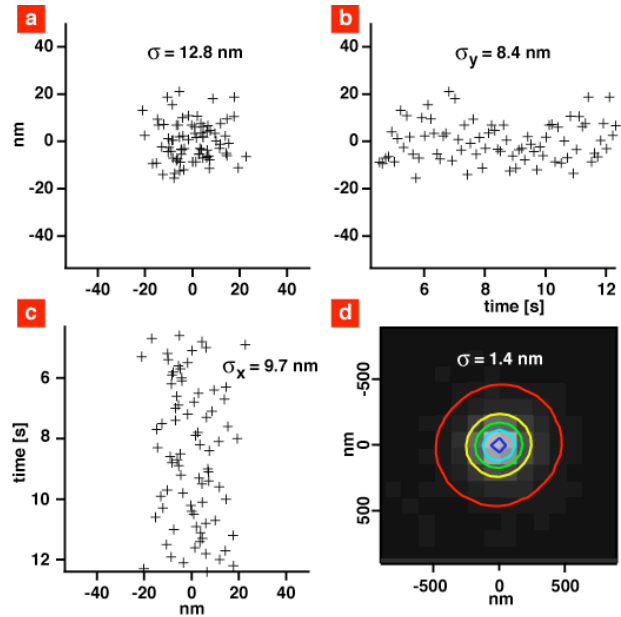


Figure 2 Nanometer precise localization of single-molecules. (a) To each frame during the lifetime of the single fluorophore deposited in Fig. 1, two-dimensional Gaussians were fitted. The temporal development of the x- and y-coordinates of the center are shown in (b) and (c). The intensity images were collected at a sampling rate of 10 Hz and the position accuracy of each fit is 13 nm. (d) Since the position of the dye was shown to be free of drift (b and c), an average intensity image of this period was summed and a single Gaussian was fit to it. The position accuracy of the optical part of the combined instrument was in this way determined to be ± 1.4 nm.

with a sampling rate of 10 Hz. This means that each frame of the movie is 100 ms long. To evaluate the mechanical stability of our combined instrument, we did not integrate the signal over the lifetime of the fluorophore. Instead for each frame the position of the fluorophore was determined and plotted in Fig. 2a. As can be seen no systematic drift of the molecule is observed and the standard deviation for the 100 ms localization was determined to be ± 13 nm. Fig. 2b and c show the temporal development of the x- and y-positions. As drift was negligible, the images were summed, whereby the S/N ratio of this image was roughly improved by a factor \sqrt{n} , where n is the number of images. This means when a single dye remains intact for about 8 s (80 frames) the S/N ratio increases by a factor of 9. Since an increase of the S/N ratio results in an increase of position accuracy, it is possible to improve the localization by calculating an averaged intensity image (Fig 2 d). This molecule that remained active for more than 8 s could thus be located with a precision better than ± 1.4 nm. This value is a benchmark for the accuracy with which we can determine the position of a single fluorophore.

Next, the spatial precision of the SMCP process was examined. As was pointed out by Smalley in his dispute with Drexler, "complete" mechanical control over an assembly process on the single-molecule level would hardly be possible because of two intrinsic fundamental limitations commonly referred as the fat and sticky finger problem. SMCP makes use of this seeming limitation in that it employs the selective "stickiness" between the DNA oligomers used for transfer and assembly. However, the spatial precision of the paste process is then limited by the size of the DNA-oligomer, by the functionalization density of the target area and by the rotational mobility of the oligomers to the surfaces. A sketch of this situation is given in Fig. 3a.

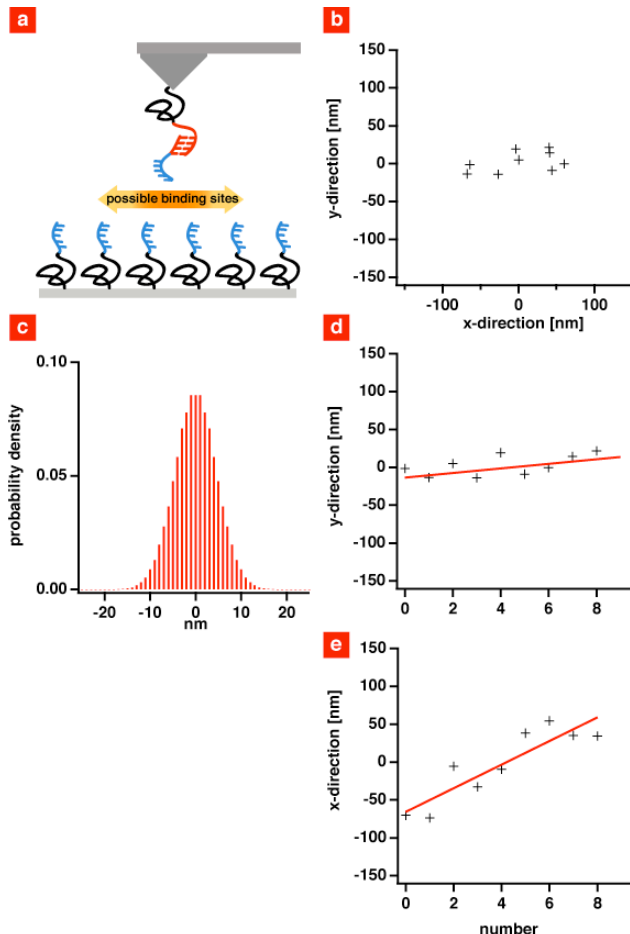


Figure 3 Long term drift and position accuracy of the SMCP process. (a) The tip of an AFM cantilever was covalently modified with a PEG-DNA complex to pick up transfer DNA strands. The substrate was also covalently modified with PEG-DNA complexes. (c) The probability density for the transfer DNA to find a certain anchor DNA is determined by a search process of the partners and could be calculated using a simple theoretical model. (b) To measure the position uncertainty, several single transfer DNA molecules were successively deposited on the same site of an image. The spatial uncertainty of the positions is comprised of both the SMCP process itself and the spatial drift of the setup. (d and e) The x - and y -positions of the deposited molecules are plotted against the number of the deposition event. A movie was recorded after each deposition process. To estimate the long term stability 5 minutes time intervals between subsequent depositions were chosen and the complete experiment lasted for about 45 minutes. During this time the experimental setup drifts laterally in the x - and y -directions. An estimate of the spatial uncertainty of the SMCP process itself can be obtained by subtracting the drift and is given by ± 11 nm.

Experimentally, the SMCP precision and the long-term stability of the setup were determined as follows. Several single-molecules were successively deposited at different positions on the target area. However, since only the sample was moved, the position of the deposited molecules relative to the optical axis of the instrument remained constant. For each deposition process a movie was recorded, and the positions of the pasted molecules were determined as described above. The positions of nine single fluorophores deposited in this way in intervals of five minutes are shown in Fig. 3b. The

spatial uncertainty of the experiment presented in Fig. 3b is comprised first of the SMCP process itself but also by spatial drift of the setup. In Fig. 3d and e the x - and y -coordinates are plotted against the number of the deposition event. Both plots clearly show a systematic and correlated drift. The drift in this particular example, which was chosen to highlight the advantage of our procedure to isolate potential artifacts, is mainly caused by temperature drift of the measurement system. An estimate of the SMCP process itself can be given by subtracting the drift (see lines in Fig. 3d and e) resulting in a precision of the y -position of ± 11 nm. Under the given conditions of spacer length and anchor density this value can be seen as a benchmark for the deposition precision.

This value agrees well with the predictions of the simple model depicted in Fig. 3a and c. Here we assumed the probability for the transfer oligomer to find an anchor oligomer while approaching the surface to be determined by a search process of the partners, both of which are constrained to the surface by PEG spacers. Provided the approach is slow compared to the search process, the area that the oligomers sample prior to finding a partner will depend on the functionalization density, the oligomer length and the end-to-end distance of the spacers. The nearly Gaussian distribution given in Fig. 3c is the result of the calculation given in the supplement.

In order to demonstrate the possibility to assemble and resolve pattern comprised of several single fluorophores we pasted six spots with a distance of $1 \mu\text{m}$ (Fig. 4a). Each spot was assembled in nine SMCP cycles as sketched in Fig. 4a. However, on average only in every second attempt a fluorophore was deposited. The goal was to identify the location of the pasted molecules by optical means. The intensity time trace of the 16 pixel sized diffraction limited spot #4 is shown in Fig. 4b. The stepwise decay with an exponential envelope is a clear indication for uncorrelated subsequent single fluorophore photobleaching. This stepwise decay of the overall intensity is also seen in the sequence of images in Fig. 4c. This sequence also contains the positional information. We used the sequential photobleaching of the fluorophores to discriminate between them in the following way. The last plateau stems from the last single fluorophore. Therefore the centroid of the corresponding image gives its position. The second to last plateau stems from the last and the second to last fluorophore. We subtracted the image of the last plateau from the image corresponding to the second to last fluorophore; its centroid was determined. With this iterative analysis we determined the position of the remaining fluorophores (Fig. 4d). As can be seen in Fig. 4e, the measured positions agree well with the expected positions in the assembly pattern. As can also be seen, the size of the error bars increases with decreasing lifetime of the fluorophore. We therefore restricted our quantitative analysis to the last 4 molecules. Nevertheless the precision of the localization of the pasted molecules within the diffraction limited ensemble by means of SRI turned out to be as good as ± 12 nm.

In summary, we have demonstrated that SMCP surface assembly combined with SRI allows monitoring of the deposition process of single fluorophores in real time and determination of the position of the deposited molecules with nanometer precision. The precision of the SMCP process was determined to ± 11 nm. This value could be improved considerably by using shorter spacers and by an optimized system of unbinding forces, e.g. by employing covalent anchor chemistry in the target area. In doing so, patterns of arbitrary shape and with arbitrary numbers of single-molecules can be created. Such patterns could be used as test systems for novel SRI techniques but could also help to investigate dye-dye interactions in a very controlled manner. While in this study we have not exploited the potential to assemble different fluorophores in well-defined pattern and to analyze

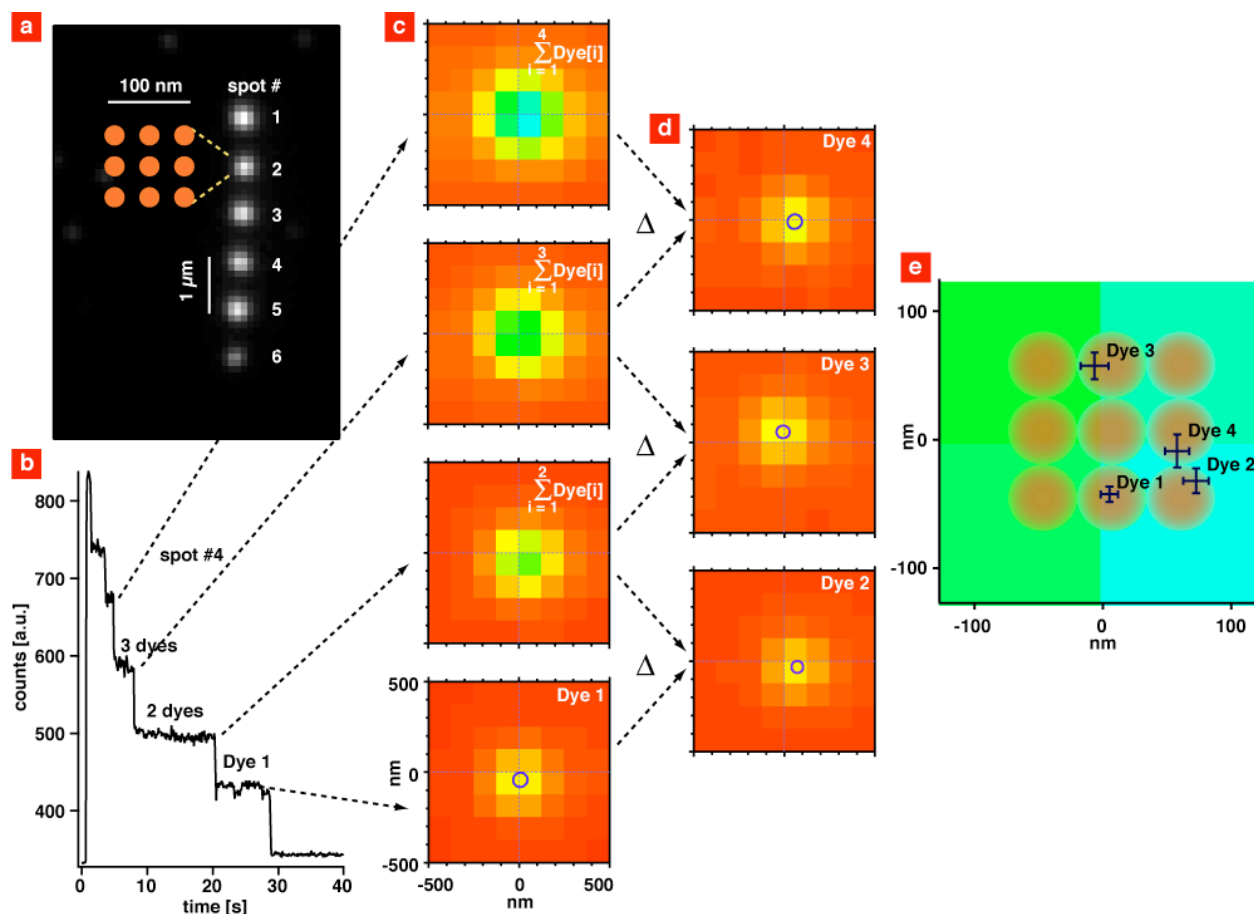


Figure 4 Super-resolution imaging with photobleaching. (a) Fluorescence micrograph of a pattern consisting of six spots with a distance of 1 μm . Each spot was assembled with nine single-molecule cut-and-paste cycles and deposited as sketched in the inset. (b) Intensity time trace of the diffraction limited spot #4. During excitation the Cy3 labels photobleach and show the typical stepwise decay of single fluorophores. After 20 s only one dye is left. (c) Average intensity images were calculated for periods of constant signal. (d) Subsequent images were subtracted to determine the intensity of the photobleached fluorophores, and 2d Gaussians were fit to each image. (e) The positions of the four dyes are shown in. The circles indicate the nine single-molecule cut-and-paste deposition sites, and their size indicates the uncertainty of the deposition.

their resulting spectral properties, such investigations are feasible and expected to shed new light on the interaction among fluorophores but also between dye molecules and photonic nanostructures or optically active nanoparticles¹⁸.

METHODS

SAMPLE-PREPARATION

Depot and target areas were prepared on a cover slip as described in¹¹. Briefly, cover slips were amino functionalized and covalently modified with NHS-PEG-maleimide ($M = 5000$ g/mol, Nektar, Huntsville, Alabama, USA). After rinsing with H_2O , a PDMS flow chamber with two channels was mounted on one cover slip. Both channels were connected to a peristaltic pump. The anchor oligomers for the depot and target area were reduced using TCEP solution (Pierce, Rockford, Illinois, USA) in order to generate free mercaptans. The left channel (depot area) was rinsed for 1 h with a 10- μM solution of depot anchor oligomers and the right one (target area) with a 10- μM solution of target anchor oligomers. Afterwards both channels were rinsed with H_2O to remove all non-covalently bound oligomers. The left channel (depot area) was rinsed with a 1- μM solution of transfer DNA dissolved in saline sodium citrate (SSC) buffer

(150 mM NaCl, 15 mM sodium citrate, pH 7) for 1 h. All oligomers used in this study were synthesized from IBA (IBA GmbH, Göttingen, Germany) and of HPLC-grade. After rinsing the depot channel for 5 min with SSC buffer to remove all non-hybridized transfer DNA, the PDMS flow chamber was removed and the cover slip was dried in a nitrogen stream. Finally the cover slip was mounted to the AFM-TIRF sample holder and immersed in SSC buffer.

TOTAL INTERNAL REFLECTION FLUORESCENCE (TIRF) MICROSCOPE

Single-molecule fluorescence microscopy was carried out in TIRF excitation. Fluorescence excitation of the Cy3 dyes is performed by a 532 nm, 75 mW DPSS laser (Crystalaser, Nevada, USA) through a 100x/1.49 oil immersion objective lens (Nikon CFI Apochromat TIRF, Japan), where the collimated laser beam is focused in the back focal plane of the objective lens such that the beam is totally reflected at the cover slip. Fluorescence light is split by color with a commercial Dual View (Optical Insights, Arizona, USA) with Brightline HC 582/75 (Semrock, New York, USA) and ET 700/75 (Chroma, Vermont, USA) as emission filters for the green and red channel respectively and a dichroic mirror with a cut-off wavelength of 630 nm (630DCLP). The emitted light is detected by a 512 x 512 pixel back-illuminated EMCCD camera (DU-897, Andor, Belfast, Ireland). Time series were recorded in frame-transfer

mode with an integration time of 100 ms per frame. The EMCCD chip was typically operated at a temperature of -75°C and an electron multiplication gain of 300x was used. The magnification was 96, i.e. 125 nm are imaged to one pixel.

AFM MEASUREMENTS

All SCMP experiments were performed with a custom build AFM¹⁹ at room temperature in SSC buffer. Silicon nitride cantilevers (MLCT-AUHW, Veeco Probes, Camarillo, California, USA) were amino functionalized and covalently modified with NHS-PEG-maleimide (M = 5000 g/mol, Nektar, Huntsville, Alabama, USA) as described in²⁰. The spring constant of the DNA modified cantilever was calibrated in solution using the equipartition theorem^{21, 22}. This method yielded a spring constant of 12.9 pN/nm and a resonance frequency of 1.24 kHz for the cantilever used in this study. The tip was withdrawn from the surface at a speed of 1500 nm/s until it was 2 μm above the surface. The protocol for the SMCP as well as the data recording was programmed using Igor Pro 5.03 (Wave Metrics, Lake Oswego, Oregon, USA). An Asylum Research controller, which provides ADC and DAC channels as well as a DSP board, was used for setting up feedback loops. Cantilever positioning for pickup and delivery was controlled in closed-loop operation. The precision was set to ±4 nm.

DATA-ANALYSIS

Fluorescence images were analyzed with Igor Pro 6.01 (Wave Metrics, Lake Oswego, Oregon, USA). Intensity time traces were produced by calculating the average intensity over 4 x 4 pixels in every frame. Centroid localization of a single-molecule was performed by fitting a 2d Gaussian distribution to a 11 x 11 pixel sized diffraction limited image. For localizing the positions of each fluorophore within a cluster, the individual contributions to the intensity images were extracted as follows: An average intensity image was calculated for every period of constant signal. Then subsequent images were subtracted from each other and the differences display the average intensities of the contributing fluorophores. The positions of the fluorophores were again determined by fitting 2d Gaussians.

REFERENCES

- Betzig, E. & Trautman, J.K. Near-Field Optics: Microscopy, Spectroscopy, and Surface Modification Beyond the Diffraction Limit. *Science* **257**, 189-195 (1992).
- Xie, X.S. & Dunn, R.C. Probing Single Molecule Dynamics. *Science* **265**, 361-364 (1994).
- Hell, S.W. & Wichmann, J. Breaking the diffraction resolution limit by stimulated emission: stimulated-emission-depletion fluorescence microscopy. *Opt. Lett.* **19**, 780 (1994).
- Lacoste, T.D. et al. Ultrahigh-resolution multicolor colocalization of single fluorescent probes. *Proceedings of the National Academy of Sciences* **97**, 9461-9466 (2000).
- Dyba, M. & Hell, S.W. Focal Spots of Size $\lambda/23$ Open Up Far-Field Fluorescence Microscopy at 33 nm Axial Resolution. *Physical Review Letters* **88**, 163901 (2002).
- Gordon, M.P., Ha, T. & Selvin, P.R. Single-molecule high-resolution imaging with photobleaching. *Proceedings of the National Academy of Sciences* **101**, 6462-6465 (2004).
- Qu, X., Wu, D., Mets, L. & Scherer, N.F. Nanometer-localized multiple single-molecule fluorescence microscopy. *Proceedings of the National Academy of Sciences* **101**, 11298-11303 (2004).
- Churchman, L.S., Okten, Z., Rock, R.S., Dawson, J.F. & Spudich, J.A. Single molecule high-resolution colocalization of Cy3 and Cy5 attached to macromolecules measures intramolecular distances through time. *Proceedings of the National Academy of Sciences* **102**, 1419-1423 (2005).
- Rust, M.J., Bates, M. & Zhuang, X. Sub-diffraction-limit imaging by stochastic optical reconstruction microscopy (STORM). *Nat Meth* **3**, 793-796 (2006).
- Betzig, E. et al. Imaging Intracellular Fluorescent Proteins at Nanometer Resolution. *Science* **313**, 1642-1645 (2006).
- Kufer, S.K., Puchner, E.M., Gumpp, H., Liedl, T. & Gaub, H.E. Single-Molecule Cut-and-Paste Surface Assembly. *Science* **319**, 594-596 (2008).
- Bobroff, N. Position measurement with a resolution and noise-limited instrument. *Review of Scientific Instruments* **57**, 1152-1157 (1986).
- Thompson, R.E., Larson, D.R. & Webb, W.W. Precise Nanometer Localization Analysis for Individual Fluorescent Probes. *Biophys. J.* **82**, 2775-2783 (2002).
- Ober, R.J., Ram, S. & Ward, E.S. Localization Accuracy in Single-Molecule Microscopy. *Biophys. J.* **86**, 1185-1200 (2004).
- Yildiz, A. et al. Myosin V Walks Hand-Over-Hand: Single Fluorophore Imaging with 1.5-nm Localization. *Science* **300**, 2061-2065 (2003).
- Tinnefeld, P. & Sauer, M. Branching Out of Single-Molecule Fluorescence Spectroscopy: Challenges for Chemistry and Influence on Biology. *Angewandte Chemie International Edition* **44**, 2642-2671 (2005).
- Gaiduk, A., Kühnemuth, R., Antonik, M. & Seidel, C.A.M. Optical Characteristics of Atomic Force Microscopy Tips for Single-Molecule Fluorescence Applications. *ChemPhysChem* **6**, 976-983 (2005).
- Bek, A. et al. Fluorescence Enhancement in Hot Spots of AFM-Designed Gold Nanoparticle Sandwiches. *Nano Lett.* **8**, 485-490 (2008).
- Kühner, F., Lugmaier, R., Mihatsch, S. & Gaub, H.E. Print your atomic force microscope. *Rev. Sci. Instrum.* **78** (2007).
- Morfill, J. et al. B-S Transition in Short Oligonucleotides. *Biophys. J.* (2007).
- Florin, E.L. et al. Sensing specific molecular interactions with the atomic force microscope. *Biosensors and Bioelectronics* **10**, 895-901 (1995).
- Butt, H.-J. & Jaschke, M. Calculation of thermal noise in atomic force microscopy. *Nanotechnology* **6**, 1-7 (1995).

ACKNOWLEDGEMENTS

We thank P. Tinnefeld and A. Fornof for helpful discussions. This work was supported by the German Science Foundation and the Nanosystems Initiative Munich.

Supplementary information

Super-Resolution Imaging of a Fluorophore Pattern Assembled by Single-Molecule Cut-and-Paste

Stefan K. Kufer¹, Mathias Strackharn¹, Stefan W. Stahl¹, Hermann Gump¹, Elias M. Puchner¹ and Hermann E. Gaub^{1*}

The SMCP force system:

The probe of an atomic force microscope (AFM) was used to assemble individual single stranded DNA (ssDNA) oligomers one by one in aqueous solutions at room temperature. The oligomers were stored on well-defined depot areas, picked up with the tip of an AFM cantilever and reassembled with nanometer precision on a spatially distinct target area. The storage, the pick up and the deposition of the DNA oligomers were realized by using an ordered system of unbinding forces based on DNA interactions.

The dissociation rates of DNA duplexes under load are highly dependent of loading geometries and DNA sequences respectively^{1,2}. When the duplex is stretched along its molecular axis, this means that the DNA duplex is loaded at opposite 5' ends or 3' ends, respectively, one speaks of "shear mode"¹ (Fig. S1e). The topological arrangement when double strands are loaded by pulling on the 5' and 3' extremities of one end of the duplex is called "unzip mode"³ (Fig. S1a). These two geometries are well distinguishable concerning their dissociation properties under load.

The rupture forces for DNA duplexes loaded in unzip mode are independent both of the length of the DNA sequence and the loading rate, but vary for G-C and A-T interactions. G-C pairing results in a dissociation force of 20 pN whereas A-T gives 10 pN². The dissociation forces for DNA duplexes loaded in shear geometry depend both on the length of the DNA sequence and the loading rate¹.

To connect the transfer DNA to the depot a 30 base pair (bp) long anchor sequence with mixed G-C and A-T is used (Fig. S1a). The transfer DNA has in addition to this 30 bp anchor sequence a 20 bp handle sequence for pick up. The AFM-tip is covalently modified with a ssDNA strand. Since this strand is complementary to the handle sequence a duplex is formed as the tip approaches the depot area (Fig. S1b). Then the tip is retraced from the depot the anchor sequence is loaded in unzip mode whereas the handle sequence in shear mode. Although the 30 bp anchor sequence is longer than the 20 bp handle sequence, its unbinding probability under load is much higher than for the handle sequence and the transfer DNA is picked up (Fig. S1c).

¹Center for Nanoscience & Physics Department, University Munich, Amalienstr. 54, 80799 Munich
* E-mail: Gaub@LMU.de

After translocation of the transfer DNA to its target site the cantilever is moved down. Since the target area is covalently modified with ssDNA oligomers that are complementary to the anchor sequence a 30 bp duplex in shear geometry is formed (Fig S1d). As the dissociation force of duplexes in shear geometry depends on the length of the DNA sequence the shorter handle sequence ruptures first and the transfer DNA is attached to the target site (Fig. S1e). The DNA sequences of the oligomers used in this study are shown in Fig. S2. The experimental setup for the SMCP process is shown in Fig. S3.

Theoretical calculation of the SCMP lateral uncertainty:

For an estimation of lateral uncertainty the total construct consisting of the transfer DNA attached to the cantilever DNA that again is bound to the tip by a PEG spacer was treated as two entropic springs connected by a stiff part (Fig. S4a). The first entropic spring corresponds to the free end of the transfer DNA. The handle duplex formed by the transfer DNA and cantilever DNA forms a stiff construct, and the PEG spacer again can be regarded as an entropic spring.

From the freely jointed chain (FJC) model⁴ we know that the distribution of end-to-end distances is

$$P(r) = \sqrt{\frac{3}{2\pi N b^2}} \exp\left(-\frac{3r^2}{2N b^2}\right),$$

where b is the Kuhn length of the Polymer and N the number of Kuhn monomers. The probability that the first entropic spring (PEG) has an end-to-end distance within the interval $[r_1, r_1+dr_1]$ and the second (ssDNA) within $[r_2, r_2+dr_2]$ is

$$P(r_1, r_2) dr_1 dr_2 = P_{PEG}(r_1) dr_1 \cdot P_{ssDNA}(r_2) dr_2.$$

This leads to the distribution of end-to-end distances of the total construct

$$P(r) = \frac{1}{A_1} \int_0^\infty \int_0^{2\pi} \int_0^{2\pi} e^{-\frac{3}{2b_{PEG}^2 N_{PEG}} r_1^2} \cdot e^{-\frac{3}{2b_{DNA}^2 N_{DNA}} \left(\sqrt{r_1^2 + d^2 + 2r_1 d \cos\phi} \cos\chi + \sqrt{(r_1^2 + d^2 - 2r_1 d \cos\phi)(\cos^2\chi - 1) + r_1^2} \right)^2} dr_1 d\phi d\chi$$

where A_1 is the normalization constant, d is the length of the stiff DNA duplex and ϕ and χ are the angles as depicted in Fig. S4a.

The sticky end of the transfer DNA molecule attached to a cantilever tip would sample at least the lower half space with according to the probability given by this radial dependency.

If the tip approaches the functionalized surface (Fig. S4b) from infinity to a distance u above the surface the probability that the end of the transfer DNA binds in a certain distance v from the center of the distribution on the surface is given by all probabilities that the molecule end reaches points with distance v from the center of the distribution on the surface. This probability is given by the integral

$$P_{binding}(v) = \frac{1}{A_2} \int_{\sqrt{u^2+v^2}}^\infty P(r) dr$$

with A_2 again a normalization constant. We evaluated the integrals numerically with the parameters $b_{PEG}=1.1 \text{ nm}^4$, $N_{PEG}=27.4^5$, $b_{ssDNA}=1.5 \text{ nm}^6$ and $N_{DNA}=8^6$, and $d=6.8 \text{ nm}^6$. The sequence that hybridizes to the target anchor was considered as a sticky

end point with no extension. The end distance from the surface was chosen to be $u=10$ nm in order to not allow the surface to strongly disturb the radial distribution $P(r)$. A_1 and A_2 were chosen such that the area under the probability distributions becomes unity.

References:

1. Strunz, T., Oroszlan, K., Schafer, R. & Guntherodt, H.J. Dynamic force spectroscopy of single DNA molecules. *Proceedings of the National Academy of Sciences of the United States of America* **96**, 11277-11282 (1999).
2. Rief, M., Clausen-Schaumann, H. & Gaub, H.E. Sequence-dependent mechanics of single DNA molecules. *Nat Struct Biol* **6**, 346-349 (1999).
3. Levinthal, C. & Crane, H.R. On the Unwinding of DNA. *PNAS* **42**, 436-438 (1956).
4. Rubinstein, R.H.C. Polymer Physics. *Oxford University Press* (2005).
5. Oesterhelt, F., Rief, M. & Gaub, H.E. Single molecule force spectroscopy by AFM indicates helical structure of poly(ethylene-glycol) in water. *New Journal of Physics* **1** (1999).
6. Smith, S.B., Cui, Y.J. & Bustamante, C. Overstretching B-DNA: The elastic response of individual double-stranded and single-stranded DNA molecules. *Science* **271**, 795-799 (1996).

Figures:

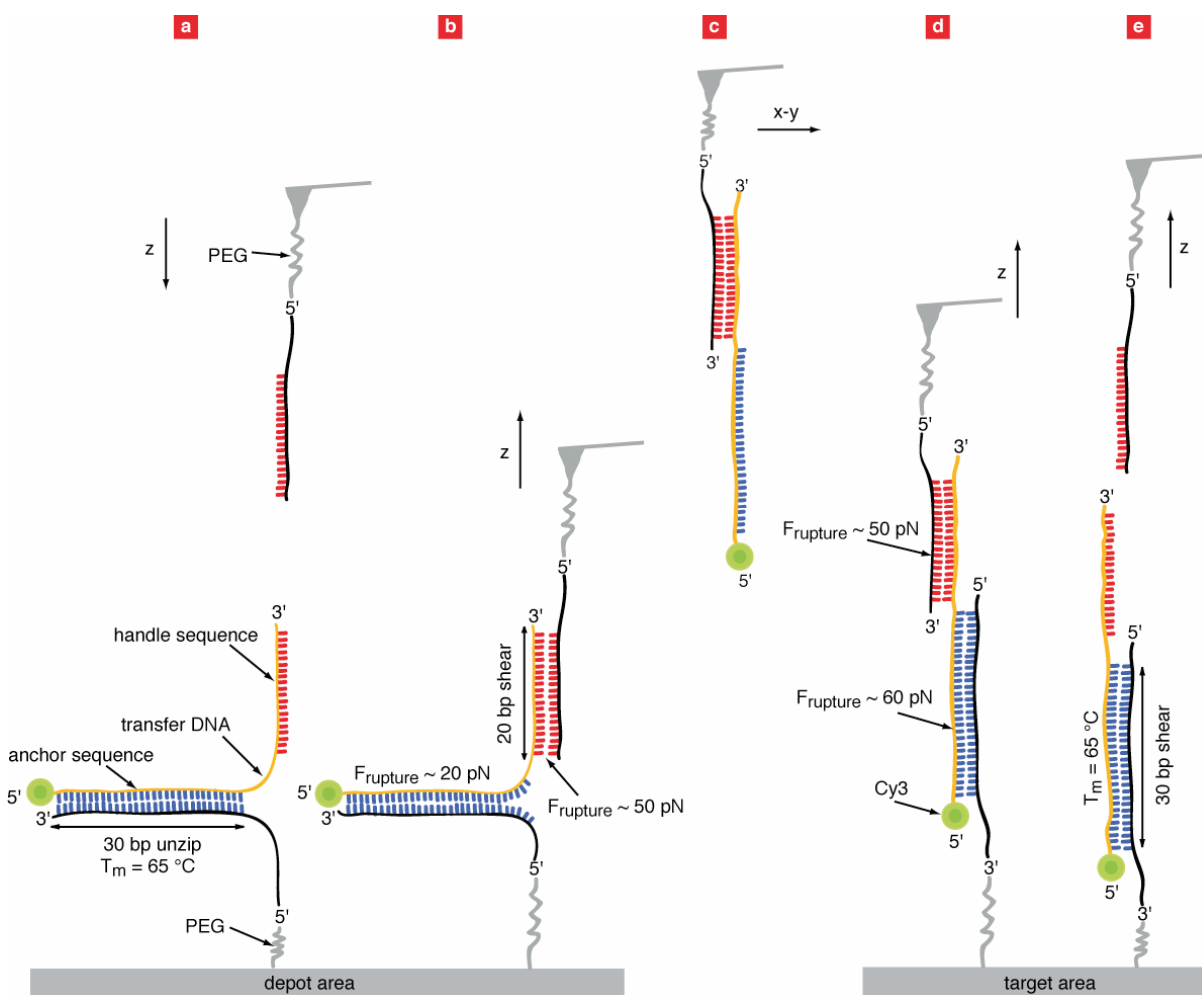


Fig. S1. Schematic illustration of the hierarchical force system. (a) To prevent unspecific adsorption, polyethyleneglycol (PEG) molecules are covalently attached to the target area. DNA oligomers, complementary to the anchor sequence of the transfer DNA, are covalently bonded with their 5' end to these PEG molecules. Transfer DNA oligomers, which were modified with Cy3 labels on the 5' end, are hybridized to this anchor sequences. The tip of an AFM cantilever is also covalently modified with PEG molecules and a single DNA oligomer, which is complementary to the handle sequence of the transfer DNA, is bonded covalently with its 5' end to a PEG molecule. (b) When the tip is in contact with the surface a duplex between the transfer DNA and the cantilever DNA is formed. When the tip is retracted the anchor sequence is loaded in unzip mode and the handle sequence in shear mode. As the unbinding probability for the anchor sequence is higher, the transfer DNA is picked up. (c and d) The target site is also covalently modified with PEG molecules. DNA oligomers, complementary to the anchor sequence of the transfer DNA, are bonded with their 3' end to the PEG molecules. After translocation the tip is moved down and a duplex is formed. When the tip is retracted the handle and the anchor sequences are loaded in shear mode, but this time the shorter handle sequence ruptures first and the transfer DNA is attached to its target site. The tip is now in its initial state and the cycle could be repeated over and over again.

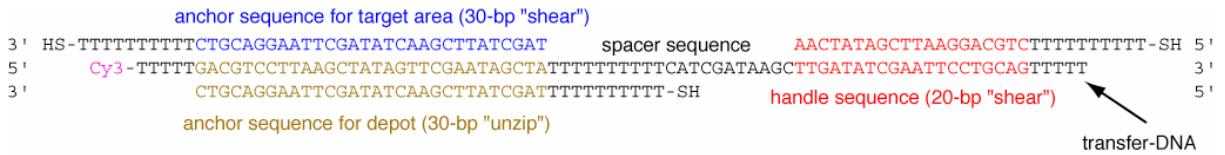


Fig. S2. Oligomers used in this study. The transfer DNA is 80 bp long and has a Cy3 label on the 5' end. The 30 bp long sequence on the 5' end is used to anchor the transfer DNA both to the depot and to the target site. The 20 bp long sequence on the 3' end is used as a handle for pick up. All oligomers were synthesized and purified (HPLC-grade) from IBA (IBA GmbH, Göttingen, Germany).

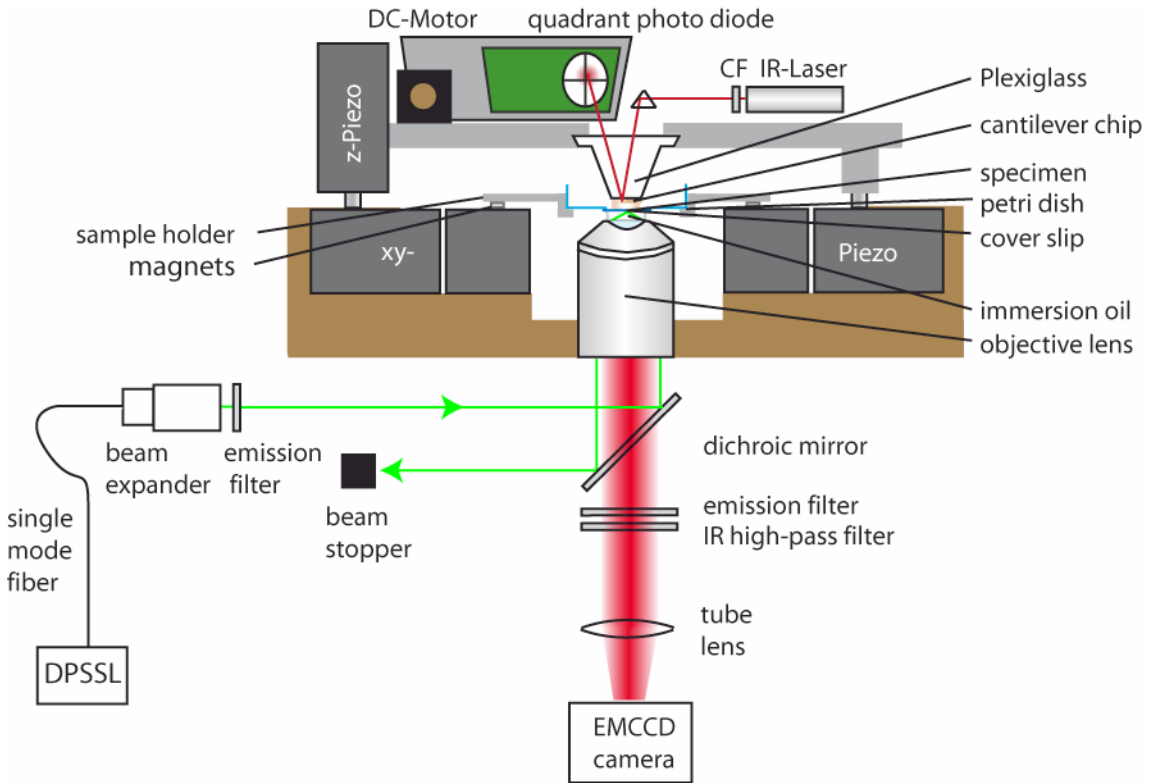


Fig. S3. Experimental setup. A custom built AFM, which is moveable in z direction via a piezo, is combined with an inverted microscope for objective-type wide-field TIRF excitation. The cover slip with the depot- and target areas on top is glued into a bored petri dish. The petri dish is placed in a sample holder, which is fixed through magnets on x-y piezo scanner.

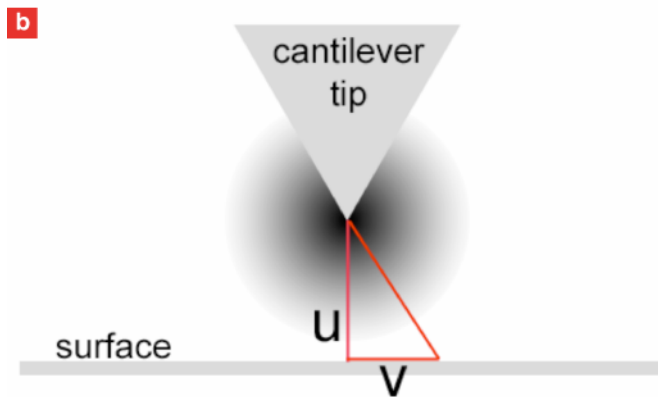
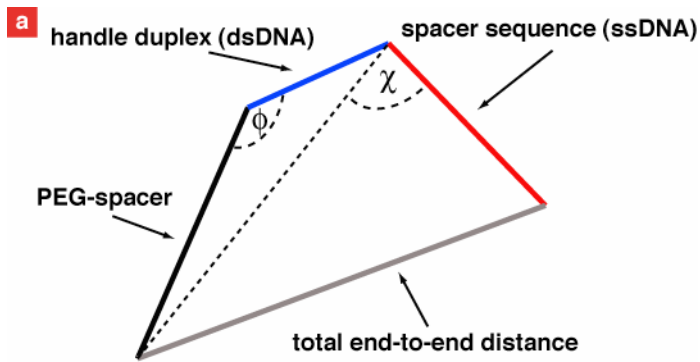


Fig. S4. Illustration of the theoretical model to calculate the spatial uncertainty of the SMCP process. a) The total end-to-end distance of the PEG-DNA complex is comprised of the PEG-spacer, the handle DNA-duplex, and the single stranded spacer sequence. The PEG-spacer and the single stranded spacer sequence are treated as entropic springs. Their end-to-end distance can easily be calculated using the freely jointed chain (FJC) model. The handle DNA-duplex is treated as a stiff part with the length $d=6.8$ nm. b) The cantilever approaches the surface until the distance is u . The binding probability distribution is calculated as a function of the distance v from the center of the distribution.

Anhang E

Nanoparticle self-assembly on a DNA-scaffold written by single-molecule cut-and-paste

Elias M. Puchner, Stefan K. Kufer, Stefan W. Stahl, Mathias Strackharn and Hermann E. Gaub

Nano Letters, eingereicht

In dieser Veröffentlichung wurde gezeigt, dass die Methode der SMCP-Oberflächenassemblierung dazu verwendet werden kann, Halbleiternanokristalle auf Oberflächen in beliebigen geometrischen Mustern anzuordnen. Dazu wurden die als Transfersystem dienenden DNA-Moleküle mit Biotin modifiziert und mittels SMCP assembliert. Streptavidin modifizierte Halbleiternanokristalle wurden anschließend an diese Muster angebunden. Die Größe der Muster variierte von nur wenigen Nanometern bis zu ausgedehnten viele Mikrometer großen Strukturen. An die Muster wurden exemplarisch Halbleiternanokristalle mit drei verschiedenen Emissionswellenlängen gebunden.

Nanoparticle self-assembly on a DNA-scaffold written by single-molecule cut-and-paste

Elias M. Puchner, Stefan K. Kufer, Mathias Strackharn, Stefan W. Stahl and Hermann E. Gaub

Center for Nanoscience & Physics Department, University Munich, Amalienstr. 54, 80799 Munich

submitted to Nano Letters

ABSTRACT

Nanoparticle self-assembly guided by molecular recognition has in the past been employed to assemble superstructures like nanoparticle molecules or hypercrystals. Recently molecule-by-molecule assembly of nanoscale superstructures was demonstrated also. Here we present a hybrid approach where we first assemble a pattern of binding sites one-by-one at a surface and then allow different nanoparticles to attach by self-assembly. For this, biotin bearing-DNA oligomers were picked up from a depot using a complementary DNA strand bound to an AFM tip. These units were deposited in the target area again by hybridization, forming a recognition pattern on this surface. Fluorescent semiconductor nanoparticles conjugated with streptavidin were allowed to assemble on this scaffold and form the final nanoparticle super structures.

Two fundamentally different strategies, commonly referred to as top-down or bottom-up, are feasible for the assembly of functional nano-systems. The bottom-up approach has two extremes. In the first the building blocks are allowed to self-assemble e.g. guided by molecular recognition, much in the way mother nature does in embryogenesis [1-7]. Alternatively the building blocks are assembled one-by-one e.g. using the tip of a scanning probe microscope, as we have demonstrated recently [8]. In this so called single-molecule cut-and-paste (SMCP) approach, we combine the precision of an AFM with the selectivity of DNA interaction. The units to be assembled, here biotins, are picked up with an AFM tip from a depot, where both the interaction of the unit with the depot surface as well as with the tip are mediated by specific DNA oligomers. Also the target area is covered with DNA oligomers. The interaction forces are chosen by geometry and by sequence such that the unit is first transferred from the depot to the tip and then from the tip to the target, allowing for a cyclic operation and thus the assembly of complex patterns of units. In this study we have merged these two very successful strategies of self- and one-by-one assembly. We combined molecule by molecule to assemble patterns of binding sites with the self-assembly of nanoparticles guided by specific molecular interactions to the scaffold.

The schematics of the surface assembly process of the binding scaffold is depicted in Fig 1. Both depot and target areas were functionalized with DNA anchor oligomers capable of hybridizing with the so-called transfer DNA via a 30 basepair (bp) DNA sequence. In the depot area the anchor oligomers are covalently attached with the 5' end and in the target area with the 3' end. The depot area was then loaded with the transfer DNA, which is used as a carrier for the binding site of the nanoparticles, in this case biotin. The transfer DNA is designed such that it hybridizes at its 5' end with the anchor sequence and has a 20 bp overhang at the 3'

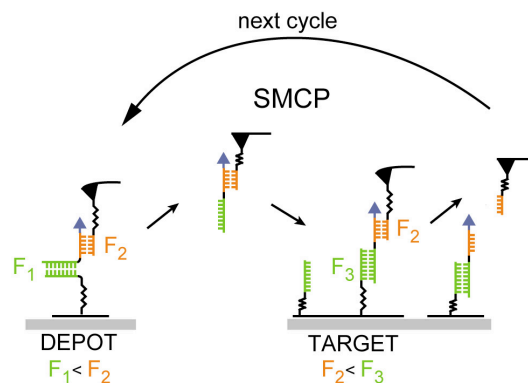


Figure 1. Schematics of SMCP process. The transfer DNA oligomers carry biotin as the functional binding site (blue). They are stored in the depot area through specific DNA hybridization (30 bp, green) to the covalently immobilized depot anchor oligomer in the zipper geometry. The overhanging sequence of the transfer DNA is complementary to a 20 bp sequence, which is covalently attached to a tip of an AFM cantilever. When the cantilever is brought into contact with the surface, a 20 bp duplex (yellow) in shear geometry is formed. Although the binding energy of the transfer DNA to the depot is higher, the unbinding force F_1 is lower than the unbinding force F_2 between the tip and the transfer DNA due to the different unbinding geometries (zipper vs. shear). Therefore the transfer DNA remains on the tip sequence upon retraction of the cantilever. The tip is then moved to the target area with nm-precision and again brought into contact with the surface. Here the free part of the transfer DNA hybridizes to the 30 bp target sequence in shear mode. Since its rupture force F_3 is the highest, the transfer DNA including its functional unit biotin remains on the target site when removing the cantilever. Having transferred one functional unit in this way, the tip sequence is free again for the next cut-and-paste cycle.

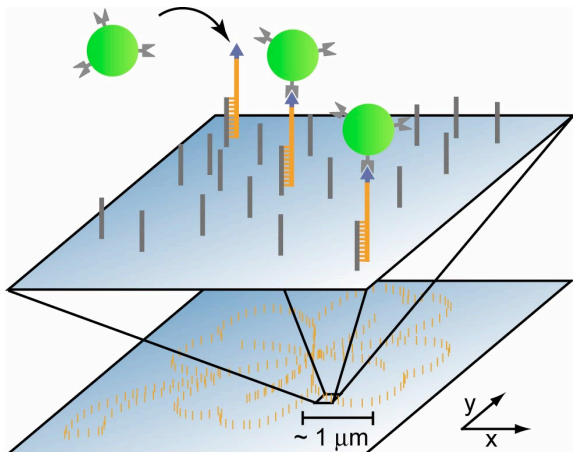


Figure 2. Sketch of the self-assembly of nanoparticles to a defined pattern guided by molecular recognition. SMCP allows the creation of DNA scaffolds of arbitrary shape and size. Here a $5\ \mu\text{m}$ sized pattern with the shape of a cloverleaf was created by transferring the biotin modified transfer DNAs one-by-one to the target area. The spacing of binding sites was chosen to be $100\ \text{nm}$. In a second step this DNA scaffold allows for the self-assembly of streptavidin conjugated nanoparticles to a superstructure.

end. An AFM cantilever was covalently functionalized with a $20\ \text{bp}$ DNA oligomer complementary to the overhang sequence. This cantilever was carefully lowered towards the depot surface allowing the tip oligomer to hybridize with the transfer DNA. This approach had been either stopped upon surface contact or alternatively, proximity had been detected by increased viscous damping of the tip vibrations and functional units were picked up. Typical force distance curves of this contact and non-contact pick up are shown in the supplement.

Upon withdrawing the tip from the surface the force that is built up in the molecular complex propagates through the two oligomers with the different geometries. Whereas the anchor duplex is loaded in unzip geometry, the tip duplex is loaded in shear geometry. As has been shown, the unbinding forces for these two configurations under load differ significantly [9,10]. The rationale behind this effect is that the mechanical work to overcome the binding energy is performed over paths of different length, resulting in different forces. Despite the higher thermodynamic stability of the $30\ \text{bp}$ anchor duplex compared to the $20\ \text{bp}$ tip duplex, the rupture probability for the anchor is higher by an order of magnitude than that of the tip duplex. For a quantitative analysis see [11]. As a result, the transfer DNA with the functional unit biotin is now bound to the tip and may be transferred to the target area.

At the target site the tip is lowered again, allowing the transfer DNA to hybridize at the chosen position with an anchor oligomer. Now, due to the different attachment both duplexes are loaded in shear geometry when the tip is withdrawn and the longer anchor oligomer keeps the transfer DNA bound, and the tip is free again and ready to pick up the next object. For a detailed description of this ordered system of unbinding forces and the experimental setup see the supplement.

All transfer steps are monitored online by force distance curves, which have clearly distinguishable fingerprints for each of the unzip or shear processes (see supplement). If needed each of the individual steps may be corrected or repeated. It should be pointed out here that this hierarchy of binding forces, which is the basis of this single-molecule cut-and-paste surface assembly (SMCP), may be established by a variety of interactions of physical, chemical or biological nature. We chose DNA here since its properties are conveniently

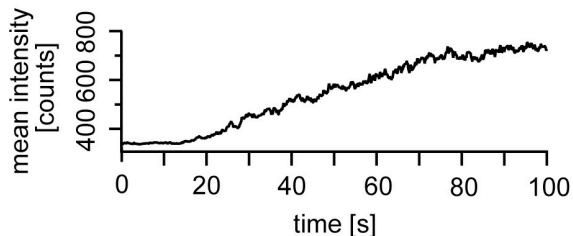
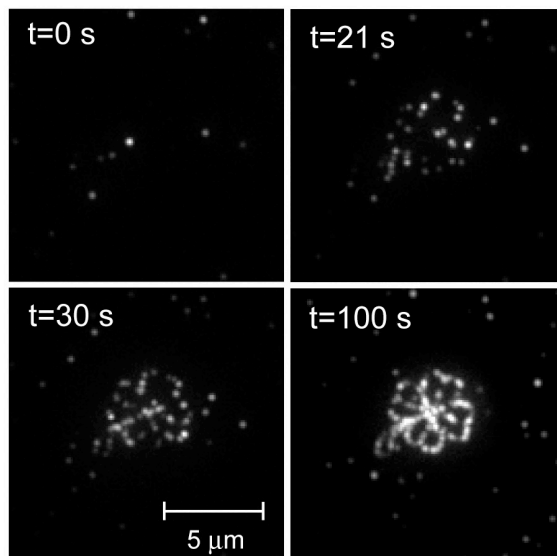


Figure 3. Time evolution of the nanoparticle superstructure formation.

At time $t=0$, streptavidin conjugated nanoparticles were incubated on the sample at a concentration of $500\ \text{pM}$. After approximately 20 seconds, the particles are close to the surface and start to specifically bind to the biotin-DNA scaffold until saturation is reached. The binding kinetics was traced by plotting the mean intensity of the observed area against the time (bottom). After already $100\ \text{s}$ the formation was completed.

programmed by their sequence and geometry. It should also be mentioned that although the AFM potentially has sub-Angstrom positioning precision, the use of the polymeric spacers that we employ for the attachment of the DNA oligomers to the tip and the surface, reduces this precision to the $10\ \text{nm}$ range, which for our purpose is easily tolerable.

Following this protocol we now assembled a pattern of attachment points at the target site. We placed individual biotins $100\ \text{nm}$ apart from each other along the outline of a cloverleaf. This is schematically shown in Fig 2. We then incubated the sample with a $500\ \text{pM}$ solution of fluorescent nanoparticles carrying an average of 7 streptavidins, which recognize and selectively bind biotin [12]. We followed this process online by fluorescence microscopy in TIRF excitation. As can be seen in the picture series in Fig 3, the beads gradually assemble on the scaffold and finally decorate the outline of the cloverleaf. We encourage the reader to watch the movie of this nanoparticle attachment to the DNA scaffold published in the supplement, as it demonstrates this process in a much clearer way.

This self-assembly process on the predefined scaffold is completed within minutes. Because of the specific binding between biotin and streptavidin and the low concentration of only $500\ \text{pM}$ of the nanoparticles, nonspecific adhesion was negligible as can be seen in Fig 3. It is interesting to note that

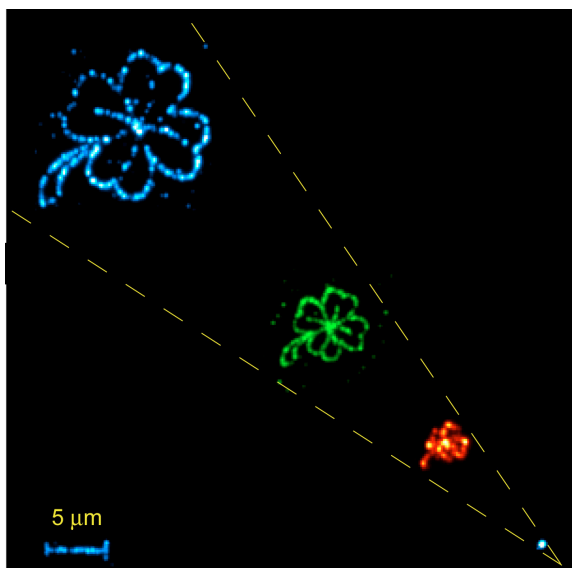


Figure 4. Nanoparticle superstructures of different sizes and compounds. To show the possibility to create freely programmable architectures of different compounds, the superstructure was scaled down and built with nanoparticles of different sizes. For the first cloverleaf (10 μm , blue) we used nanoparticles emitting at a wavelength of 525 nm, for the second one (5 μm , green), particles emitting at 565 nm and for the third one (2.5 μm , red), already close to the optical resolution, particles emitting at a wavelength of 705 nm. Please note that the 5 μm scalebar also represents a nanoparticle superstructure. The images are standard deviation maps of the recorded movies.

not all of the positions light up, although our transfer protocols corroborate that a biotin was deposited at these optical voids. A comparison of AFM images (not shown here) with the fluorescence images demonstrated that beads had bound at these positions. Obviously those nanoparticles had been optically inactive, a fact that was frequently described in the literature [13,14].

For demonstration purposes we rewrote the pattern in different sizes and allowed different nanoparticles to assemble on them (see Fig 4). Again a sizable fraction of the nanoparticles was optically inactive. In the assembly of the yellow pattern thermal drift caused a slight distortion of the pattern, but even the scale bar could be trustfully assembled. Since for this study we always used the biotin-streptavidin interaction as the coupler, only single component structures were assembled. However since a multitude of couplers with orthogonal affinities is available, the assembly of multicomponent structures would be straightforward [15,16].

Nanoparticle self-assembly guided by specific molecular interactions has in the past been very successfully used to design complex structures with novel functions promising a richness of new applications [17-22]. Here we have expanded this concept by a written scaffold and demonstrated that molecule-by-molecule assembly of a binding pattern combined with the self-assembly of semiconductor nanoparticles guided by molecular interactions is a straightforward and very general means to create nanoparticle superstructures [23]. Whereas the assembly of planar nanoparticle structures of arbitrary design can easily be assembled this way, an expansion into the third dimension appears challenging but achievable. Covalent crosslinking of the DNA oligomers after hybridization can be employed to stabilize the scaffold, and multifunctionality of the nanoparticles attachment sites may be used to build subsequent layers of structures. This could lead to a new dimension of complexity and novel effects.

Acknowledgment. We thank A. Fornof and P. Tinnefeld for helpful discussions. This work was supported by the German Science Foundation and the Nanosystems Initiative Munich (NIM).

References

- (1) Park, S.Y., A.K. Lytton-Jean, B. Lee, S. Weigand, G.C. Schatz, and C.A. Mirkin. 2008. DNA-programmable nanoparticle crystallization. *Nature* 451(7178):553-556.
- (2) Shevchenko, E.V., M. Ringler, A. Schwemer, D.V. Talapin, T.A. Klar, A.L. Rogach, J. Feldmann, and A.P. Alivisatos. 2008. Self-assembled binary superlattices of CdSe and Au nanocrystals and their fluorescence properties. *J Am Chem Soc* 130(11):3274-3275.
- (3) Nykypanchuk, D., M.M. Maye, D. van der Lelie, and O. Gang. 2008. DNA-guided crystallization of colloidal nanoparticles. *Nature* 451(7178):549-552.
- (4) Mirkin, C.A., R.L. Letsinger, R.C. Mucic, and J.J. Storhoff. 1996. A DNA-based method for rationally assembling nanoparticles into macroscopic materials. *Nature* 382(6592):607-609.
- (5) Alivisatos, A.P., K.P. Johnsson, X. Peng, T.E. Wilson, C.J. Loweth, M.P. Bruchez, Jr., and P.G. Schultz. 1996. Organization of 'nanocrystal molecules' using DNA. *Nature* 382(6592):609-611.
- (6) Maye, M.M., D. Nykypanchuk, D. van der Lelie, and O. Gang. 2007. DNA-regulated micro- and nanoparticle assembly. *Small* 3(10):1678-1682.
- (7) Mirkin, C.A. 2000. Programming the assembly of two- and three-dimensional architectures with DNA and nanoscale inorganic building blocks. *Inorg Chem* 39(11):2258-2272.
- (8) Kufer, S.K., E.M. Puchner, H. Gumpf, T. Liedl, and H.E. Gaub. 2008. Single-molecule cut-and-paste surface assembly. *Science* 319(5863):594-596.
- (9) Rief, M., H. Clausen-Schaumann, and H.E. Gaub. 1999. Sequence-dependent mechanics of single DNA molecules. *Nat Struct Biol* 6(4):346-349.
- (10) Strunz, T., K. Oroszlan, R. Schafer, and H.J. Guntherodt. 1999. Dynamic force spectroscopy of single DNA molecules. *Proc Natl Acad Sci U S A* 96(20):11277-11282.
- (11) Morfill, J., F. Kuhner, K. Blank, R.A. Lugmaier, J. Sedlmair, and H.E. Gaub. 2007. B-S transition in short oligonucleotides. *Biophys J* 93(7):2400-2409.
- (12) Mann, S., W. Shenton, M. Li, S. Connolly, and D. Fitzmaurice. 2000. Biologically programmed nanoparticle assembly. *ADVANCED MATERIALS* 12(12):147-150.
- (13) M. Kuno, D.P. Fromm, H.F. Hamann, A. Gallagher, D.J. Nesbitt. 2000. Nonexponential "blinking" kinetics of single CdSe quantum dots: A universal power law behavior. *The Journal of Chemical Physics* 112(7):3117-3120.
- (14) M. Kuno, D.P. Fromm, S.T. Johnson, A. Gallagher, D.J. Nesbitt. 2003. Modeling distributed kinetics in isolated semiconductor quantum dots. *Phys. Rev. B* 67(12):125304.
- (15) Lacoste, T.D., X. Michalet, F. Pinaud, D.S. Chemla, A.P. Alivisatos, and S. Weiss. 2000. Ultrahigh-resolution multicolor colocalization of single fluorescent probes. *Proc Natl Acad Sci U S A* 97(17):9461-9466.
- (16) Gerion, D., W.J. Parak, S.C. Williams, D. Zanchet, C.M. Micheel, and A.P. Alivisatos. 2002. Sorting fluorescent nanocrystals with DNA. *J Am Chem Soc* 124(24):7070-7074.
- (17) Bek, A., R. Jansen, M. Ringler, S. Mayilo, T.A. Klar, and J. Feldmann. 2008. Fluorescence enhancement in hot spots of AFM-designed gold nanoparticle sandwiches. *Nano Lett* 8(2):485-490.
- (18) Clapp, A.R., I.L. Medintz, H.T. Uyeda, B.R. Fisher, E.R. Goldman, M.G. Bawendi, and H. Mattoussi. 2005. Quantum dot-based multiplexed fluorescence resonance energy transfer. *J Am Chem Soc* 127(51):18212-18221.
- (19) Huang, Y., X. Duan, Y. Cui, L.J. Lauhon, K.H. Kim, and C.M. Lieber. 2001. Logic gates and computation from assembled nanowire building blocks. *Science* 294(5545):1313-1317.
- (20) Fu, A., W. Gu, B. Boussert, K. Koski, D. Gerion, L. Manna, M. Le Gros, C.A. Larabell, and A.P. Alivisatos. 2007. Semiconductor quantum rods as single molecule fluorescent biological labels. *Nano Lett* 7(1):179-182.

- (21) Brennan, J.L., N.S. Hatzakis, T.R. Tshikhudo, N. Dirvianskyte, V. Razumas, S. Patkar, J. Vind, A. Svendsen, R.J. Nolte, A.E. Rowan, and M. Brust. 2006. Bionanoconjugation via click chemistry: The creation of functional hybrids of lipases and gold nanoparticles. *Bioconjug Chem* 17(6):1373-1375.
- (22) Zhou, D., J.D. Piper, C. Abell, D. Klenerman, D.J. Kang, and L. Ying. 2005. Fluorescence resonance energy transfer between a quantum dot donor and a dye acceptor attached to DNA. *Chem Commun (Camb)*(38):4807-4809.
- (23) Pellegrino, T., S. Kuder, T. Liedl, A. Munoz Javier, L. Manna, and W.J. Parak. 2005. On the development of colloidal nanoparticles towards multifunctional structures and their possible use for biological applications. *Small* 1(1):48-63.

Supplementary Information

**Nanoparticle self-assembly on a
DNA-scaffold written by single-molecule
cut-and-paste**

E. M. Puchner, S. K. Kufer, M. Strackharn, S. Stahl and H. E. Gaub*

Center for Nanoscience & Physics Department, University Munich,
Amalienstr. 54, 80799 Munich

*To whom correspondence should be addressed.
Email: gaub@lmu.de

Sample Preparation

Depot and target areas were prepared on a cover slip as described in [1]. Briefly, cover slips were amino functionalized and covalently modified with NHS-PEG-maleimide ($M = 5000$ g/mol, Nektar, Huntsville, Alabama, USA). After rinsing with H_2O , a PDMS flow chamber with two channels was mounted on one cover slip. Both channels were connected to a peristaltic pump. The anchor oligomers for the depot and target area were reduced using TCEP solution (Pierce, Rockford, Illinois, USA) in order to generate free mercaptans. The left channel (depot area) was rinsed for 1 h with a $10\text{-}\mu\text{M}$ solution of depot anchor oligomers and the right one (target area) with a $10\text{-}\mu\text{M}$ solution of target anchor oligomers. Afterwards both channels were rinsed with H_2O to remove all non-covalently bound oligomers. The left channel (depot area) was rinsed with a $1\text{-}\mu\text{M}$ solution of transfer DNA dissolved in saline sodium citrate (SSC) buffer (150 mM NaCl, 15 mM sodium citrate, pH 7) for 1 h. All oligomers used in this study were synthesized from IBA (IBA GmbH, Göttingen, Germany) and of HPLC-grade. After rinsing the depot channel for 5 min with SSC buffer to remove all non-hybridized transfer DNA, the PDMS flow chamber was removed and the cover slip was dried in a nitrogen stream. Finally the cover slip was mounted to the AFM-TIRF sample holder and immersed in SSC buffer.

AFM Measurements

All SCMP experiments were performed with a custom build combined AFM [2] at room temperature in SSC buffer (Fig. S1). Silicon nitride cantilevers (MLCT-AUHW, Veeco Probes, Camarillo, California, USA) were amino functionalized and covalently modified with NHS-PEG-maleimide ($M = 5000$ g/mol, Nektar, Huntsville, Alabama, USA) as described in [1]. The spring constant of the DNA modified cantilever was calibrated in solution using the equipartition [3,4]. This method yielded a spring constant of about 15 pN/nm and a resonance frequency of 1.24 kHz for the cantilever used in this study. The tip was withdrawn from the surface at a speed of 1500 nm/s until it was 2 μm above the surface. The protocol for the SMCP as well as the data recording was programmed using Igor Pro 5.03 (Wave Metrics, Lake Oswego, Oregon, USA). An Asylum Research controller, which provides ADC and DAC channels as well as a DSP board, was used for setting up feedback loops. Cantilever positioning for pickup and delivery was controlled in closed-loop operation. The precision was set to ± 4 nm.

Total Internal Reflection Fluorescence (TIRF) Microscope

Single-molecule fluorescence microscopy was carried out in TIRF excitation (Fig. S1). Fluorescence excitation of nanoparticles was performed by a 532 nm, 75 mW DPSS laser (Crystalaser, Nevada, USA) and by a 473nm, 100 mW DPSS laser (Ciel Laser Quantum, UK) through a 100x/1.49 oil immersion objective lens (Nikon CFI Aplanachromat TIRF, Japan), where the collimated laser beam is focused in the back focal plane of the objective lens such that the beam is totally reflected at the cover slip. Fluorescence light is either split by color with a commercial Dual View (Optical Insights, Arizona, USA) with Brightline HC 582/75 (Semrock, New York, USA) and ET 700/75 (Chroma, Vermont, USA) as emission filters for the green and red channel respectively and a dichroic mirror with a cut-off wavelength of 630 nm (630DCLP) when using 532 nm excitation or filtered by a bandpass filter HQ 525/50 (Chroma, Vermont, USA) when using 473 nm excitation wavelength. The emitted light is detected by a 512 x 512 pixel back-illuminated EMCCD camera (DU-897, Andor, Belfast,

Ireland). Time series were recorded in frame-transfer mode with an integration time of 100 ms per frame. The EMCCD chip was typically operated at a temperature of -75°C and an electron multiplication gain of 300x was used. The magnification was 96, i.e. 125 nm are imaged to one pixel.

The SMCP force system:

The probe of an atomic force microscope (AFM) was used to assemble individual single stranded DNA (ssDNA) oligomers one by one in aqueous solutions at room temperature. The oligomers were stored on well-defined depot areas, picked up with the tip of an AFM cantilever and reassembled with nanometer precision on a spatially distinct target area. The storage, the pick up and the deposition of the DNA oligomers were realized by using an ordered system of unbinding forces based on DNA interactions.

The dissociation rates of DNA duplexes under load are highly dependent of loading geometries and DNA sequences respectively [5,6]. When the duplex is stretched along its molecular axis, this means that the DNA duplex is loaded at opposite 5' ends or 3' ends, respectively, one speaks of "shear mode" [5] (Fig. S2e). The topological arrangement when double strands are loaded by pulling on the 5' and 3' extremities of one end of the duplex is called "unzip mode" [7] (Fig. S2a). These two geometries are well distinguishable concerning their dissociation properties under load.

The rupture forces for DNA duplexes loaded in unzip mode are independent both of the length of the DNA sequence and the loading rate, but vary for G-C and A-T interactions. G-C pairing results in a dissociation force of 20 pN whereas A-T gives 10 pN [6]. The dissociation forces for DNA duplexes loaded in shear geometry depend both on the length of the DNA sequence and the loading rate [5].

To connect the transfer DNA to the depot a 30 base pair (bp) long anchor sequence with mixed G-C and A-T is used (Fig. S2a). The transfer DNA has in addition to this 30 bp anchor sequence a 20 bp handle sequence for pick up. The AFM-tip is covalently modified with a ssDNA strand. Since this strand is complementary to the handle sequence a duplex is formed as the tip approaches the depot area (Fig. S2b). Then the tip is retraced from the depot the anchor sequence is loaded in unzip mode whereas the handle sequence in shear mode. Although the 30 bp anchor sequence is longer than the 20 bp handle sequence, its unbinding probability under load is much higher than for the handle sequence and the transfer DNA is picked up (Fig. S2c, Fig. 4).

After translocation of the transfer DNA to its target site the cantilever is moved down. Since the target area is covalently modified with ssDNA oligomers that are complementary to the anchor sequence a 30 bp duplex in shear geometry is formed (Fig S2d). As the dissociation force of duplexes in shear geometry depends on the length of the DNA sequence the shorter handle sequence ruptures first and the transfer DNA is attached to the target site (Fig. S2e, Fig. 4). The DNA sequences of the oligomers used in this study are shown in Fig. S3.

Hybridization of fluorescent nanoparticles to the DNA scaffold:

For the modification to the DNA-biotin scaffold, the following fluorescent semiconductor nanoparticles were used: Invitrogen, Germany, streptavidin conjugate, 1 μ M solution, Qdot 525 (colored blue), Qdot 565 (colored green), and Qdot 705 (colored red). The nanoparticles were incubated on the written DNA-biotin pattern at a final concentration of 500 pM in 0.1x SSC buffer. After about one minute, the self-assembly process of nanoparticles to the pattern was complete.

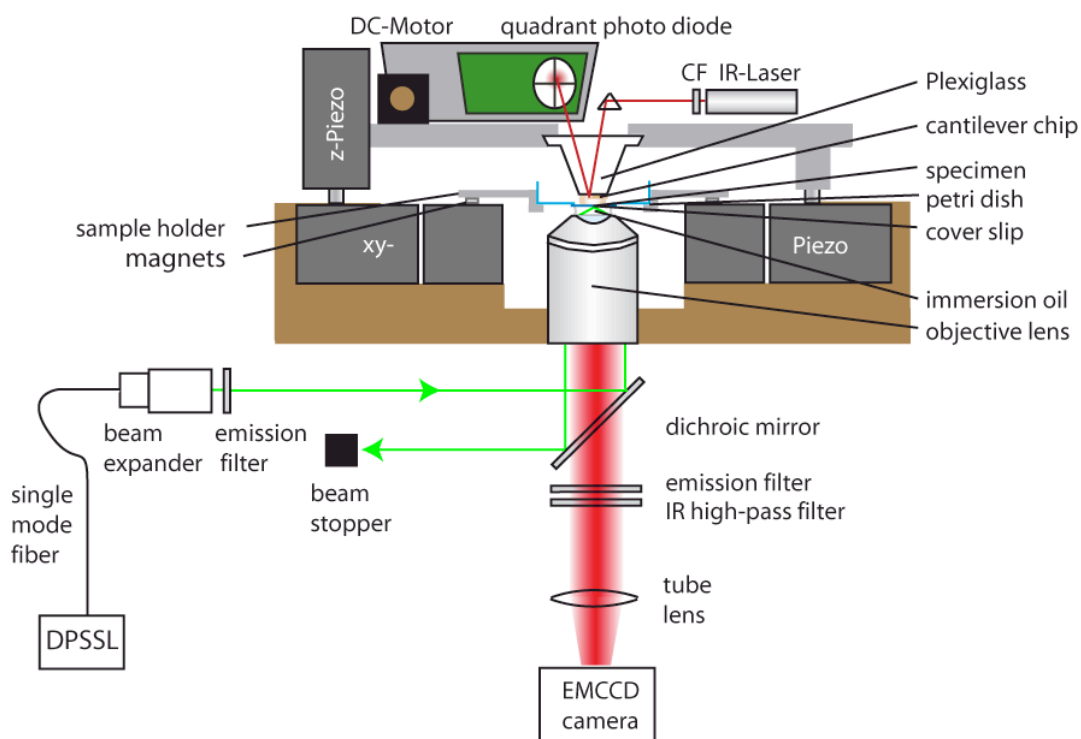


Fig. S1. Experimental setup. A custom built AFM, which is moveable in z direction via a piezo, is combined with an inverted microscope for objective-type TIRF excitation. The cover slip with the depot- and target areas on top is glued into a drilled petri dish. The petri dish is placed in a sample holder, which is fixed through magnets on x-y piezo scanner.

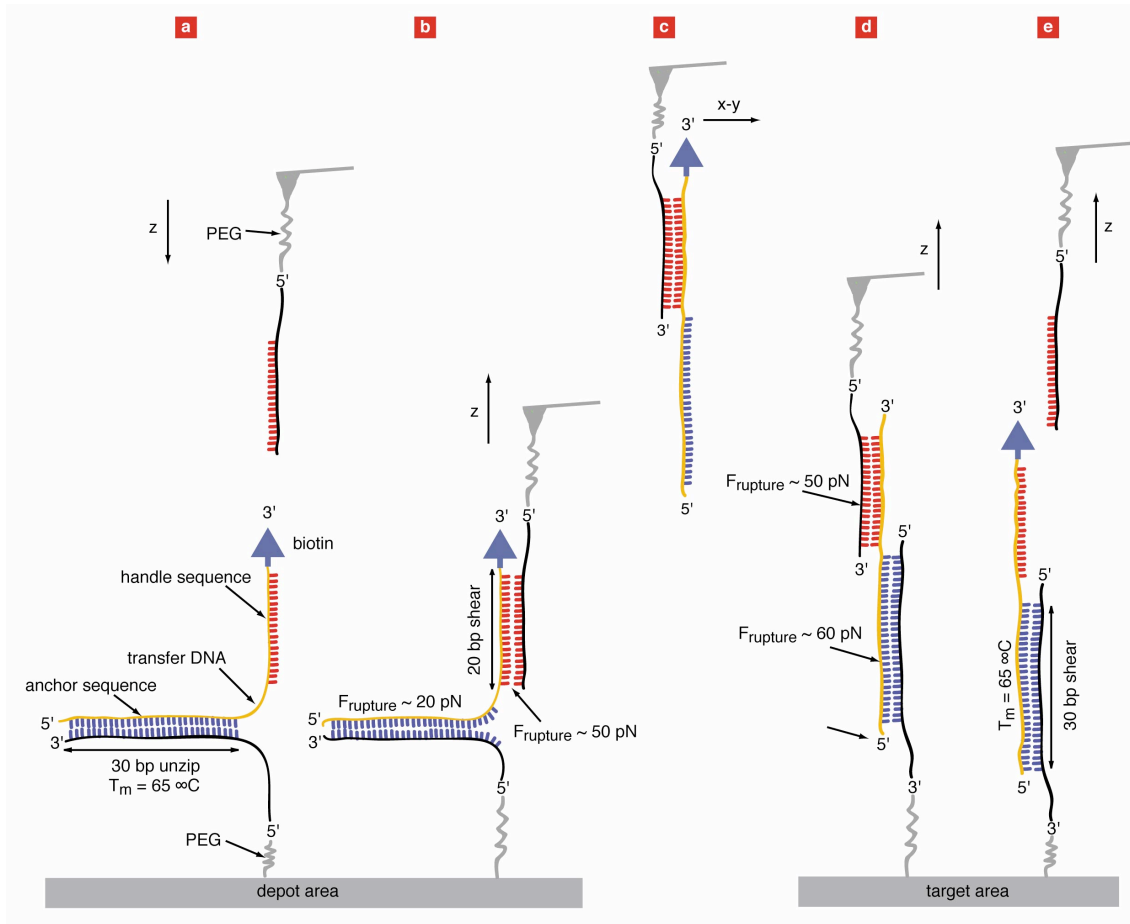


Fig. S2. Schematic illustration of the hierarchical force system. (a) To prevent unspecific adsorption, polyethyleneglycol (PEG) molecules are covalently attached to the target area. DNA oligomers, complementary to the anchor sequence of the transfer DNA, are covalently bonded with their 5' end to these PEG molecules. Transfer DNA oligomers, which were modified with biotin labels at the 3' end, are hybridized to this anchor sequences. The tip of an AFM cantilever is also covalently modified with PEG molecules and a single DNA oligomer, which is complementary to the handle sequence of the transfer DNA, is bonded covalently with its 5' end to a PEG molecule. (b) When the tip is in contact with the surface a duplex between the transfer DNA and the cantilever DNA is formed. When the tip is retracted the anchor sequence is loaded in unzip mode and the handle sequence in shear mode. As the unbinding probability for the anchor sequence is higher, the transfer DNA is picked up. (c and d) The target site is also covalently modified with PEG molecules. DNA oligomers, complementary to the anchor sequence of the transfer DNA, are bonded with their 3' end to the PEG molecules. After translocation the tip is moved down and a duplex is formed. When the tip is retracted the handle and the anchor sequences are loaded in shear mode, but this time the shorter handle sequence ruptures first and the transfer DNA is attached to its target site. The tip is now in its initial state and the cycle could be repeated over and over again.

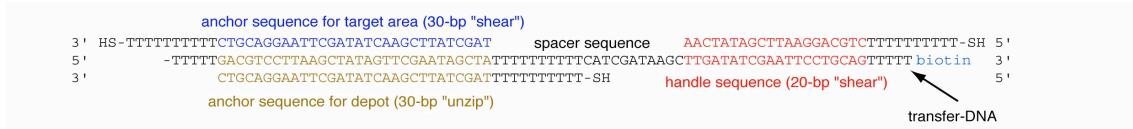


Fig. S3. Oligomers used in this study. The transfer DNA is 80 bp long and has a biotin label on the 3' end. The 30 bp long sequence on the 5' end is used to anchor the transfer DNA both to the depot and to the target site. The 20 bp long sequence on the 3' end is used as a handle for pick up. All oligomers were synthesized and purified (HPLC-grade) from IBA (IBA GmbH, Göttingen, Germany).

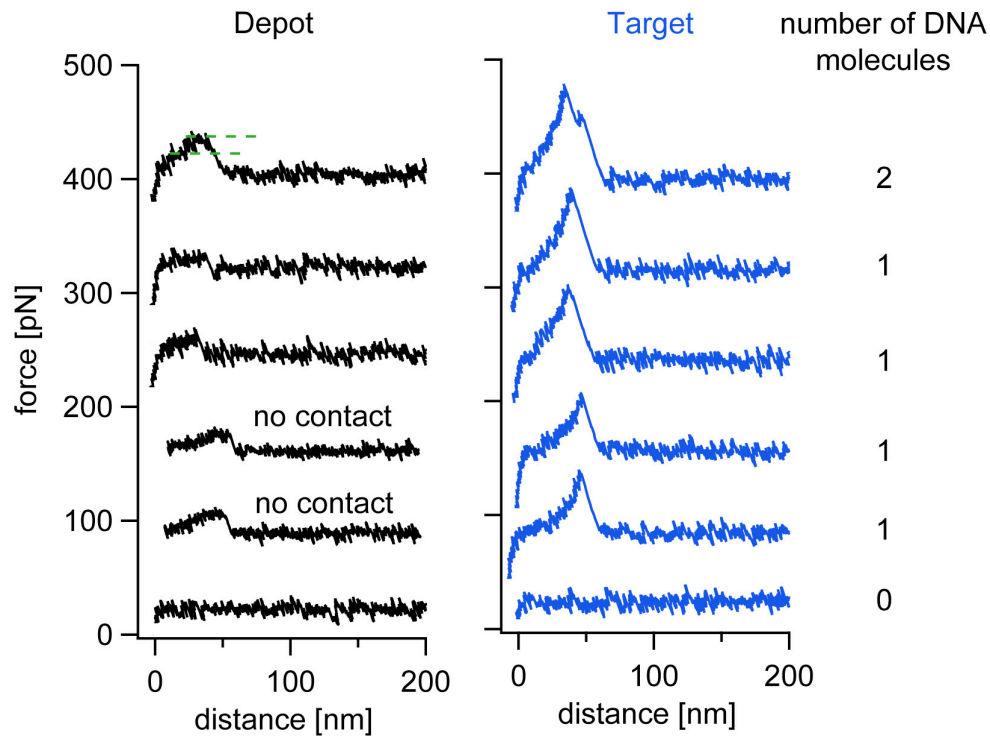


Fig. S4. Typical force distance curves of the depot and target region. In the depot region, the transfer DNA is separated from the depot oligomer in the zipper geometry. This separation process results in a force plateau of about 18 pN. As indicated, the transfer DNA can also be picked up without contacting the surface. In the target region the transfer DNA is separated from the tip oligomer in the shear geometry. Here, the force distance curves follows the elasticity of the PEG-spacer and the DNA until the DNA oligomers are separated at forces of about 50 pN. For each cut-and-paste cycle, the number of picked up and delivered DNA oligomers can be counted. As an example we show traces were two, one and no DNA molecule was detected.

References:

1. Kufer, S.K., Puchner, E.M., Gump, H., Liedl, T. & Gaub, H.E. Single-Molecule Cut-and-Paste Surface Assembly. *Science* 319, 594-596 (2008).
2. Kühner, F., Lugmaier, R., Mihatsch, S. & Gaub, H.E. Print your atomic force microscope. *Rev. Sci. Instrum.* 78 (2007).
3. Florin, E.L. et al. Sensing specific molecular interactions with the atomic force microscope. *Biosensors and Bioelectronics* 10, 895-901 (1995).
4. Butt, H.-J. & Jaschke, M. Calculation of thermal noise in atomic force microscopy. *Nanotechnology* 6, 1-7 (1995).
5. Strunz, T., Oroszlan, K., Schafer, R. & Guntherodt, H.J. Dynamic force spectroscopy of single DNA molecules. *Proceedings of the National Academy of Sciences of the United States of America* 96, 11277-11282 (1999).
6. Rief, M., Clausen-Schaumann, H. & Gaub, H.E. Sequence-dependent mechanics of single DNA molecules. *Nat Struct Biol* 6, 346-349 (1999).
7. Levinthal, C. & Crane, H.R. On the Unwinding of DNA. *PNAS* 42, 436-438 (1956).
4. Rubinstein, R.H.C. *Polymer Physics*. Oxford University Press (2005).
5. Oesterhelt, F., Rief, M. & Gaub, H.E. Single molecule force spectroscopy by AFM indicates helical structure of poly(ethylene-glycol) in water. *New Journal of Physics* 1 (1999).
6. Smith, S.B., Cui, Y.J. & Bustamante, C. Overstretching B-DNA: The elastic response of individual double-stranded and single-stranded DNA molecules. *Science* 271, 795-799 (1996).

Anhang F

Methoden zur Oberflächenfunktionalisierung für SMCP-Experimente

SMCP wurde als Methode entwickelt, eine große Anzahl unterschiedlicher molekularer Bausteine, die in Depotbereichen stabil gelagert werden, mechanisch kontrolliert in Zielbereichen zu assemblieren. Da die Bausteine sowohl zum Depot als auch zum Ziel eine hohe Affinität zeigen, muss die „Befüllung“ der Depots so durchgeführt werden, dass die Zielflächen dabei nicht kontaminiert werden. Ferner ist die Transportstrecke durch die Reichweite des xy-Piezotisches limitiert¹, weshalb die verschiedenen Bereiche innerhalb dieser Region erzeugt werden müssen. Strategien zur Oberflächenfunktionalisierung werden im Folgenden kurz besprochen.

Oberflächenfunktionalisierung mittels Mikrofluidik

Die Depot- und Zielbereiche aller in dieser Arbeit verwendeten Proben wurden mikrofluidisch hergestellt. Das genaue Protokoll hierzu ist im Anhang C beschrieben. Das dort gezeigte Mikrofluidik-System besteht aus zwei 100 μm breiten und 20 μm hohen Kanälen, die durch einen 15 μm breiten Spalt voneinander getrennt sind. Auf diese Weise können auf einem Deckglas zwei räumlich getrennte Bereiche erzeugt werden. Prinzipiell lassen sich durch Verkleinerung der Kanäle wesentlich mehr Bereiche innerhalb der Verfahrstrecke des Piezos unterbringen². Die vier Bereiche der Abbildung F.1 wurden beispielsweise durch eine 4-Kanal-Mikrofluidik hergestellt.

Oberflächenfunktionalisierung durch lokales Heizen

Eine weitere Möglichkeit zur Herstellung von Depot- und Zielbereichen ergibt sich durch die Ausnützung der Hybridisierungseigenschaften von DNA-Molekülen. Doppelsträngige DNA

¹Derzeit 150 μm .

²Hierbei nimmt der experimentelle Aufwand aufgrund der vielen Zu- und Abflüsse beträchtlich zu.

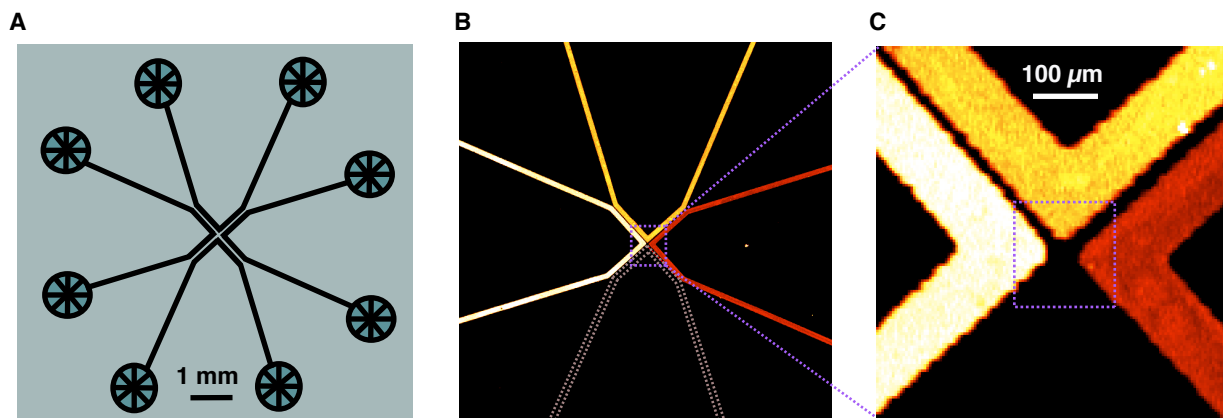


Abbildung F.1: 4-Kanal-Mikrofluidik. (A) Schematische Zeichnung des mikrostrukturierten Silizium-Wafers, der als Gussform zur Herstellung der 4-Kanal PDMS-Flusskammern dient. Die Kanäle sind $100\ \mu\text{m}$ breit, $20\ \mu\text{m}$ hoch und durch einen $15\ \mu\text{m}$ breiten Steg getrennt. Die runden Strukturen am Ende der Kanäle dienen als Anschluß an eine Peristaltikpumpe. (B) Fluoreszenzaufnahme eines mit vier Kanälen funktionalisierten Deckglases. Drei der Kanäle dienen als Depot und wurden mit verschiedenen, fluoreszenzmarkierten Transfer-DNAs bestückt. Der untere schraffierte Kanal dient als Ziel und ist kovalent mit Ziel-DNA funktionalisiert. (C) Detailansicht des Zentrums. Das schraffierte Quadrat illustriert den für den Piezo zugänglichen Bereich.

lässt sich abhängig von Art und Anzahl der Basenpaare durch Erhitzen in einzelsträngige DNA denaturieren. Die zur Anbindung der Transfer-DNA verwendeten Ankersequenzen haben Längen zwischen 30 und 35 Basenpaaren. Ihre Schmelztemperaturen liegen zwischen 60 °C und 65 °C. In [88] wurde ein Infrarot-Laser benützt, um eine zwischen zwei Grenzflächen eingeschlossene Wasserschicht aufzuheizen. Innerhalb der Kammer ergeben sich abhängig von der Kammerdicke und vom verwendeten Material der Grenzflächen starke Temperaturgradienten. Dadurch ist es möglich, DNA-Oligomere, die an eine Oberfläche hybridisiert sind, mit hoher lateraler Auflösung lokal abzuschmelzen. Durch Verwendung eines in xy-Richtung ablenkbaren Infrarot-Lasers [89] können dadurch beliebige Bereiche auf einer Oberfläche abgeschmolzen werden. In Abbildung F.2 (A und B) wird die auf diesem Prinzip beruhende Methode zur Oberflächenfunktionalisierung schematisch dargestellt. Die in Abbildung F.2 (C - E) gezeigten Fluoreszenzbilder wurden mit dieser Methode erzeugt.

Oberflächenfunktionalisierung auf räumlich getrennten Flächen

Der allgemeinste Ansatz zur Herstellung von Depot- und Zielbereichen besteht darin, die Beschichtung auf getrennten Substraten durchzuführen. Das Prinzip ist in Abbildung F.3 schematisch dargestellt. Mehrere räumlich getrennte Substrate werden jeweils mit einer Sorte molekularer Bausteine großflächig beschichtet. In einem zweiten Schritt fügt man die Depots auf einer gemeinsamen Fläche zusammen. Diese Fläche ist gegen die Zielfläche lateral verschiebbar. Die Anzahl an Depotflächen ist dadurch nicht mehr durch die Verfahrstrecke des Piezotisches eingeschränkt.

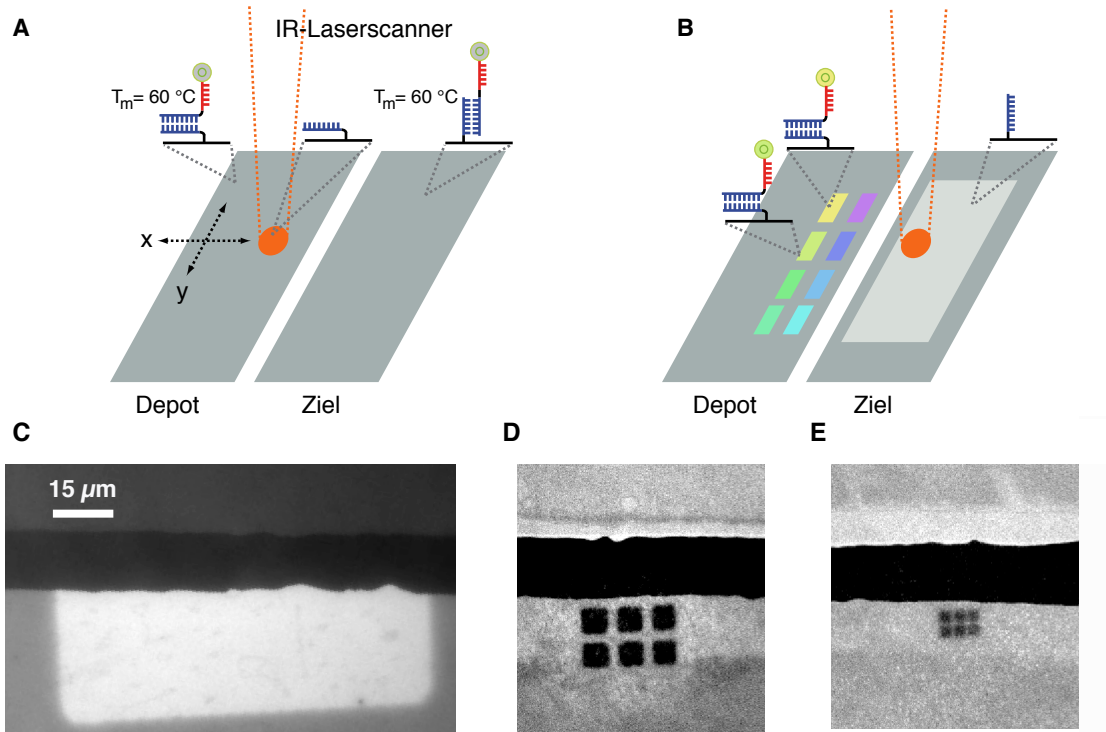


Abbildung F.2: Oberflächenfunktionalisierung durch lokales Heizen. (A) Depot- und Zielflächen werden mikrofluidisch mit den entsprechenden DNA-Oligomeren kovalent beschichtet. Anschließend werden Transfer-DNA-Moleküle flächig angebunden. Durch lokales Heizen mittels eines Infrarot-Lasers kann die Transfer-DNA punktuell mit einer lateralen Auflösung von bis zu $1 \mu\text{m}$ abgeschmolzen werden. (B) Der freigeschmolzene Depotbereich kann mit einer weiteren Sorte Transfer-DNA beschichtet werden. Durch sukzessives Abschmelzen und Hybridisieren können viele verschiedene Depotbereiche erzeugt werden. Im letzten Schritt wird der Zielbereich freigeschmolzen. (C) Das Fluoreszenzbild zeigt eine auf diese Weise erzeugte Oberfläche, wobei lediglich ein Schmelz- und Hybridisierungszyklus durchgeführt wurde. (D und E) Die freigeschmolzenen Bereiche wurden sukzessive verkleinert. Die Größe der Bereiche in (E) beträgt ca. $2,5 \mu\text{m}$. Auf eine Anbindung verschiedener Bausteine wurde verzichtet.

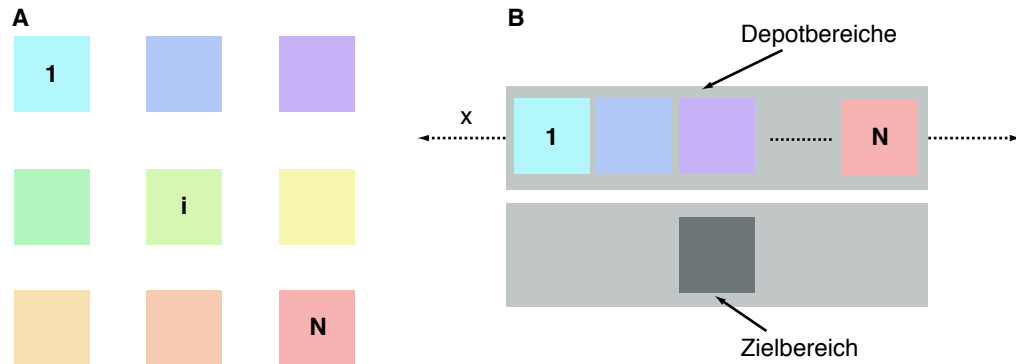


Abbildung F.3: Oberflächenfunktionalisierung durch laterales Verschieben. (A) Auf räumlich getrennten Flächen werden die verschiedenen Depotbereiche mit unterschiedlichen molekularen Bausteinen beschichtet. Ein *Cross-Talk* kann dadurch vollständig vermieden werden. (B) In einem zweiten Schritt werden die Depots auf einer gemeinsamen Fläche zusammengefügt. Die Depotbereiche lassen sich lateral gegen die Zielbereiche verschieben. Dadurch ist die Anzahl der Depots nicht mehr durch die Verfahrstrecke des Piezos limitiert.

Anhang G

SMCP als entkoppeltes Transportsystem für verschiedenste molekulare Bausteine

Die Transfer-DNA kann mit verschiedenen *Tags* modifiziert werden, wodurch die Möglichkeit besteht, variabel molekulare Bausteine daran zu koppeln, d.h. das Transportsystem DNA arbeitet entkoppelt vom zu transportierenden Baustein.

Tags an der Transfer-DNA

- Biotin: Die Biotin/Streptavidin Bindung ist eine der stärksten nichtkovalenten Verbindungen, die in der Biologie vorkommt [33]. Es besteht die Möglichkeit, die Transfer-DNA am 5'- sowie am 3' Ende mit Biotin zu modifizieren. Für die in Abbildung G.1 mittels SMCP erzeugten Muster, wurde fluoreszenzmarkiertes Streptavidin an die mit Biotin modifizierte Transfer-DNA gebunden.
- Benzylguanin: Das Biotin/Streptavidin System ist eine Standardmethode der Biotechnologie. Aus diesem Grund gibt es eine Vielzahl Streptavidin modifizierter Stoffe, die kommerziell erhältlich sind. Die Halbleiternanopartikel aus Anhang E wurden beispielsweise bei Invitrogen gekauft. Streptavidin hat allerdings den Nachteil, dass es als Tetramer vorkommt¹, daher ist es nicht als rekombinantes Fusionsprotein herstellbar. Für viele Anwendungen ist daher das in Anhang B beschriebene Benzylguanin/hAGT System besser geeignet. Das Benzylguanin kann ebenfalls sowohl am 5'- sowie am 3' Ende an die Transfer-DNA gebunden werden.

DNA-Sequenzen

Eine weitere Möglichkeit molekulare Bausteine zu koppeln, besteht darin, die Transfer-DNA selbst als *Tag* zu benützen (Abbildung G.2). Derzeit besteht die Transfer-DNA aus

¹Die Primärstruktur des Monomers besteht aus 159 Aminosäuren und hat ein Molekulargewicht von 16807 Da.

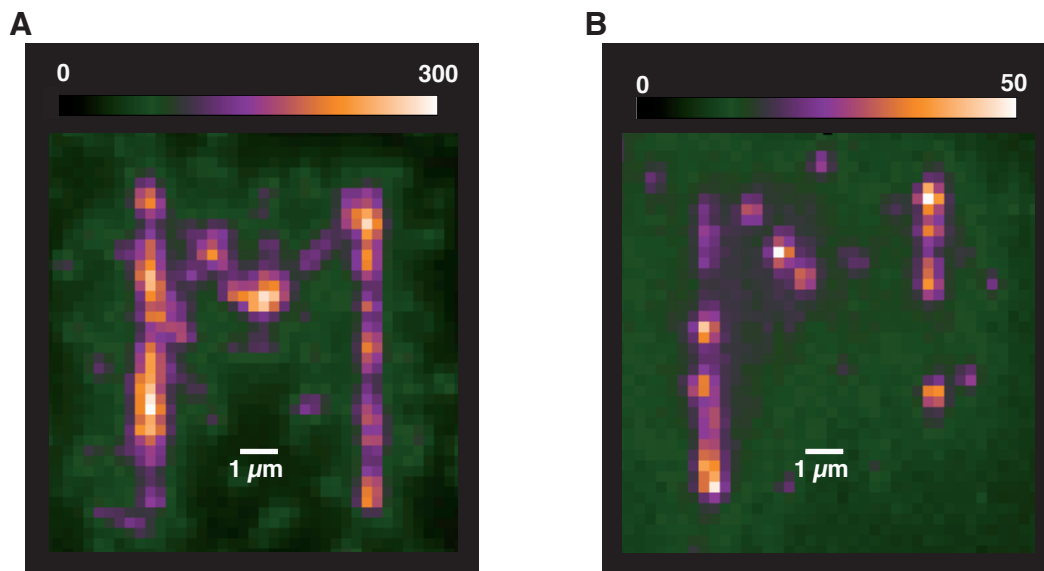


Abbildung G.1: SMCP mit Polypeptiden. (A) Biotin modifizierte Transfer-DNA-Moleküle wurden durch 400 SMCP-Zyklen im Zielbereich zu einem „M“ assembliert. Anschließend wurde die Oberfläche mit einer 1 nM fluoreszenzmarkierten Streptavidin Lösung inkubiert. Nach 60 Sekunden Inkubationszeit wurde die Oberfläche mit 1*SSC Puffer gespült und ein TIRF-Bild aufgenommen. (B) Die Biotin modifizierte DNA wurde bereits im Depot mit fluoreszenzmarkierten Streptavidin inkubiert. Anschließend wurde mit 1*SSC Puffer gründlich gespült. Anschließend wurde durch 400 SMCP Zyklen im Zielbereich ein „M“ assembliert.



Abbildung G.2: Transfer-DNA als frei programmierbarer *Tag*. Die Transfer-DNA besteht aus 80 Basenpaare, wovon 50 Basenpaare für das hierarchische Kraftsystem verwendet werden. Die restlichen 30 Basenpaare sind frei programmierbar. Dadurch ergeben sich theoretisch 4^{30} verschiedene Kopplungsstellen.

80 Basenpaare, wovon lediglich 50 Basenpaare für das hierarchische Kraftsystem verwendet werden. Die restlichen 30 Basenpaare sind frei „programmierbar“, wodurch sich theoretisch 4^{30} verschiedene Kopplungsstellen ergeben.

Anhang H

Verbesserungsmöglichkeiten bei der SMCP-Oberflächenassemblierung

Mit der SMCP-Oberflächenassemblierung ist eine einfache, robuste und zuverlässige Methode entwickelt worden, mit der es erstmals gelungen ist, unter physiologischen Bedingungen eine sehr große Anzahl molekularer Bausteine einzeln und mechanisch kontrolliert auf Oberflächen anzubinden. Eine wesentliche Eigenschaft dieser Technik besteht darin, molekulare Bindungen selektiv zu öffnen und anschließend neue Bindungen zu formen. Dabei erlaubt es das auf DNA-DNA Wechselwirkung basierende Kraftsystem, die einzelnen Schritte (öffnen der Zipper-Sequenz im Depot und absetzen der Transfer-DNA im Ziel) über eindeutige Kraft-Abstandskurven zu charakterisieren. Auf diese Weise kann die exakte Anzahl der aufgenommenen und platzierten Bausteine bestimmt werden. Um das Potential der Methode voll auszuschöpfen, können folgende Verbesserungen durchgeführt werden:

- Messaufbau: Das derzeitige kombinierte AFM-TIRF Mikroskop erlaubt die Anregung der Farbstoffe mit einer festen Wellenlänge und die Detektion von zwei Emissionswellenlängen. Für viele Anwendungen wäre es jedoch hilfreich, schnell die Anregungswellenlänge zu ändern und somit verschieden markierte molekulare Bausteine in getrennten Kanälen zu detektieren. Außerdem könnte durch Integration eines Infrarot-Lasers von der Möglichkeit Gebrauch gemacht werden, beschriebene Zielbereiche durch Abschmelzen der Transfer-DNA wieder zu regenerieren. Wie im Anhang F gezeigt, können auf diese Weise Bereiche mit einer lateralen Auflösung bis zu $1\ \mu\text{m}$ selektiv gelöscht werden.
- Temperaturstabilisierung: Der größte Unsicherheitsfaktor bei der Durchführung der Experimente kommt durch temperaturbedingte Drift zustande (siehe auch Anhang D). In Abbildung H.1 wurde beispielsweise die Position eines einzelnen Halbleiternanokristalls über einen Zeitraum von 180 s bestimmt. Während dieser Zeit wurde die Temperatur linear von $20\ \text{°C}$ auf $25\ \text{°C}$ erhöht¹. Die Position des Nanokristalls

¹Der AFM-TIRF Aufbau befindet sich in einer Schallschutzbox. Wird während des SMCP-Prozesses

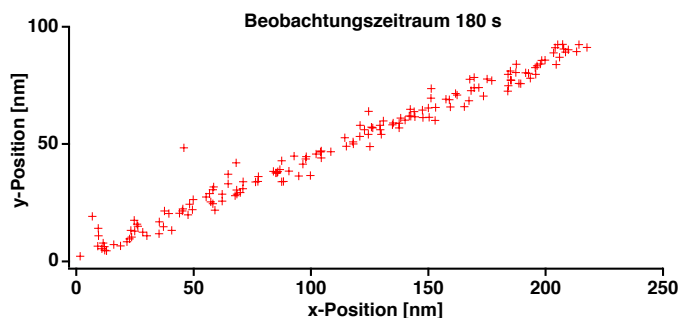


Abbildung H.1: Temperaturbedingte Drift. Ein Halbleiternanokristall wurde über Biotin/Streptavidin fest an eine Oberfläche gebunden. Seine Position wurde über einen Zeitraum von 180 s verfolgt. In dieser Zeit wurde die Temperatur linear von 20 °C auf 25 °C erhöht, was zu einer temperaturbedingten Drift von ca. 240 nm des Partikels relativ zum Objektiv führte.

relativ zum Objektiv änderte sich dabei um ca. 240 nm. Die Unsicherheit der SMCP-Oberflächenassemblierung wurde in Anhang D bestimmt und beträgt ca. ± 11 nm. Um nicht durch temperaturbedingte Drift limitiert zu sein, ist es daher zwingend nötig, eine Temperaturstabilisierung zu integrieren.

- Kombinierte AFM-TIRF *realtime* Evaluierung: Derzeit wird das SMCP-Protokoll unabhängig von den Einzelmolekülfluoreszenzdaten durchgeführt. Für Experimente bei denen mehrere molekulare Bausteine mit Nanometerpräzision relativ zueinander positioniert werden sollen, ist es sinnvoll das SMCP-Protokoll durch die Einzelmolekülfluoreszenzdaten zu steuern. Dazu kann die tatsächliche Istposition eines assemblierten Bausteins aus den Einzelmolekülfluoreszenzdaten bestimmt und mit seiner Sollposition verglichen werden. Die auf diese Weise bestimmte Istposition dient dann als *Feedback*-Parameter für die weiteren SMCP-Positionen. Auf diese Weise können trotz der intrinsischen Ortsunsicherheit der SMCP-Oberflächenassemblierung, die bei ca. ± 11 nm liegt, die molekularen Bausteine mit Nanometerpräzision angeordnet werden.

die Box geschlossen, erhöhen die elektronischen Geräte im Inneren (EMCCD-Kamera, Stable-Table, etc.) die Temperatur. Die Temperatur kann dabei auf bis zu 40 °C ansteigen.

Abkürzungsverzeichnis

AFM	Atomic Force Microscope (Rasterkraftmikroskop)
APD	Avalanche Photo Diode (Lawinen-Photodiode)
BG	<i>O</i> ⁶ -Benzylguanin
CCD	Charge Coupled Device (Ladungsgekoppeltes Bauteil)
DNA	Desoxyribonukleinsäure
FCS	Fluorescence Correlation Spectroscopy (Fluoreszenz-Korrelations-Spektroskopie)
GFP	Grün Fluoreszierendes Protein
hAGT	Human Alkylguanine-DNA-Alkyltransferase
MEMS	Micro Electro Mechanical System (Mikrosystemtechnik)
PDMS	Polydimethylsiloxan
PEG	Polyethylenglykol
PMT	Photomultiplier Tube (Photomultiplier)
PSF	Point Spread Funktion (Punktverwaschungsfunktion)
REM	Rasterelektronenmikroskop
RNA	Ribonukleinsäure
SSC	Saline Sodium Citrate (Natriumchlorid Ziträt)
SMCP	Single-Molecule Cut-and-Paste
SPR	Surface Plasmon Resonance (Oberflächenplasmonenresonanz)
STM	Scanning Tunneling Microscope (Rastertunnelmikroskop)
TIRFM	Total Interne Reflexion Fluoreszenz Mikroskopie

Literaturverzeichnis

- [1] M. M. Tice and D. R. Lowe. Photosynthetic microbial mats in the 3,416-Myr-old ocean. *Nature*, 431:549–552, 2006.
- [2] J. W. Schopf and B. M. Packer. Early Archean (3.3-billion to 3.5-billion-year-old) microfossils from Warrawoona Group, Australia. *Science*, 237(4810):70–73, 1987.
- [3] W. Gilbert. Origin of life: The RNA world. *Nature*, (319):618, 1986.
- [4] M. J. Russell, A. J. Hall, A. G. Cairns-Smith, and P. S. Braterman. Submarine hot springs and the origin of life. *Nature*, (336):117, 1988.
- [5] P. Baaske, F. M. Weinert, S. Duhr, K. H. Lemke, M. J. Russell, and D. Braun. From the Cover: Extreme accumulation of nucleotides in simulated hydrothermal pore systems. *Proceedings of the National Academy of Sciences*, 104(22):9346–9351, 2007.
- [6] J. A. Doudna and J. W. Szostak. RNA-catalysed synthesis of complementary-strand RNA. *Nature*, (339):519–522, 1989.
- [7] R. F. Gesteland, T. R. Cech, and J. F. Atkins. *The RNA World*. Cold Spring Harbor Laboratory Press, 1999.
- [8] N. A. Campbell. *Biologie*. Spektrum Akademischer Verlag, 1997.
- [9] W. B. Whitman, D. C. Coleman, and W. J. Wiebe. Prokaryotes: The unseen majority. *Proceedings of the National Academy of Sciences*, 95(12):6578–6583, 1998.
- [10] E. G. Roussel, M. A. C. Bonavita, J. Querellou, B. A. Cragg, G. Webster, D. Prieur, and R. J. Parkes. Extending the Sub-Sea-Floor Biosphere. *Science*, 320(5879):1046–, 2008.
- [11] W. M. X. Zimmer, M. P. Johnson, A. D’Amico, and P. L. Tyack. Combining data from a multisensor tag and passive sonar to determine the diving behavior of a sperm whale (*Physeter macrocephalus*). *IEEE Journal of Oceanic Engineering*, 28:13–28, Jan 2003.
- [12] Z. Shao and F. Vollrath. Materials: Surprising strength of silkworm silk. *Nature*, 418:741, 2002.

- [13] S. Rammensee, U. Slotta, T. Scheibel, and A. R. Bausch. Assembly mechanism of recombinant spider silk proteins. *Proceedings of the National Academy of Sciences*, 105(18):0709246105, 2008.
- [14] A. M. Turing. Computing machinery and intelligence. *Mind*, 59:433–460, 1950.
- [15] A. Bird. DNA methylation patterns and epigenetic memory. *Genes Development*, 16(1):6–21, 2002.
- [16] C. D. Allis, T. Jenuwein, and D. Reinberg. *Epigenetics*. Cold Spring Harbor Laboratory Press, 2007.
- [17] G. Binnig, C. F. Quate, and Ch. Gerber. Atomic Force Microscope. *Physical Review Letters*, 56(9):930–933, 1986.
- [18] A. Ashkin, J. M. Dziedzic, J. E. Bjorkholm, and S. Chu. Observation of a single-beam gradient force optical trap for dielectric particles. *Optics Letters*, 11(5):288, 1986.
- [19] S. B. Smith, L. Finzi, and C. Bustamante. Direct mechanical measurements of the elasticity of single DNA molecules by using magnetic beads. *Science*, 258(5085):1122–1126, 1992.
- [20] S. Weiss. Fluorescence Spectroscopy of Single Biomolecules. *Science*, 283(5408):1676–1683, 1999.
- [21] R. Merkel, P. Nassoy, A. Leung, K. Ritchie, and E. Evans. Energy landscapes of receptor–ligand bonds explored with dynamic force spectroscopy. *Nature*, 397:50–53, 1999.
- [22] A. Yildiz, J. N. Forkey, S. A. McKinney, T. Ha, Y. E. Goldman, and P. R. Selvin. Myosin V Walks Hand-Over-Hand: Single Fluorophore Imaging with 1.5-nm Localization. *Science*, 300(5628):2061–2065, 2003.
- [23] A. Yildiz, M. Tomishige, R. D. Vale, and P. R. Selvin. Kinesin Walks Hand-Over-Hand. *Science*, 303(5658):676–678, 2004.
- [24] S. B. Smith, Y. Cui, and C. Bustamante. Overstretching B-DNA: The Elastic Response of Individual Double-Stranded and Single-Stranded DNA Molecules. *Science*, 271(5250):795–799, 1996.
- [25] T. R. Strick, J.-F. Allemand, D. Bensimon, A. Bensimon, and V. Croquette. The Elasticity of a Single Supercoiled DNA Molecule. *Science*, 271(5257):1835–1837, 1996.
- [26] B. Essevaz-Roulet, U. Bockelmann, and F. Heslot. Mechanical separation of the complementary strands of DNA. *Proceedings of the National Academy of Sciences of the United States of America*, 94(22):11935–11949, 1997.

- [27] M. Rief, H. Clausen-Schaumann, and H. E. Gaub. Sequence-dependent mechanics of single DNA molecules. *Nature Structural Biology*, 6(4):346, 1999.
- [28] R. Krautbauer, M. Rief, and H. E. Gaub. Unzipping DNA oligomers. *Nano Letters*, 3(4):493–496, 2003.
- [29] J. Morfill, F. Kuhner, K. Blank, R. A. Lugmaier, J. Sedlmair, and H. E. Gaub. B-S Transition in Short Oligonucleotides. *Biophysical Journal*, 93(7):2400–2409, 2007.
- [30] M. Rief, M. Gautel, F. Oesterhelt, J. M. Fernandez, and H. E. Gaub. Reversible Unfolding of Individual Titin Immunoglobulin Domains by AFM. *Science*, 276(5315):1109–1112, 1997.
- [31] H. Dietz and M. Rief. Exploring the energy landscape of GFP by single-molecule mechanical experiments. *Proceedings of the National Academy of Sciences*, 101(46):16192–16197, 2004.
- [32] H. Dietz and M. Rief. Protein structure by mechanical triangulation. *Proceedings of the National Academy of Sciences*, 103(5):1244–1247, 2006.
- [33] E. L. Florin, V. T. Moy, and H. E. Gaub. Adhesion forces between individual ligand-receptor pairs. *Science*, 264(5157):415–417, 1994.
- [34] V. T. Moy, E. L. Florin, and H. E. Gaub. Intermolecular forces and energies between ligands and receptors. *Science*, 266(5183):257–259, 1994.
- [35] J. Morfill, K. Blank, C. Zahnd, B. Luginbuhl, F. Kuhner, K. E. Gottschalk, A. Pluckthun, and H. E. Gaub. Affinity-Matured Recombinant Antibody Fragments Analyzed by Single-Molecule Force Spectroscopy. *Biophysical Journal*, 93(10):3583–3590, 2007.
- [36] C. Albrecht, K. Blank, M. Lalic-Multhaler, S. Hirler, T. Mai, I. Gilbert, S. Schiffmann, T. Bayer, H. Clausen-Schaumann, and H. E. Gaub. DNA: A Programmable Force Sensor. *Science*, 301(5631):367–370, 2003.
- [37] C. Dose, D. Ho, H. E. Gaub, P. B. Dervan, and C. H. Albrecht. Recognition of „Mirror-Image“ DNA by Small Molecules. *Angewandte Chemie International Edition*, 46(44):8384–8387, 2007.
- [38] A. J. Turberfield, J. C. Mitchell, B. Yurke, A. P. Mills, M. I. Blakey, and F. C. Simmel. DNA Fuel for Free-Running Nanomachines. *Physical Review Letters*, 90(11):118102, Mar 2003.
- [39] B. Yurke, A. J. Turberfield, A. P. Mills, F. C. Simmel, and J. L. Neumann. A DNA-fuelled molecular machine made of DNA. *Nature*, 406:605–608, 2000.
- [40] E. Winfree, F. Liu, L. A. Wenzler, and N. C. Seeman. Design and self-assembly of two-dimensional DNA crystals. *Nature*, 394:539–544, 1998.

- [41] P. W. K. Rothemund. Folding DNA to create nanoscale shapes and patterns. *Nature*, 440(7082):297–302, 2006.
- [42] J. Chen and N. C. Seeman. Synthesis from DNA of a molecule with the connectivity of a cube. *Nature*, 350:631–633, 1991.
- [43] L. M. Adleman. Molecular computation of solutions to combinatorial problems. *Science*, 266(5187):1021–1024, 1994.
- [44] R. J. Lipton. DNA solution of hard computational problems. *Science*, 268(5210):542–545, 1995.
- [45] Q. Ouyang, P. D. Kaplan, S. Liu, and A. Libchaber. DNA Solution of the Maximal Clique Problem. *Science*, 278(5337):446–449, 1997.
- [46] K. Sakamoto, H. Gouzu, K. Komiya, D. Kiga, S. Yokoyama, T. Yokomori, and M. Hagiya. Molecular Computation by DNA Hairpin Formation. *Science*, 288(5469):1223–1226, 2000.
- [47] D. M. Eigler and E. K. Schweizer. Positioning single atoms with a scanning tunnelling microscope. *Nature*, (344):524–526, 1990.
- [48] M. F. Crommie, C. P. Lutz, and D. M. Eigler. Confinement of Electrons to Quantum Corrals on a Metal Surface. *Science*, 262(5131):218–220, 1993.
- [49] J. K. Gimzewski, C. Joachim, R. R. Schlittler, V. Langlais, H. Tang, and I. Johannsen. Rotation of a Single Molecule Within a Supramolecular Bearing. *Science*, 281(5376):531–533, 1998.
- [50] S. W. Hla, L. Bartels, G. Meyer, and K. H. Rieder. Inducing All Steps of a Chemical Reaction with the Scanning Tunneling Microscope Tip: Towards Single Molecule Engineering. *Physical Review Letters*, 85(13):2777–2780, Sep 2000.
- [51] R. E. Smalley. Of Chemistry, Love and Nanobots. *Scientific American*, 285(3):76–77, 2001.
- [52] G. Binnig, H. Rohrer, Ch. Gerber, and E. Weibel. Surface Studies by Scanning Tunneling Microscopy. *Physical Review Letters*, 49(1):57–61, 1982.
- [53] Y. Martin and H. K. Wickramasinghe. Magnetic imaging by “force microscopy” with 1000 Å resolution. *Applied Physics Letters*, 50(20):1455–1457, 1987.
- [54] E. Betzig and J. K. Trautman. Near-Field Optics: Microscopy, Spectroscopy, and Surface Modification Beyond the Diffraction Limit. *Science*, 257(5067):189–195, 1992.
- [55] G. Binnig, H. Rohrer, C. Gerber, and E. Weibel. Tunneling through a Controllable Vacuum Gap. *Applied Physics Letters*, 40(2):178–180, 1982.

- [56] G. Binnig and H. Rohrer. Scanning tunneling microscopy. *IBM Journal of Research and Development*, 44(1/2), 2000.
- [57] G. Meyer and N. M. Amer. Novel optical approach to atomic force microscopy. *Applied Physics Letters*, 53(12):1045–1047, 1988.
- [58] J. L. Hutter and J. Bechhoefer. Calibration of atomic-force microscope tips. *Review of Scientific Instruments*, 64(7):1868, 1993.
- [59] H. J. Butt and M. Jaschke. Calculation of thermal noise in atomic force microscopy. *Nanotechnology*, 6(1):1, 1995.
- [60] E. L. Florin, M. Rief, H. Lehmann, M. Ludwig, C. Dornmair, V. T. Moy, and H. E. Gaub. Sensing specific molecular interactions with the atomic force microscope. *Biosensors and Bioelectronics*, (10):895–901, 1995.
- [61] N. A. Burnham, X. Chen, C. S. Hodges, G. A. Matei, E. J. Thoreson, C. J. Roberts, M. C. Davies, and S. J. B. Tendler. Comparison of calibration methods for atomic-force microscopy cantilevers. *Nanotechnology*, 14(1):1, 2003.
- [62] D. Sarid. *Scanning force microscopy*. Oxford Press, 1994.
- [63] D. A. Walters, J. P. Cleveland, N. H. Thomson, P. K. Hansma, M. A. Wendman, G. Gurley, and V. Elings. Short cantilevers for atomic force microscopy. *Review of Scientific Instruments*, 67:3583, 1996.
- [64] M. B. Viani, T. E. Schaffer, A. Chand, M. Rief, H. E. Gaub, and P. K. Hansma. Small cantilevers for force spectroscopy of single molecules. *Journal of Applied Physics*, 86(4):2258–2262, 1999.
- [65] E. Chargaff. *The Nucleic Acids. Chemistry and Biology*. Academic Press, 1955.
- [66] M. K. Cheezum, W. F. Walker, and W. H. Guilford. Quantitative Comparison of Algorithms for Tracking Single Fluorescent Particles. *Biophysical Journal*, 81(4):2378–2388, 2001.
- [67] N. Bobroff. Position measurement with a resolution and noise-limited instrument. *Review of Scientific Instruments*, 57(6):1152–1157, 1986.
- [68] J. Enderlein, E. Toprak, and P. R. Selvin. Polarization effect on position accuracy of fluorophore localization. *Optics Express*, 14(18):8111–8120, 2006.
- [69] C. E. Shannon. Communication in the Presence of Noise. *PROCEEDINGS OF THE IRE*, 37(1):10–21, 1949.
- [70] H. Nyquist. Certain Topics in Telegraph Transmission Theory. *Trans. Amer. Inst. Elect. Eng.*, 47:617–644, 1928.

- [71] R. J. Ober, S. Ram, and E. S. Ward. Localization Accuracy in Single-Molecule Microscopy. *Biophysical Journal*, 86(2):1185–1200, 2004.
- [72] J. R. Lakowics. *Principles of Fluorescence Spectroscopy*. Kluwer Academic/Plenum Publishers, 1999.
- [73] T. Hirschfeld. Optical microscopic observation of single small molecules. *Applied Optics*, 15:2965–2966, 1976.
- [74] C. Zander, J. Enderlein, and R. A. Keller. *Single Molecule Detection in Solution*. WILEY-VCH, 2002.
- [75] R. Riegler and E. Elson. *Fluorescence Correlation Spectroscopy*. Springer, 2001.
- [76] S. W. Hell and J. Wichmann. Breaking the diffraction resolution limit by stimulated emission: stimulated-emission-depletion fluorescence microscopy. *Optics Letters*, 19(11):780, 1994.
- [77] T. D. Lacoste, X. Michalet, F. Pinaud, D. S. Chemla, A. P. Alivisatos, and S. Weiss. Ultrahigh-resolution multicolor colocalization of single fluorescent probes. *Proceedings of the National Academy of Sciences*, 97(17):9461–9466, 2000.
- [78] M. P. Gordon, T. Ha, and P. R. Selvin. Single-molecule high-resolution imaging with photobleaching. *Proceedings of the National Academy of Sciences*, 101(17):6462–6465, 2004.
- [79] X. Qu, D. Wu, L. Mets, and N. F. Scherer. Nanometer-localized multiple single-molecule fluorescence microscopy. *Proceedings of the National Academy of Sciences*, 101(31):11298–11303, 2004.
- [80] E. Betzig, G. H. Patterson, R. Sougrat, O. W. Lindwasser, S. Olenych, J. S. Bonifacino, M. W. Davidson, J. Lippincott-Schwartz, and H. F. Hess. Imaging Intracellular Fluorescent Proteins at Nanometer Resolution. *Science*, 313(5793):1642–1645, 2006.
- [81] B. Huang, W. Wang, M. Bates, and X. Zhuang. Three-Dimensional Super-Resolution Imaging by Stochastic Optical Reconstruction Microscopy. *Science*, 319(5864):810–813, 2008.
- [82] Y. Ke, S. Lindsay, Y. Chang, Y. Liu, and H. Yan. Self-Assembled Water-Soluble Nucleic Acid Probe Tiles for Label-Free RNA Hybridization Assays. *Science*, 319(5860):180–183, 2008.
- [83] H. C. Kolb, M. G. Finn, and K. B. Sharpless. Click Chemistry: Diverse Chemical Function from a Few Good Reactions. *Angewandte Chemie International Edition*, (40):2004–2021, 2001.

-
- [84] D. I. Rozkiewicz, J. G. Glenn, B. K. Gutsmedl, T. Carell, B. J. Ravoo, and D. N. Reinhoudt. Transfer Printing of DNA by „Click“ Chemistry. *ChemBioChem*, (8):1997–2002, 2007.
- [85] A. Bek, R. Jansen, M. Ringler, S. Mayilo, T. A. Klar, and J. Feldmann. Fluorescence Enhancement in Hot Spots of AFM-Designed Gold Nanoparticle Sandwiches. *Nano Letters*, 8(2):485–490, 2008.
- [86] A. R. Clapp, I. L. Medintz, J. M. Mauro, B. R. Fisher, M. G. Bawendi, and H. Mattoussi. Fluorescence Resonance Energy Transfer Between Quantum Dot Donors and Dye-Labeled Protein Acceptors. *Journal of the American Chemical Society*, 126(1):301–310, 2004.
- [87] H. D. Mootz, E. S. Blum, A. B. Tyszkiewicz, and T. W. Muir. Conditional Protein Splicing: A New Tool to Control Protein Structure and Function in Vitro and in Vivo. *Journal of the American Chemical Society*, 125(35):10561–10569, 2003.
- [88] S. Duhr, S. Arduini, and D. Braun. Thermophoresis of DNA determined by microfluidic fluorescence. *European Physical Journal E*, (15):277–286, 2004.
- [89] F. M. Weinert, J. A. Kraus, T. Franosch, and D. Braun. Microscale Fluid Flow Induced by Thermoviscous Expansion Along a Traveling Wave. *Physical Review Letters*, 100(16):164501, 2008.

Danksagung

An dieser Stelle sei all jenen gedankt, die zum Gelingen dieser Arbeit beigetragen haben.

Allen voran möchte ich Herrn Professor Dr. Hermann E. Gaub für die Betreuung meiner Diplom- und Doktorarbeit danken. Ich hatte dadurch 5 Jahre lang die Möglichkeit, an einem der weltweit renommiertesten Lehrstühlen für Biophysik zu arbeiten. Seine Geduld in schwierigen Phasen wurde nur von seiner Begeistungsfähigkeit für ungelöste Probleme übertroffen. Sein Vertrauen in mich und meine Arbeitsweise hat mich bis zum heutigen Tag immer wieder aufs neue verblüfft. Danke Gambi!

Ganz besonders möchte ich auch Elias Puchner für die Entwicklung und Programmierung der „Nähmaschine“ danken. Ohne sein großes persönliches Engagement, bereits zu einer Zeit, in der oftmals als Kommentar lediglich ein „das funktioniert eh nicht“ kam, wäre meine Doktorarbeit in dieser Form sicher nicht möglich gewesen.

Hermann Gump für seinen tollen (First-Generation) AFM-TIRF-Aufbau, der wirklich alles detektiert, das ihm vor die Optik läuft.

Tim Liedl, der in einer sehr kritischen Phase die erlösende Idee hatte und mit seinen Kenntnissen über Mikrofluidik meine Defizite darin kompensierte.

Mathias Strackharn und Stefan Stahl für den (Second-Generation) AFM-TIRF-Aufbau und ihre Ausdauer beim Durchführen vieler Messungen - „aber ihr könntet doch vielleicht auch gleich noch schnell mal wenn ihr schon dabei seid...“.

Angelika Kardinal für die Organisation des Chemielabors und für vieles, vieles mehr.

Lars Sonnenberg dafür, dass er sich mehr als 3 Jahre lang mein ständiges Gejammer angehört hat.

Allen (ganz besonders Sabine), die meine Arbeit durchgelesen und mich auf Fehler hingewiesen haben.

Julia, Anna, Thomas, Flo, Dominik, Hendrik und Franz, die mich während der letzten

Jahre als Freund ertragen haben und mich beim Kartenspielen gewinnen ließen.

Der ganzen Gambicrew für die tolle Atmosphäre, die am Lehrstuhl herrscht und den Lehrstuhl Gaub zum LEHRSTUHL GAUB macht.

Ganz besonders möchte ich auch meiner Frau Steffi für die schöne gemeinsame Zeit und für unsere Töchter Lea und Romy danken.

Danke!

Curriculum Vitae

1. Persönliche Daten

Dipl. Phys. (Univ.) Stefan Kaspar Kufer
Goethestr. 19
85117 Eitensheim

geb. am 23.10.1975 in Freising
Familienstand: verheiratet
Kinder: Lea Franziska
Romy Katharina
Staatsangehörigkeit: deutsch
Telefon: 08458/346797
e-mail: Stefan.Kufer@physik.uni-muenchen.de

2. Ausbildung

seit 09/04: **Promotion in Physik**, Ludwig-Maximilians-Universität München, Dissertation am Lehrstuhl für Angewandte Physik bei Prof. Dr. Hermann E. Gaub, Thema: „AFM-basierte Assemblierung biomolekularer Bausteine auf Festkörperoberflächen“

11/98 - 06/04: **Studium der Physik**, Ludwig-Maximilians-Universität München, Diplomarbeit am Lehrstuhl für Angewandte Physik bei Prof. Dr. Hermann E. Gaub, Thema: „Kovalente und selektive Verankerung rekombinanter Proteine auf festen Oberflächen“, Abschluss: Diplom (Note: sehr gut, 1.1)

10/96 - 08/98: **Studium der physikalischen Technik**, Fachhochschule München, Abschluss: Vordiplom

3. Berufspraxis

seit 09/04: Wissenschaftlicher Angestellter an der Ludwig-Maximilians-Universität München, Lehrstuhl für Angewandte Physik

09/00 - 04/01: Werkstudent bei Solon Management Consulting in München

04/98 - 10/98: Werkstudent bei Texas Instruments in Freising

10/97 - 03/98: Praktikum bei Texas Instruments in Freising

4. Grundwehrdienst

10/95 - 07/96: Gebirgsjägerbataillon 232, Strub, Berchtesgaden

5. Auszeichnungen

03/05: SNAP-tag Award 2005 für die Veröffentlichung: Kufer S. K., et al.: „Covalent immobilization of recombinant fusion proteins with hAGT for single molecule force spectroscopy.“ Eur Biophys J (2005), 35(1), pp. 72-78

